ABSTRACT

ELECTROMAGNETIC SCATTERING FROM A
PLASMA-COATED CYLINDER

By

Chen Yi Lee

The present study deals with the problem of electromagnetic scattering from a plasma-coated object. An infinite cylinder of a finite radius is covered by a layer of inhomogeneous, lossy and hot plasma. This plasma-coated cylinder is assumed to be illuminated by a plane wave with either TE or TM polarization. When the temperature effect of the plasma is considered, an electroacoustic wave in addition to the electromagnetic wave is excited in the plasma layer. The effects of this electroacoustic wave on the electromagnetic scattering are studied. It is found that if the plasma-coated cylinder is illuminated by a TM plane wave, no electroacoustic wave can be excited in the plasma layer. To handle the wave propagation in the inhomogeneous plasma medium, the stratification method is applied.

In the analysis, the dipolar, quadrupolar and temperature resonances have been found to exist in the plasma layer. The effect of various parameters on the electromagnetic scattering are also studied.

An experiment was conducted to verify the theory.

ELECTROMAGNETIC SCATTERING FROM A PLASMA-COATED CYLINDER

By

Chen Yi Lee

A THESIS

Submitted to
Michigan State University
in partial fulfillment of the requirements
for the degree of

DOCTOR OF PHILOSOPHY

Department of Electrical Engineering

1971

To my parents

Mr. & Mrs. Sun Ri Lee

ACKNOWLEDGMENTS

The author wishes to express his sincere appreciation to his major professor, Dr. K. M. Chen, for his guidance, counsel and encouragement throughout the course of this investigation.

He also wishes to thank the committee member, Dr. B. Ho, for his valuable suggestions and help in the experimental part of this research, and to the other members, Drs. D. P. Nyquist, J. Asmussen Jr. and W. Benenson, for their time and interest in this research.

Finally, the author especially wishes to thank his wife, Hsin-huei, for her typing and proofreading the manuscript, as well as for her encouragement throughout the major part of his graduate study.

The research reported in this thesis was supported by the National Science Foundation under Grant GK-2952.

TABLE OF CONTENTS

LIST OF FIGURES

CHAPTER 1

INTRODUCTION

The electromagnetic scattering of the object surrounded by or immersed in a plasma medium has been a subject received a great deal of attention from researchers in recent years. The interest was motivated by the problems of electromagnetic wave propagation in the ionosphere, the electromagnetic reflection from meteor trails and the radar reflection from a re-entry vehicle.

This dissertation deals with the electromagnetic scattering from a plasma-coated metallic cylinder and some other related subjects. Similar problems have been considered by other researchers. In 1952, Kaiser and Closs[1] studied the electromagnetic reflections from meteor trails. In 1955, Keitel[2] investigated the forward electromagnetic scatterings by meteor trails. Later, a number of investigators including Ohba,[3] Chen and Cheng[4] and Yeh and Rusch,[5] have studied the electromagnetic scattering from a plasma-coated metallic cylinder. Many other workers have studied the related problem and will be cited later. Most of previous workers, however, assumed the plasma medium as a dielectric with an equivalent dielectric constant or using so called cold plasma model. It is well known that if the temperature effect of the plasma is not ignored, an electroacoustic wave in addition to an electromagnetic wave can be excited in the plasma medium. This electroacoustic wave may have significant

effects on the electromagnetic scattering from a plasma-coated object. For this reason, both the cold plasma and hot plasma models are used to analyze the plasma surrounding the object.

Since the plasma layer which surrounds an object is usually inhomogeneous, a certain density distribution is assumed for the plasma medium in the analysis. To solve the problem of propogation of waves in an inhomogeneous medium, the stratification method is used. The plasma layer is divided into a number of thin sublayers and a step function approximation is used to describe the density distribution of the plasma medium. In the course of applying the stratification method a difficulty was encountered which led to a series of numerical singularities. These singularities or "mathematical resonances" bear no physical meanings and were carefully handled in the analysis.

Throughout this study, the macroscopic approach which uses the hydrodynamic equations instead of the Boltzmann equation is used to describe the dynamic behaviors of the plasma. The problem was solved based on the hydrodynamic equations and Maxwell's equations.

In Chapter 2, the electromagnetic scattering from a plasma-coated cylinder illuminated by a plane wave with the $\vec{E}$ field perpendicular to the cylinder is studied based on the cold plasma model. The plasma layer surrounding the cylinder is assumed to be inhomogeneous.

The same problem is treated in Chapter 3, but based on a much more complicated hot plasma model. Effects of the electroacoustic wave are studied.

In Chapter 4, the same plasma-coated cylinder is assumed to be illuminated by a plane wave with the $\vec{E}$ field in parallel with the

cylinder. Under this illumination, it is shown that no electro-acoustic wave can be excited in the plasma layer.

An experimental study on the subject is described in Chapter 5. Experimental results agree qualitatively with the theoretical results obtained in Chapters 2, 3, and 4.

CHAPTER 2

SCATTERING FROM A METALLIC CYLINDER SURROUNDED BY A LAYER OF LOSSY, COLD PLASMA ILLUMINATED BY A TE WAVE

2.1 Introduction

The scattering of an electromagnetic wave by a plasma-coated metallic cylinder when it is illuminated by a normally incident plane wave with its $\vec{H}$ field parallel to the cylinder axis is studied in this chapter. In the analysis, the plasma is assumed to be cold and non-uniform. Also an equivalent permittivity and a collision frequency are assigned to describe the characteristics of the plasma.

A number of workers have studied this problem. Tang[6] studied the backscattering from an infinite cylindrical obstacle coated by a homogeneous dielectric. In treating the reflection from meteor trails Kaiser and Closs[1] considered a meteor trail as a plasma cylinder which was then treated as a lossless dielectric column. Ohba[3] and Chen[4] studied the scattering from an anisotropic and uniform cylinder and considered the plasma as a medium with an equivalent tensor permittivity in the presence of a steady magnetic field. Vandenplas[7] also studied the same problem but treated the plasma as a medium with a equivalent complex permittivity taking into account of the collision loss in the plasma. Yeh and Rusch[5] studied the scattering from an inhomogeneous plasma cylinder with a differential equation method. Fong[8] calculated briefly the radar cross section of a plasma-coated

metallic cylinder by the stratification method.

In this chapter the temperature effect of the plasma is neglected. Due to the existence of a static potential on the metallic cylinder and other boundaries the density distribution of the plasma is assumed to be inhomogeneous. The stratification method is used in the analysis. The inhomogeneous plasma layer is subdivided into a number of concentric sublayers of sufficiently small thickness compared with the electromagnetic wave length. The plasma density is assumed to be constant in each sublayer so that a step function approximation for the density profile is adopted. The wave equation is, then, solved in each sublayer resulting in two cylindrical waves with unknown magnitudes and propagating in opposite directions. The magnitudes of waves are determined by matching the boundary conditions at the interface of two ajacent sublayers. This boundary matching process will lead to the final determination of the scattered fields in space.

To compare with experimental results, a glass wall is assumed to surround the plasma in theoretical model.

2.2 Geometry of the Problem

An infinitely long metallic cylinder with a radius a and covered by a layer of non-uniform cold plasma is confined in a glass tube with inner radius b and outer radius c. This plasma-coated cylinder is placed along the z axis and is illuminated normally by a plane electromagnetic wave with its $\vec{E}$ field perpendicular to the z axis and $\vec{H}$ field parallel to the z axis (TE wave). The layer of non-uniform cold plasma is subdivided into a number of sublayers as shown in Fig 2.1 for the analysis. These sublayers are counted from outmost sublayer and

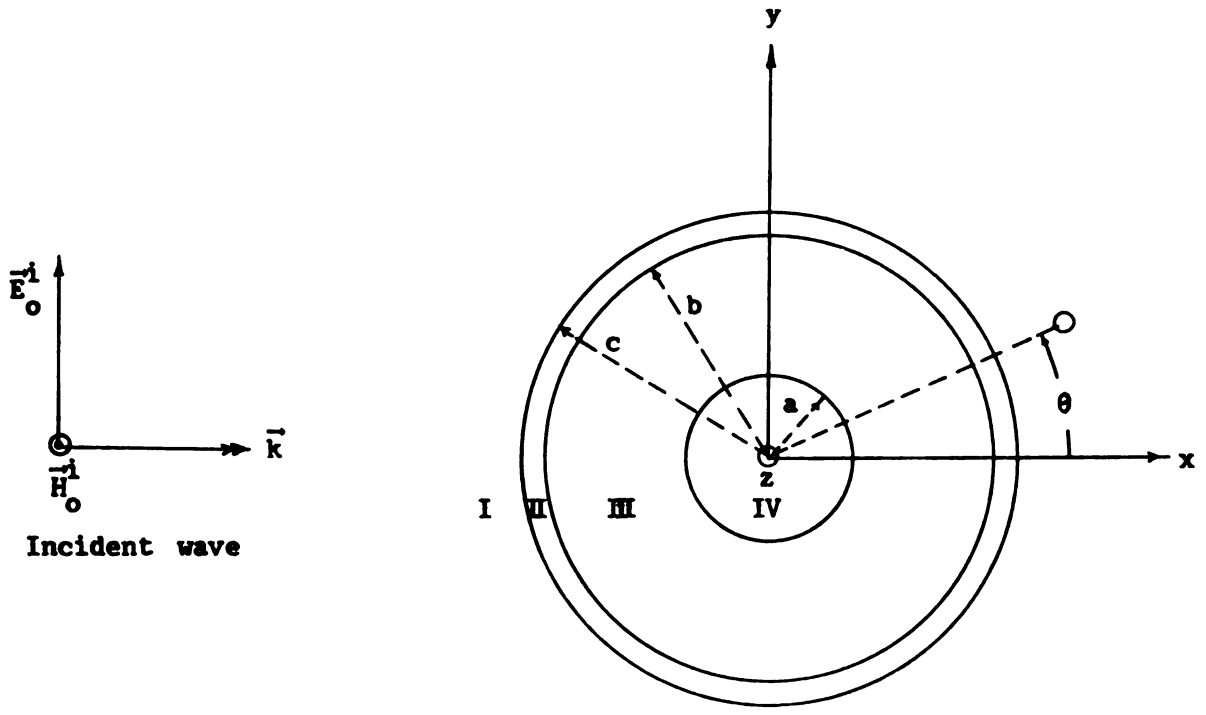

Region I: free space

Region II: glass wall

Region III: cold plasma

Region IV: metallic cylinder

Fig. 2.1.(a) A plasma-coated metallic cylinder illuminated by a TE wave from the left. (cold plasma model)

inwardly. For example, the first sublayer is located immediately inside the glass wall and the last sublayer is located immediately outside the metallic cylinder. The radius between two adjacent mth and (m+1)th sublayers is denoted as r_m. In the mth sublayer, we assume that the plasma density is $n_{o,m}$, the collision frequency is ν_m, the propagation constant is $k_{e,m}$ and the equivalent complex permittivity is ξ_m.

The cylinder is assumed to be infinitely long in the analysis so that there is no field variation along the z direction. The angle θ in the cylindrical coordinates starts from the x axis and increases in the counter clockwise direction. The time dependence of $\exp(j\omega t)$ is assumed and the field of incident plane wave are given by[9]

$$H_{oz}^{i} = e^{-jk_o x} = e^{-jk_o r\cos\theta}$$

$$= \sum_{n=o}^{\infty} \epsilon_{on}(-j)^n \cos(n\theta)\, J_n(k_o r) \qquad (2.1)$$

$$H_{or}^{i} = H_{o\theta}^{i} = 0 \qquad (2.2)$$

$$E_{or}^{i} = -\frac{j}{\omega\epsilon_o r}\frac{\partial}{\partial\theta} H_{oz}^{i}$$

$$= \frac{j}{\omega\epsilon_o r}\sum_{n=o}^{\infty} \epsilon_{on}(-j)^n n\sin(n\theta)\, J_n(k_o r) \qquad (2.3)$$

$$E_{o\theta}^{i} = \frac{j}{\omega\epsilon_o}\frac{\partial}{\partial r} H_{oz}^{i}$$

$$= j\zeta_o \sum_{n=o}^{\infty} \epsilon_{on}(-j)^n \cos(n\theta)\, J_n'(k_o r) \qquad (2.4)$$

$$E_{oz}^{i} = 0 \quad . \qquad (2.5)$$

In these expressions, the superscript "i" represents incident wave. k_o is the propagation constant of free space and is defined as $k_o = \omega\sqrt{\mu_o \epsilon_o}$. ϵ_{on} is the Neumann factor defined as $\epsilon_{on} = 1$ when n=0 and $\epsilon_{on} = 2$

when $n \neq 0$. $J_n(k_o r)$ is Bessel function of the first kind with integer order n and argument $k_o r$. $J_n'(k_o r)$ is the first derivative of $J_n(k_o r)$. ζ_o is the impedance of free space and is defined as $\zeta_o = \sqrt{\frac{\mu_o}{\epsilon_o}} = 120\pi$ ohms. μ_o and ϵ_o are permeability and permttivity of free space respectively.

2.3 Fields in Free Space Region

In the free space region the Maxwell's equations are

$$\nabla \times \vec{E}_o^s = -j\omega\mu_o \vec{H}_o^s \tag{2.6}$$

$$\nabla \times \vec{H}_o^s = j\omega\epsilon_o \vec{E}_o^s \tag{2.7}$$

where $\vec{E}_o^s$, $\vec{H}_o^s$ are the scattered electric and magnetic fields, and μ_o, ϵ_o are the permeability and permittivity of free space respectively. Due to geometrical symmetry, all fields are symmetrical with respect to the $\theta = 0$ axis.

From Eqs. (2.7) and (2.6) we obtain

$$\nabla \times \nabla \times \vec{H}_o^s = \omega^2 \mu_o \epsilon_o \vec{H}_o^s \ . \tag{2.8}$$

Due to TE polarization of incident electromagnetic plane wave and the geometry of problem, $\vec{E}$ field does not have z component and is independent of z. With these two conditions the lefthand side of Eq. (2.6) reduces to a z component equation as

$$\frac{1}{r}\left[\frac{\partial}{\partial r}(rE_{o\theta}^s) - \frac{\partial E_{or}^s}{\partial \theta}\right]\hat{z} = -j\omega\mu_o \vec{H}_o^s \ . \tag{2.9}$$

Equation (2.9) shows that $\vec{H}_o^s$ is allowed to have z component only. Assuming that $\vec{H}_o^s = H_{oz}^s \hat{z}$, Eq. (2.8) reduces to

$$\frac{\partial^2 H_{oz}^s}{\partial r^2} + \frac{\partial H_{oz}^s}{r\partial r} + \frac{\partial^2 H_{oz}^s}{r^2 \partial \theta^2} + k_o^2 H_{oz}^s = 0 \ . \tag{2.10}$$

Equation (2.10) can be solved by the method of separation of variables. We assume that

$$H_{oz}^{s} = H(r)\,H(\theta) \tag{2.11}$$

where H(r) and H(θ) are functions of r and θ respectively. The substitution of Eq. (2.11) in Eq. (2.10) leads to

$$\frac{r^2}{H(r)}\frac{\partial^2 H(r)}{\partial r^2} + \frac{r}{H(r)}\frac{\partial H(r)}{\partial r} + k_o^2 r^2 = n^2 \tag{2.12}$$

$$\frac{1}{H(\theta)}\frac{\partial^2 H(\theta)}{\partial \theta^2} = n^2 . \tag{2.13}$$

Considering the symmetry of problem and the degeneracy of angle θ, the solution for H(θ) is

$$H(\theta) = \cos(n\theta) \tag{2.14}$$

where n is an integer.

Equation (2.12) can be rearranged to

$$\frac{\partial^2 H(r)}{\partial (k_o r)^2} + \frac{1}{(kr)}\frac{\partial H(r)}{\partial (k_o r)} + \left(1 - \frac{n^2}{(k_o r)^2}\right) H(r) = 0 \tag{2.15}$$

which is a Bessel equation.

The solution to Eq. (2.15) is a Bessel function of order n with an argument of $k_o r$. Because only an outgoing cylindrical wave is expected to exist in the free space, the proper solution for Eq. (2.15) is the second kind of the Hankel function such as

$$H(r) = H_n^{(2)}(k_o r) . \tag{2.16}$$

With Eqs. (2.14) and (2.16), the final solution for H_{oz}^{s} can be written as

$$H_{oz}^{s} = \sum_{n=o}^{\infty} \cos(n\theta)\, H_n^{(2)}(k_o r)\, A_n \tag{2.17}$$

where A_n is a constant to be determined by the boundary conditions.

The corresponding $\vec{E}_o^s$ field can be found from

$$\vec{E}_o^s = \frac{1}{j\omega\epsilon_o} \nabla \times \vec{H}_o^s$$

$$= \frac{1}{j\omega\epsilon_o} \left(\frac{1}{r} \frac{\partial H_{oz}^s}{\partial \theta}\right) \hat{r} - \frac{1}{j\omega\epsilon_o} \left(\frac{\partial H_{oz}^s}{\partial r}\right) \hat{\theta} \tag{2.18}$$

or

$$E_{or}^{s} = \frac{j}{\omega\epsilon_o r} \sum_{n=o}^{\infty} n\sin(n\theta)\, H_n^{(2)}(k_o r)\, A_n \tag{2.19}$$

$$E_{o\theta}^{s} = j\zeta_o \sum_{n=o}^{\infty} \cos(n\theta)\, H_n^{(2)'}(k_o r)\, A_n \tag{2.20}$$

where $\zeta_o = \sqrt{\frac{\mu_o}{\epsilon_o}} = 120\pi$ ohms and $H_n^{(2)'}(k_o r)$ is the first derivative of $H_n^{(2)}(k_o r)$ with respect to $(k_o r)$.

The total fields in the free space region can be obtained by summing the incident and scattered fields to be

$$H_{oz}^{t} = \sum_{n=o}^{\infty} \cos(n\theta) \left[\epsilon_{on}(-j)^n J_n(k_o r) + H_n^{(2)}(k_o r)\, A_n\right] \tag{2.21}$$

$$H_{or}^{t} = H_{o\theta}^{t} = 0 \tag{2.22}$$

$$E_{or}^{t} = \frac{j}{\omega\epsilon_o r} \sum_{n=o}^{\infty} n\sin(n\theta) \left[\epsilon_{on}(-j)^n J_n(k_o r) + H_n^{(2)}(k_o r)\, A_n\right] \tag{2.23}$$

$$E_{o\theta}^{t} = j\zeta_o \sum_{n=o}^{\infty} \cos(n\theta) \left[\epsilon_{on}(-j)^n J_n'(k_o r) + H_n^{(2)'}(k_o r)\, A_n\right] \tag{2.24}$$

$$E_{oz}^{t} = 0 \,. \tag{2.25}$$

2.4 Fields in Glass Wall Region

In the glass wall region the Maxwell's equations are

$$\nabla \times \vec{E}_g = -j\omega\mu_o \vec{H}_g \tag{2.26}$$

$$\nabla \times \vec{H}_g = j\omega \epsilon_o \epsilon_g \vec{E}_g \tag{2.27}$$

where ϵ_g is the dielectric constant of glass.

If we allow an incoming and an outgoing (reflected) waves to exist in the glass wall region, the solution for $\vec{H}_g$ field can be expressed as

$$\vec{H}_g = H_{gz}\hat{z} \tag{2.28}$$

where

$$H_{gz} = \sum_{n=o}^{\infty} \cos(n\theta) \left[H_n^{(1)}(k_g r) B_n + H_n^{(2)}(k_g r) C_n \right] . \tag{2.29}$$

In Eq. (2.29), B_n and C_n are the constants to be determined by the boundary conditions and k_g is propagation constant of glass defined as $k_g = k_o\sqrt{\epsilon_g}$.

The corresponding $\vec{E}_g$ field has components given by

$$E_{gr} = \frac{j}{\omega \epsilon_o \epsilon_g r} \sum_{n=o}^{\infty} n\sin(n\theta) \left[H_n^{(1)}(k_g r) B_n + H_n^{(2)}(k_g r) C_n \right] \tag{2.30}$$

$$E_{g\theta} = \frac{j\zeta_o}{\sqrt{\epsilon_g}} \sum_{n=o}^{\infty} \cos(n\theta) \left[H_n^{(1)'}(k_g r) B_n + H_n^{(2)'}(k_g r) C_n \right] \tag{2.31}$$

$$E_{gz} = 0. \tag{2.32}$$

2.5 Fields in Plasma Region

As mentioned before, the plasma layer is subdivided into a number of concentric sublayers of sufficiently small thickness. The plasma density is then considered to be uniform within each sublayer,

but it varies from sublayer to sublayer in radial direction. In the mth sublayer the plasma medium is considered as a frequency and collision dependent dielectric. The equivalent complex permittivity can be expressed as

$$\xi_m = \epsilon_o \left[\left(1 - \frac{\omega_{p,m}^2}{\omega^2 + \nu_m^2}\right) - \frac{j\omega_{p,m}^2 \nu_m}{\omega(\omega^2 + \nu_m^2)} \right] \tag{2.33}$$

where $\omega_{p,m}$ is the plasma frequency associated with density $n_{o,m}$ in the mth sublayer and is given by

$$\omega_{p,m} = \sqrt{\frac{e^2 n_{o,m}}{M \epsilon_o}} \ . \tag{2.34}$$

e and M are the charge and mass of electrons respectively in Eq. (2.34). Also ν_m is the collision frequency in the mth sublayer.

The field in the mth sublayer of plasma medium can be obtained from the Maxwell's equations,

$$\nabla \times \vec{E}_m = -j\omega\mu_o \vec{H}_m \tag{2.35}$$

$$\nabla \times \vec{H}_m = j\omega\xi_m \vec{E}_m \ . \tag{2.36}$$

The components of $\vec{H}_m$ and $\vec{E}_m$ fields can be expressed as

$$H_{mz} = \sum_{n=o}^{\infty} \cos(n\theta) \left[H_n^{(1)}(k_{e,m} r) D_{m,n} + H_n^{(2)}(k_{e,m} r) F_{m,n} \right] \tag{2.37}$$

$$H_{mr} = H_{m\theta} = 0 \tag{2.38}$$

$$E_{mr} = \frac{j}{\omega \xi_m r} \sum_{n=o}^{\infty} n\sin(n\theta) \left[H_n^{(1)}(k_{e,m} r) D_{m,n} + H_n^{(2)}(k_{e,m} r) F_{m,n} \right] \tag{2.39}$$

$$E_{m\theta} = j\sqrt{\frac{\mu_o}{\xi_m}} \sum_{n=o}^{\infty} \cos(n\theta) \left[H_n^{(1)'}(k_{e,m} r) D_{m,n} + H_n^{(2)'}(k_{e,m} r) F_{m,n} \right] \tag{2.40}$$

$$E_{mz} = 0 \tag{2.41}$$

where $D_{m,n}$ and $F_{m,n}$ are constants to be determined by boundary conditions

and $k_{e,m}$ is the propagation constant in the mth sublayer of the plasma layer and is given by

$$k_{e,m} = \omega\sqrt{\mu_o \xi_m} \ . \tag{2.42}$$

If we denote $k_{e,m}$ as

$$k_{e,m} = \beta_{e,m} - j\alpha_{e,m} \tag{2.43}$$

and after substituting ξ_m with Eq. (2.33), $\beta_{e,m}$ and $\alpha_{e,m}$ can be expressed as

$$\beta_{e,m} = \frac{\beta_o}{\sqrt{2}}\left\{ 1 - \frac{\omega_{p,m}^2}{\omega^2+\nu_m^2} + \left[1 - \frac{2\omega_{p,m}^2}{\omega^2+\nu_m^2} + \frac{\omega_{p,m}^4}{\omega^2(\omega^2+\nu_m^2)} \right]^{\frac{1}{2}} \right\}^{\frac{1}{2}} \tag{2.44}$$

$$\alpha_{e,m} = \frac{\beta_o}{\sqrt{2}}\left\{ -1 + \frac{\omega_{p,m}^2}{\omega^2+\nu_m^2} + \left[1 - \frac{2\omega_{p,m}^2}{\omega^2+\nu_m^2} + \frac{\omega_{p,m}^4}{\omega^2(\omega^2+\nu_m^2)} \right]^{\frac{1}{2}} \right\}^{\frac{1}{2}} \tag{2.45}$$

with

$$\beta_o = \omega\sqrt{\mu_o \epsilon_o} \ . \tag{2.46}$$

Up to this point, the fields in the mth sublayer have been solved. Similarly, the solutions of the fields in the other sublayers will have the same forms as that in the mth sublayer with appropriate change in the quantities of k_e, ξ, n_o and ν etc.

2.6 Matching the Boundary Conditions at Interfaces

In the solutions for $\vec{E}_m$ and $\vec{H}_m$ obtained in Sec. 2.5, there are two unknown constants to be determined by boundary conditions. In order to express the constants in one sublayer in terms of the constants of its adjacent sublayer, it is necessary to have two boundary conditions at the

interface of these two sublayers. Consider the boundary at $r = r_m$ between the mth and the (m+1)th sublayers (refer to Fig. 2.1). The boundary conditions at this interface are the continuity of tangential components of $\vec{E}$ and $\vec{H}$ fields. In symbols,

$$H_{mz} = H_{(m+1)z} \qquad \text{at } r = r_m \tag{2.47}$$

$$E_{m\theta} = E_{(m+1)\theta} \qquad \text{at } r = r_m \tag{2.48}$$

or

$$\sum_{n=o}^{\infty} \cos(n\theta)\left[H_n^{(1)}(k_{e,m}\, r_m)\, D_{m,n} + H_n^{(2)}(k_{e,m}\, r_m)\, F_{m,n}\right]$$

$$= \sum_{n=o}^{\infty} \cos(n\theta)\left[H_n^{(1)}(k_{e,m+1}\, r_m)\, D_{m+1,n} + H_n^{(2)}(k_{e,m+1}\, r_m) F_{m+1,n}\right] \tag{2.49}$$

and

$$j\sqrt{\frac{\mu_o}{\xi_m}} \sum_{n=o}^{\infty} \cos(n\theta)\left[H_n^{(1)'}(k_{e,m}\, r_m)\, D_{m,n} + H_n^{(2)'}(k_{e,m}\, r_m)\, F_{m,n}\right]$$

$$= j\sqrt{\frac{\mu_o}{\xi_{m+1}}} \sum_{n=o}^{\infty} \cos(n\theta)\left[H_n^{(1)'}(k_{e,m+1}\, r_m)\, D_{m+1,n} + H_n^{(2)'}(k_{e,m+1}\, r_m) F_{m+1,n}\right]. \tag{2.50}$$

Due to the orthogonality of $\cos(n\theta)$ functions, Eqs. (2.49) and (2.50) lead to the following matrix equation

$$\begin{bmatrix} H_n^{(1)}(k_{e,m}\, r_m) & H_n^{(2)}(k_{e,m}\, r_m) \\ \sqrt{\frac{1}{\xi_m}}\, H_n^{(1)'}(k_{e,m}\, r_m) & \sqrt{\frac{1}{\xi_m}}\, H_n^{(2)'}(k_{e,m}\, r_m) \end{bmatrix} \begin{bmatrix} D_{m,n} \\ F_{m,n} \end{bmatrix}$$

$$= \begin{bmatrix} H_n^{(1)}(k_{e,m+1}r_m) & H_n^{(2)}(k_{e,m+1}r_m) \\ \sqrt{\frac{1}{\xi_{m+1}}}\, H_n^{(1)'}(k_{e,m+1}r_m) & \sqrt{\frac{1}{\xi_{m+1}}}\, H_n^{(2)'}(k_{e,m+1}r_m) \end{bmatrix} \begin{bmatrix} D_{m+1,n} \\ F_{m+1,n} \end{bmatrix} . \tag{2.51}$$

Equation (2.51) gives

$$\begin{bmatrix} D_{m,n} \\ F_{m,n} \end{bmatrix} = \begin{bmatrix} H_n^{(1)}(k_{e,m}r_m) & H_n^{(2)}(k_{e,m}r_m) \\ \sqrt{\frac{1}{\xi_m}}\, H_n^{(1)'}(k_{e,m}r_m) & \sqrt{\frac{1}{\xi_m}}\, H_n^{(2)'}(k_{e,m}r_m) \end{bmatrix}^{-1}$$

$$\begin{bmatrix} H_n^{(1)}(k_{e,m+1}r_m) & H_n^{(2)}(k_{e,m+1}r_m) \\ \sqrt{\frac{1}{\xi_{m+1}}}\, H_n^{(1)'}(k_{e,m+1}r_m) & \sqrt{\frac{1}{\xi_{m+1}}}\, H_n^{(2)'}(k_{e,m+1}r_m) \end{bmatrix} \begin{bmatrix} D_{m+1,n} \\ F_{m+1,n} \end{bmatrix} . \tag{2.52}$$

We can write Eq. (2.52) as

$$\begin{bmatrix} D_{m,n} \\ F_{m,n} \end{bmatrix} = \left[L_n(k_{e,m}r_m)\right]^{-1} \left[L_n(k_{e,m+1}r_m)\right] \begin{bmatrix} D_{m+1,n} \\ F_{m+1,n} \end{bmatrix} \tag{2.53}$$

where

$$\left[L_n(k_{e,m}r_m)\right] = \begin{bmatrix} H_n^{(1)}(k_{e,m}r_m) & H_n^{(2)}(k_{e,m}r_m) \\ \sqrt{\frac{1}{\xi_m}}\, H_n^{(1)'}(k_{e,m}r_m) & \sqrt{\frac{1}{\xi_m}}\, H_n^{(2)'}(k_{e,m}r_m) \end{bmatrix} . \tag{2.54}$$

Similarly at the interface of $r = r_{m+1}$ we have

$$\begin{bmatrix} D_{m+1,n} \\ F_{m+1,n} \end{bmatrix} = \left[L_n(k_{e,m+1}r_{m+1})\right]^{-1} \left[L_n(k_{e,m+2}r_{m+1})\right] \begin{bmatrix} D_{m+2,n} \\ F_{m+2,n} \end{bmatrix} \tag{2.55}$$

Thus, combining Eqs. (2.53) and (2.55), the constants $D_{m,n}$ and $F_{m,n}$ in the mth sublayer can be expressed in terms of the constants $D_{m+2,n}$ and $F_{m+2,n}$ in the (m+2)th sublayer as

$$\begin{bmatrix} D_{m,n} \\ F_{m,n} \end{bmatrix} = \left[L_n(k_{e,m}r_m)\right]^{-1}\left[L_n(k_{e,m+1}r_m)\right] \left[L_n(k_{e,m+1}r_{m+1})\right]^{-1}\left[L_n(k_{e,m+2}r_{m+1})\right] \begin{bmatrix} D_{m+2,n} \\ F_{m+2,n} \end{bmatrix} . \tag{2.56}$$

By carrying out the successive operation of Eq. (2.56) to cover all the interfaces, the constants of the outmost sublayer can be expressed in terms of that of the inmost sublayer as follows:

$$\begin{bmatrix} D_{1,n} \\ F_{1,n} \end{bmatrix} = \left[L_n(k_{e,1}r_1)\right]^{-1}\left[L_n(k_{e,2}r_1)\right]\left[L_n(k_{e,2}r_2)\right]^{-1}\left[L_n(k_{e,3}r_2)\right]\cdots \cdot\cdot\left[L_n(k_{e,s-1}r_{s-1})\right]^{-1}\left[L_n(k_{e,s}r_{s-1})\right] \begin{bmatrix} D_{s,n} \\ F_{s,n} \end{bmatrix} \tag{2.57}$$

where the sth sublayer is the inmost sublayer. Equation (2.57) can be expressed in shorthand as

$$\begin{bmatrix} D_{1,n} \\ F_{1,n} \end{bmatrix} = \begin{bmatrix} M_n(1,1) & M_n(1,2) \\ M_n(2,1) & M_n(2,2) \end{bmatrix} \begin{bmatrix} D_{s,n} \\ F_{s,n} \end{bmatrix} \tag{2.58}$$

where $M_n(i,j)$'s are the entries of the matrix which is the product of those $[L_n]$ matrices in Eq. (2.57).

Let's now consider the interface between free space and glass wall at r = c. The tangential components of $\vec{E}$ and $\vec{H}$ fields are continuous

at this interface. This leads to

$$H_{oz}^{t} = H_{gz} \qquad \text{at } r = c \tag{2.59}$$

$$E_{o\theta}^{t} = E_{g\theta} \qquad \text{at } r = c \tag{2.60}$$

where H_{oz}^{t} and $E_{o\theta}^{t}$ are given in Eqs. (2.21) and (2.24) respectively and H_{gz} and $E_{g\theta}$ are given in Eqs. (2.29) and (2.31) respectively. With Eqs. (2.21), (2.24), (2.29) and (2.31), Eqs. (2.59) and (2.60) lead to

$$- H_n^{(2)}(k_o c)\, A_n + H_n^{(1)}(k_g c)\, B_n + H_n^{(2)}(k_g c)\, C_n = \epsilon_{on}(-j)^n J_n(k_o c) \tag{2.61}$$

$$- H_n^{(2)'}(k_o c)\, A_n + \frac{1}{\sqrt{\epsilon_g}} H_n^{(1)'}(k_g c)\, B_n + \frac{1}{\sqrt{\epsilon_g}} H_n^{(2)'}(k_g c)\, C_n = \epsilon_{on}(-j)^n J_n'(k_o c). \tag{2.62}$$

We consider next the interface between the glass wall and the first sublayer of plasma at $r = b$. The continuity of the tangential components of $\vec{E}$ and $\vec{H}$ fields leads to

$$- H_n^{(1)}(k_g b)\, B_n - H_n^{(2)}(k_g b)\, C_n + H_n^{(1)}(k_{e,1} b)\, D_{1,n} + H_n^{(2)}(k_{e,1} b)\, F_{1,n} = 0 \tag{2.63}$$

$$- \frac{1}{\sqrt{\epsilon_g}} H_n^{(1)'}(k_g b)\, B_n - \frac{1}{\sqrt{\epsilon_g}} H_n^{(2)'}(k_g b)\, C_n + \sqrt{\frac{\epsilon_o}{\xi_1}} H_n^{(1)'}(k_{e,1} b)\, D_{1,n} + \sqrt{\frac{\epsilon_o}{\xi_1}} H_n^{(2)'}(k_{e,1} b)\, F_{1,n} = 0. \tag{2.64}$$

Expressing $D_{1,n}$, $F_{1,n}$ in terms of $D_{s,n}$, $F_{s,n}$ by Eq. (2.58), Eqs. (2.63) and (2.64) lead to

$$- H_n^{(1)}(k_g b)\, B_n - H_n^{(2)}(k_g b)\, C_n + \left[R_n(1)\right] D_{s,n} + \left[R_n(2)\right] F_{s,n} = 0 \tag{2.65}$$

and

$$- \frac{1}{\sqrt{\epsilon_g}} H_n^{(1)'}(k_g b)\, B_n - \frac{1}{\sqrt{\epsilon_g}} H_n^{(2)'}(k_g b)\, C_n + \left[R_n(3)\right] D_{s,n} + \left[R_n(4)\right] F_{s,n} = 0 \tag{2.66}$$

where

$$R_n(1) = H_n^{(1)}(k_{e,1} b)\, M_n(1,1) + H_n^{(2)}(k_{e,1} b)\, M_n(2,1) \tag{2.67}$$

$$R_n(2) = H_n^{(1)}(k_{e,1} b)\, M_n(1,2) + H_n^{(2)}(k_{e,1} b)\, M_n(2,2) \tag{2.68}$$

$$R_n(3) = \sqrt{\frac{\epsilon_0}{\xi_1}}\, H_n^{(1)'}(k_{e,1} b)\, M_n(1,1) + \sqrt{\frac{\epsilon_0}{\xi_1}}\, H_n^{(2)'}(k_{e,1} b)\, M_n(2,1) \tag{2.69}$$

$$R_n(4) = \sqrt{\frac{\epsilon_0}{\xi_1}}\, H_n^{(1)'}(k_{e,1} b)\, M_n(1,2) + \sqrt{\frac{\epsilon_0}{\xi_1}}\, H_n^{(2)'}(k_{e,1} b)\, M_n(2,2) \,. \tag{2.70}$$

Finally, we consider the interface on the metallic cylinder surface at $r = a$. If the cylinder is assumed to be a perfect conductor, the tangential component of the $\vec{E}$ field at its surface vanishes. That is

$$E_{s\theta} = 0 \qquad \text{at } r = a \,. \tag{2.71}$$

This leads to

$$H_n^{(1)'}(k_{e,s} a)\, D_{s,n} + H_n^{(2)'}(k_{e,s} a)\, F_{s,n} = 0 \,. \tag{2.72}$$

Equations (2.61), (2.62), (2.65), (2.66) and (2.72) can be represented in a matrix equation as

$$\begin{bmatrix} Q_n(1,1) & Q_n(1,2) & Q_n(1,3) & 0 & 0 \\ Q_n(2,1) & Q_n(2,2) & Q_n(2,3) & 0 & 0 \\ 0 & Q_n(3,2) & Q_n(3,3) & Q_n(3,4) & Q_n(3,5) \\ 0 & Q_n(4,2) & Q_n(4,3) & Q_n(4,4) & Q_n(4,5) \\ 0 & 0 & 0 & Q_n(5,4) & Q_n(5,5) \end{bmatrix} \begin{bmatrix} A_n \\ B_n \\ C_n \\ D_{s,n} \\ F_{s,n} \end{bmatrix} = \begin{bmatrix} Q_n(1,6) \\ Q_n(2,6) \\ 0 \\ 0 \\ 0 \end{bmatrix} \tag{2.73}$$

where

$$Q_n(1,1) = -H_n^{(2)}(k_o c) \tag{2.74}$$

$$Q_n(1,2) = H_n^{(1)}(k_g c) \tag{2.75}$$

$$Q_n(1,3) = H_n^{(2)}(k_g c) \tag{2.76}$$

$$Q_n(1,6) = \epsilon_{on}(-j)^n J_n(k_o c) \tag{2.77}$$

$$Q_n(2,1) = -H_n^{(2)'}(k_o c) \tag{2.78}$$

$$Q_n(2,2) = \frac{1}{\sqrt{\epsilon_g}} H_n^{(1)'}(k_g c) \tag{2.79}$$

$$Q_n(2,3) = \frac{1}{\sqrt{\epsilon_g}} H_n^{(2)'}(k_g c) \tag{2.80}$$

$$Q_n(2,6) = \epsilon_{on}(-j)^n J_n'(k_o c) \tag{2.81}$$

$$Q_n(3,2) = -H_n^{(1)}(k_g b) \tag{2.82}$$

$$Q_n(3,3) = -H_n^{(2)}(k_g b) \tag{2.83}$$

$$Q_n(3,4) = H_n^{(1)}(k_{e,1} b)\, M_n(1,1) + H_n^{(2)}(k_{e,1} b)\, M_n(2,1) \tag{2.84}$$

$$Q_n(3,5) = H_n^{(1)}(k_{e,1} b)\, M_n(1,2) + H_n^{(2)}(k_{e,1} b)\, M_n(2,2) \tag{2.85}$$

$$Q_n(4,2) = -\frac{1}{\sqrt{\epsilon_g}} H_n^{(1)'}(k_g b) \tag{2.86}$$

$$Q_n(4,3) = -\frac{1}{\sqrt{\epsilon_g}} H_n^{(2)'}(k_g b) \tag{2.87}$$

$$Q_n(4,4) = \sqrt{\frac{\epsilon_o}{\xi_1}} H_n^{(1)'}(k_{e,1} b)\, M_n(1,1) + \sqrt{\frac{\epsilon_o}{\xi_1}} H_n^{(2)'}(k_{e,1} b)\, M_n(2,1) \tag{2.88}$$

$$Q_n(4,5) = \sqrt{\frac{\epsilon_o}{\xi_1}} H_n^{(1)'}(k_{e,1} b)\, M_n(1,2) + \sqrt{\frac{\epsilon_o}{\xi_1}} H_n^{(2)'}(k_{e,1} b)\, M_n(2,2) \tag{2.89}$$

$$Q_n(5,4) = H_n^{(1)'}(k_{e,s} a) \tag{2.90}$$

$$Q_n(5,5) = H_n^{(2)'}(k_{e,s} a)\,. \tag{2.91}$$

2.7 Scattered Field in Free Space Region

The constant A_n is of main interest and can be obtained from Eq. (2.73) by Cramer's Rule as

$$A_n = \frac{\Delta_{n1}}{\Delta_n}\,. \tag{2.92}$$

Two determinants, Δ_n and Δ_{n1}, are given as

$$\Delta_n = \begin{vmatrix} Q_n(1,1) & Q_n(1,2) & Q_n(1,3) & 0 & 0 \\ Q_n(2,1) & Q_n(2,2) & Q_n(2,3) & 0 & 0 \\ 0 & Q_n(3,2) & Q_n(3,3) & Q_n(3,4) & Q_n(3,5) \\ 0 & Q_n(4,2) & Q_n(4,3) & Q_n(4,4) & Q_n(4,5) \\ 0 & 0 & 0 & Q_n(5,4) & Q_n(5,5) \end{vmatrix} \tag{2.93}$$

and

$$\Delta_{n1} = \begin{vmatrix} Q_n(1,6) & Q_n(1,2) & Q_n(1,3) & 0 & 0 \\ Q_n(2,6) & Q_n(2,2) & Q_n(2,3) & 0 & 0 \\ 0 & Q_n(3,2) & Q_n(3,3) & Q_n(3,4) & Q_n(3,5) \\ 0 & Q_n(4,2) & Q_n(4,3) & Q_n(4,4) & Q_n(4,5) \\ 0 & 0 & 0 & Q_n(5,4) & Q_n(5,5) \end{vmatrix} . \tag{2.94}$$

Finally, the scattered fields in free space region are obtained as

$$H_{oz}^s = \sum_{n=o}^{\infty} \cos(n\theta)\, H_n^{(2)}(k_o r)\, A_n \tag{2.95}$$

$$H_{or}^s = H_{o\theta}^s = 0 \tag{2.96}$$

$$E_{or}^s = \frac{j}{\omega \epsilon_o r} \sum_{n=o}^{\infty} n\sin(n\theta)\, H_n^{(2)}(k_o r)\, A_n \tag{2.97}$$

$$E_{o\theta}^s = j\zeta_o \sum_{n=o}^{\infty} \cos(n\theta)\, H_n^{(2)'}(k_o r)\, A_n \tag{2.98}$$

$$E_{oz}^s = 0 \tag{2.99}$$

with A_n expressed as Eq. (2.92).

For the scattered fields observed at a large distance, Hankel function can be expressed in its asymptotic form as

$$H_n^{(2)}(k_o r) \approx \sqrt{\frac{2}{\pi k_o r}}\, e^{-j(k_o r - \frac{1}{2}n\pi - \frac{1}{4}\pi)} . \tag{2.100}$$

And the scattered fields at a large distance are then obtained as

$$H_{oz}^s = \sqrt{\frac{2}{\pi k_o r}}\, e^{-j(k_o r - \frac{1}{4}\pi)} \sum_{n=o}^{\infty} \cos(n\theta)\, e^{j\frac{1}{2}n\pi} A_n \tag{2.101}$$

$$H_{or}^s = H_{o\theta}^s = 0 \tag{2.102}$$

$$E_{or}^s = j\sqrt{\frac{2}{\pi k_o r}}\, \frac{1}{\omega \epsilon_o r}\, e^{-j(k_o r - \frac{1}{4}\pi)} \sum_{n=o}^{\infty} n\sin(n\theta)\, e^{j\frac{1}{2}n\pi} A_n$$

$$\doteq 0 \tag{2.103}$$

$$E_{o\theta}^{s} = j\zeta_o\sqrt{\frac{2}{\pi k_o r}}\sum_{n=o}^{\infty}\cos(n\theta)\left[-e^{-j(k_o r - \frac{1}{2}(n+1)\pi - \frac{1}{4}\pi)}\right.$$

$$\left. + \frac{n}{k_o r}e^{-j(k_o r - \frac{1}{2}n\pi - \frac{1}{4}\pi)}\right]A_n$$

$$\approx \zeta_o\sqrt{\frac{2}{\pi k_o r}}e^{-j(k_o r - \frac{1}{4}\pi)}\sum_{n=o}^{\infty}\cos(n\theta)\,e^{j\frac{1}{2}n\pi}A_n \qquad (2.104)$$

after neglecting the $r^{-\frac{3}{2}}$ term

$$E_{oz}^{s} = 0 \,. \qquad (2.105)$$

To derive Eq. (2.104) the relation of

$$H_n^{(2)'}(k_o r) = -H_{n+1}^{(2)}(k_o r) + \frac{n}{k_o r}H_n^{(2)}(k_o r) \qquad (2.106)$$

is used.

2.8 Some Special Cases

In section 2.6 we have developed a theory and a set of five simultaneous linear equations with five unknowns which can be solved to determine the scattering from a plasma-coated metallic cylinder. We will show that with a slight modification this theory can be used to determine the scatterings by a plain plasma cylinder and by a plasma-coated dielectric cylinder.

2.8.1 The Scattered Field from a Plain Plasma Cylinder

For this case the plasma fills the whole glass tube in the absence of metallic cylinder. If we let the inmost sublayer be the plasma cylinder with an extremely small radius and located along the z axis, the whole plasma cylinder is subdivided into an extremely thin

plasma cylinder at the center and a number of concentric sublayers extended from radius r = 0 to radius r = b up to the glass wall (Refer to Fig. 2.1). Since the Bessel function of the second kind, $Y_n(k_{e,s}r)$, has a singularity at r = 0, the proper solution for the fields in the inmost sublayer or the thin cylinder at the center is the Bessel function of the first kind, $J_n(k_{e,s}r)$, only. This condition can be achieved by setting the constants $D_{s,n}$ and $F_{s,n}$ to be equal, because

$$J_n(k_{e,s}r) = \frac{1}{2}\left[H_n^{(1)}(k_{e,s}r) + H_n^{(2)}(k_{e,s}r)\right] . \tag{2.107}$$

Thus for a plain plasma cylinder, the simultaneous equations are Eqs. (2.61), (2.62), (2.65), (2.66) and the following equation:

$$D_{s,n} - F_{s,n} = 0 . \tag{2.108}$$

With this set of equations A_n can be solved and consequently the scattered field.

2.8.2 The Scattered Field from a Plasma-Coated Dielectric Cylinder

In this case a dielectric cylinder instead of a metallic cylinder is located in the center of the plasma column. The tangential component of $\vec{E}$ field will not vanish on the surface of the dielectric cylinder. Due to the singularity of the Bessel function of the second kind, the proper solution for the $\vec{H}$ field in the dielectric cylinder is

$$\vec{H}_d = H_{dz}\,\hat{z} = \sum_{n=0}^{\infty} \cos(n\theta)\, J_n(k_d r)\, G_n\, \hat{z} \tag{2.109}$$

where subscript d implies the dielectric regon. G_n is a constant to be determined by boundary conditions. k_d is the propagation constant of the dielectric cylinder and is given by

$$k_d = \omega\sqrt{\mu_o \epsilon_o \epsilon_d} \tag{2.110}$$

where ϵ_d is the dielectric constant of the dielectric cylinder.

The corresponding $\vec{E}$ field can be obtained from a Maxwell's equation,

$$\vec{E}_d = \frac{1}{j\omega\epsilon_o\epsilon_d} \nabla \times \vec{H} \ , \tag{2.111}$$

to yield the following components

$$E_{dr} = \frac{j}{\omega\epsilon_o\epsilon_d r} \sum_{n=o}^{\infty} n\sin(n\theta)\, J_n(k_d r)\, G_n \tag{2.112}$$

$$E_{d\theta} = \frac{j\zeta_o}{\sqrt{\epsilon_d}} \sum_{n=o}^{\infty} \cos(n\theta)\, J_n'(k_d r)\, G_n \tag{2.113}$$

$$E_{dz} = 0 \ . \tag{2.114}$$

The boundary conditions at the interface between the plasma region and dielectric cylinder are the continuity of the tangential components of $\vec{E}$ and $\vec{H}$ fields. These boundary conditions lead to

$$- H_n^{(1)}(k_{e,s}a)\, D_{s,n} - H_n^{(2)}(k_{e,s}a)\, F_{s,n} + J_n(k_{e,d}a)\, G_n = 0 \tag{2.115}$$

and

$$-\sqrt{\frac{\epsilon_o}{\xi_s}}\, H_n^{(1)'}(k_{e,s}a)\, D_{s,n} - \sqrt{\frac{\epsilon_o}{\xi_s}}\, H_n^{(2)'}(k_{e,s}a)\, F_{s,n} + \frac{1}{\sqrt{\epsilon_d}}\, J_n'(k_{e,d}a)\, G_n = 0 \ . \tag{2.116}$$

With this modification, Eqs. (2.61), (2.62), (2.65), (2.66), (2.115) and (2.116) form a set of six simultaneous linear equations with six unknowns which can be solved to determine the scattered fields.

2.9 Numerical Results

The back scattered E fields from a plasma-coated metallic cylinder, a plain plasma cylinder and a plasma-coated dielectric cylinder have been calculated as a function of $(\omega_p/\omega)^2$. Although in the development of theory the collision frequency ν is treated as a variable, in our numerical calculation ν is assumed to be a constant for all sublayers for simplicity. For a laboratory plasma the ionization degree is very low and the electron-neutral particle collision usually is the predominant effect. Even though the electron density of the plasma may be non-uniform, the density of neutral particles can be uniform in the plasma. Thus the assumption of a constant collision frequency in a non-uniform plasma may be reasonable. The series solution is produced by summing up the first four terms only (up to n=3). The accuracy of the numerical results based on four-term summation is quite satisfactory since these results deviate less than one percent from the numerical results based on ten-term summation. The scattered fields are calculated at a distance from the z axis with $k_o r = 10$ for convenience. And these fields are plotted in figures with its normalized value, E_o^s/E_o^i where E_o^s and E_o^i are the scattered and incident fields respectively. From Fig. 2.2 through Fig. 2.6, the dimensions for the glass tube, plasma layer and central cylindrical conductor are based on the actual dimensions of the experimental model. Those dimensions, dielectric constant of glass and the operating frequency are given in Table 2.1.

Operating frequency	a (mm)	b (mm)	c (mm)	ϵ_g
f = 2.3 GHz	2.158	7	8	5

Table 2.1 Physical dimensions of plasma tube, dielectric constant of glass and operating frequency.

Figure 2.2 shows the back scattered E field in the direction of $\theta = 180^{o}$ as a function of $(\omega_p/\omega)^2$ for various collision frequencies for the case of a uniform density distribution in the plasma region ($b \geq r \geq a$). The main resonance occured at $(\omega_p/\omega)^2 = 2.58$ is the so called the dipolar resonance which corresponds to the resonance due to the n = 1 term of the series solution. The sharp peak at the right main resonance is the quadrupolar resonance.[10,7] The hexapolar resonance or n=3 resonance does not appear in the figure although the resonance does occur at a higher value of $(\omega_p/\omega)^2$. It is observed in Fig. 2.2 that when collision frequency is increased to a value of the order of $\nu/\omega = 0.5$ no resonance appears any longer. Also the quadrupolar resonance seems to be damped out by the collision more strongly than the dipolar resonance.

Figure 2.3 is a plot of the determinant Δ_n given by Eq. (2.93) for various values of n as a function of $(\omega_p/\omega)^2$. Because of rapid convergence of the series, the terms with $n \geq 4$ are neglected. The real and imaginary parts of the determinant are calculated separately. The determinant is plotted for the region of $1 < (\omega_p/\omega)^2 \leq 5$ only to show the locations of resonances. Figure 2.3.1 shows the smooth behavior of the n=0 term of the series. In Fig. 2.3.2, the point of rapid sign change of the real part of the determinant for n=1 occurs at $(\omega_p/\omega)^2 = 2.58$ and it corresponds to the dipolar resonance. A similar behavior of rapid sign change of the determinant for n=2 case is shown in Fig. 2.3.3 and this point of rapid sign change corresponds to the quadrupolar resonance. In Fig. 2.3.4 although the hexapolar (n=3) resonance is clearly seen, due to an extremely small value of

A_3 compared with A_o, A_1 and A_2, the effect of hexapolar resonance is not detectable in the scattered field as shown in Fig. 2.2.

Figure 2.4 shows the effect of the dielectric constant of the glass tube. Three curves of back scattered E field are plotted for the glass tube with dielectric constants of $\epsilon_g = 1$, 2.5 and 5. The case of $\epsilon_g = 1$ is equivalent to the absence of the glass tube. It is observed that as the dielectric constant of glass tube is increased the location of the dipolar resonance shifts to a higher value of $(\omega_p/\omega)^2$ and the separation between the dipolar and quadrupolar resonances becomes greater. These three curves are plotted with an assumption of a collision frequency of $\nu/\omega = 0.001$ and an operating frequency of 2.3 GHz.

Figures 2.5 and 2.6 show the back scattered E field from a metallic cylinder covered by a layer of non-uniform plasma as a function of $(\omega_p/\omega)^2_{ave.}$ which corresponds to the average plasma density. The density distribution of the plasma layer is assumed to be given by

$$n_{o,r} = n_{o,c}\left[1 - \alpha\left(\frac{2r-b-a}{b-a}\right)^p\right] \qquad (2.117)$$

where $n_{o,c}$ is the plasma density at $r = \frac{b+a}{2}$, and α and p are constants which are used to adjust the density distribution. The formula (2.117) gives a similar parabolic density profile adopted by Vandenplas [11] and Killian [12] in their studies for a plain plasma column. In our calculation we assign the values of $p = 2$ and $\alpha = 0.6$. The layer of non-uniform plasma is then subdivided into 3, 7 or 13 sublayers with a constant density assigned in each sublayer. This gives a step function type of density distribution. The numerical calculations based on this scheme are shown in Figures 2.5 and 2.6. In these two figures, it is

observed that the general shapes of curves and the locations of the dipolar and quadrupolar resonances remain quite unchanged as the number of sublayers in numerical calculation is varied. However, a series of small peaks appears to the left hand side of the main (dipolar) resonance. The number of these small peaks increases as the number of sublayer is increased. Obviously, these small peaks can not be physical since they are created in the process of subdividing the plasma layer. In the paper by Shohet and Hatch [13] in solving eigenvalues of a microwave cavity filled with a plasma of variable radial density, a stratification method similar to our method has been used, and they observed the number of the eigenvalues increases as the number of sublayers is increased. They attributed this phenomenon to the mathematical process involved in the stratification method. Any resonance associated with the stratification method in a non-uniform plasma should be termed as a mathematical resonance which has no physical meaning what so ever. In our analysis, we have found that each mathematical resonance occurs when the density of a sublayer approaches to a value when its ω_p/ω is approximately equal to 1. The location of main (dipolar) resonance tends to approach to a value of $(\omega_p/\omega)^2 = 2.8$ as the number of sublayers is increased. While the location of quadrupolar resonance converges to a value of $(\omega_p/\omega)^2 = 3.6$ as the number of sublayer is increased. The values of $(\omega_p/\omega)^2_{ave.}$ where both physical and mathematical resonances occur is listed in Table 2.2 for the case of collision frequency of $\nu/\omega = 0.001$ and for various stratifications.

Model	Mathematical Resonance $(\omega_p/\omega)^2_{ave.}$	Dipolar $(\omega_p/\omega)^2_{ave.}$	Quadrupolar $(\omega_p/\omega)^2_{ave.}$
Uniform	None	2.57	3.25
3 sublayers	.8839, 1.089	2.631	3.37
5 sublayers	.8282, 1.0504, 1.2726	2.747	3.47
7 sublayers	.8242, .9046, 1.186, 1.387	2.76	3.54
13 sublayers	.8212, .8813, .9814, 1.1417, 1.2218, 1.4421, 1.6024	2.804	3.60

Table 2.2 Locations of resonances in a plasma layer coating a metallic cylinder.

Figure 2.7 is a plot of the back scattered E field from a plasma-coated metallic cylinder as a function of $(\omega_p/\omega)^2_{ave.}$ with various dimensions of plasma layer and glass wall but with a fixed conductor radius of a = 2.158 mm and a fixed operating frequency of 2.3 GHz. The density distribution is assumed to be expressed by Eq. (2.117) with $\alpha = 0.6$ and $p = 2$. The calculation was made based on a 13-sublayer model and those mathematical resonances are ignored in the figure. Theoretical calculation shows that the location of the main (dipolar) resonance shifts to a larger value of $(\omega_p/\omega)^2_{ave.}$ as the thickness of the plasma layer is increased. On the other hand, the location of the quadrupolar resonance shifts to a lower value of $(\omega_p/\omega)^2_{ave.}$ as the thickness of the plasma is increased.

Figure 2.8 shows the plot of the back scattered E field from a plasma-coated metallic cylinder as a function of $(\omega_p/\omega)^2_{ave.}$ with various radii of metallic cylinder while the dimension of glass wall is kept

constant with b = 7 mm and c = 8 mm. The density distribution is assumed to be expressed by Eq. (2.117) with $\alpha = 0.6$ and $p = 2$. It is observed that the amplitude of main (dipolar) resonance remains approximately the same while the location of the main (dipolar) resonance tends to move to a smaller value of $(\omega_p/\omega)^2_{ave.}$ as the radius of the metallic cylinder is increased. In the calculation, the 13-sublayer model is again used and the mathematical resonances are ignored in the figure.

Figure 2.9 shows the back scattered E field from a plasma-coated metallic cylinder with the dimensions given in Table 2.1 as a function of $(\omega_p/\omega)^2_{ave.}$ with various plasma density profiles. Again the 13 - sublayer model is used and the mathematical resonances are neglected in the figure. Three different density profiles are assumed for the plasma layer in the calculation. The first density profile as shown in curve (1) in Fig. 2.9 is a distribution with plasma density increasing linearly from glass wall (r = b) to the metallic cylinder (r = a) and can be expressed mathematically by

$$n_{o,r} = n_{o,c}\left[1 - 0.4\left(\frac{2r-b-a}{b-a}\right)\right] \tag{2.118}$$

where $n_{o,c}$ is the plasma density at $r = \frac{b+a}{2}$.

The second density profile as shown in curve (2) has a density distribution linearly decreasing from r = b to r = a and can be expressed by

$$n_{o,r} = n_{o,c}\left[1 + 0.4\left(\frac{2r-b-a}{b-a}\right)\right] . \tag{2.119}$$

The third density profile as shown in curve (3) has a combined distributions of the first and the second profiles. Its density distribution in the region of $b \geq r \geq \frac{b+a}{2}$ obeys Eq. (2.118) and for the region of $\frac{b+a}{2} \geq r \geq a$

it follows Eq. (2.119). All curves in the figure are plotted with a constant collision frequency of $\nu/\omega = 0.01$ and the operating frequency of 2.3 GHz. It is ovserved in Fig. 2.9 that the density profile of the plasma layer has little effect on the behavior of the back scattered E field from a plasma-coated metallic cylinder.

Figure 2.10 shows the back scattered E field from a plain plasma cylinder which has been discussed in section 2.7 as a special case. The curve is plotted for a plasma cylinder with the dimension of $b = 7$ mm and $c = 8$ mm. The operating frequency again is 2.3 GHz. A 13-sublayer model with a density profile given by [11]

$$n_{o,r} = n_{o,c}\left[1-0.6\left(\frac{r}{b}\right)^2\right] \qquad (2.120)$$

is used in the calculation. The behavior of the back scattered E field from a plain plasma cylinder is similar to that from a plasma-coated metallic cylinder. However, the locations of dipolar and quadrupolar resonances of former cylinder tend to move to a larger value of $(\omega_p/\omega)^2_{ave.}$. Not included in Fig. 2.10, the calculations based on 3, 5 or 7-sublayer model were made and the locations of mathematical, dipolar and quadrupolar resonances obtained based on different sublayer models are shown in Table 2.3.

Figure 2.11 is a plot of theoretical back scattered E field from a plasma-coated glass cylinder which was used in the experiment conducted by Vandenplas.[7] The dimensions of the experimental plasma tube are $a = 1.10$ mm, $b = 3.97$ mm and $c = 5.25$ mm. The dielectric constant of the glass is assumed to be $\epsilon_g = 4.3$ and the operating frequency is fixed at 2.7 GHz. A uniform density distribution and a collision

frequency of $\nu/\omega = 0.005$ are assumed in the numerical calculation. The results shown in Fig. 2.11 agree well with the experimental and theoretical results of Vandenplas. The main difference between the numerical results of our theory and that of Vandenplas' theory, which was based on quasi-static approximation, is that our theory predicts finite resonance peaks and a quadrupolar resonance while Vandenplas' theory yields infinite resonance peaks and total absence of quadrupolar resonance.

Model	Mathematical Resonance $(\omega_p/\omega)^2_{ave.}$	Dipolar $(\omega_p/\omega)^2_{ave.}$	Quadrupolar $(\omega_p/\omega)^2_{ave.}$
Uniform	None	2.9	3.3
3 sublayers	.788, 1.061	3.01	3.727
5 sublayers	.791, .932, 1.228	3.06	3.954
7 sublayers	.8015, .9 , 1.05, 1.336	3.07	4.0
13 sublayers	.813, .885, .911, .995, 1.1074, 1.2616, 1.5	3.08	4.0

Table 2.3 Locations of resonances in a plain plasma cylinder.

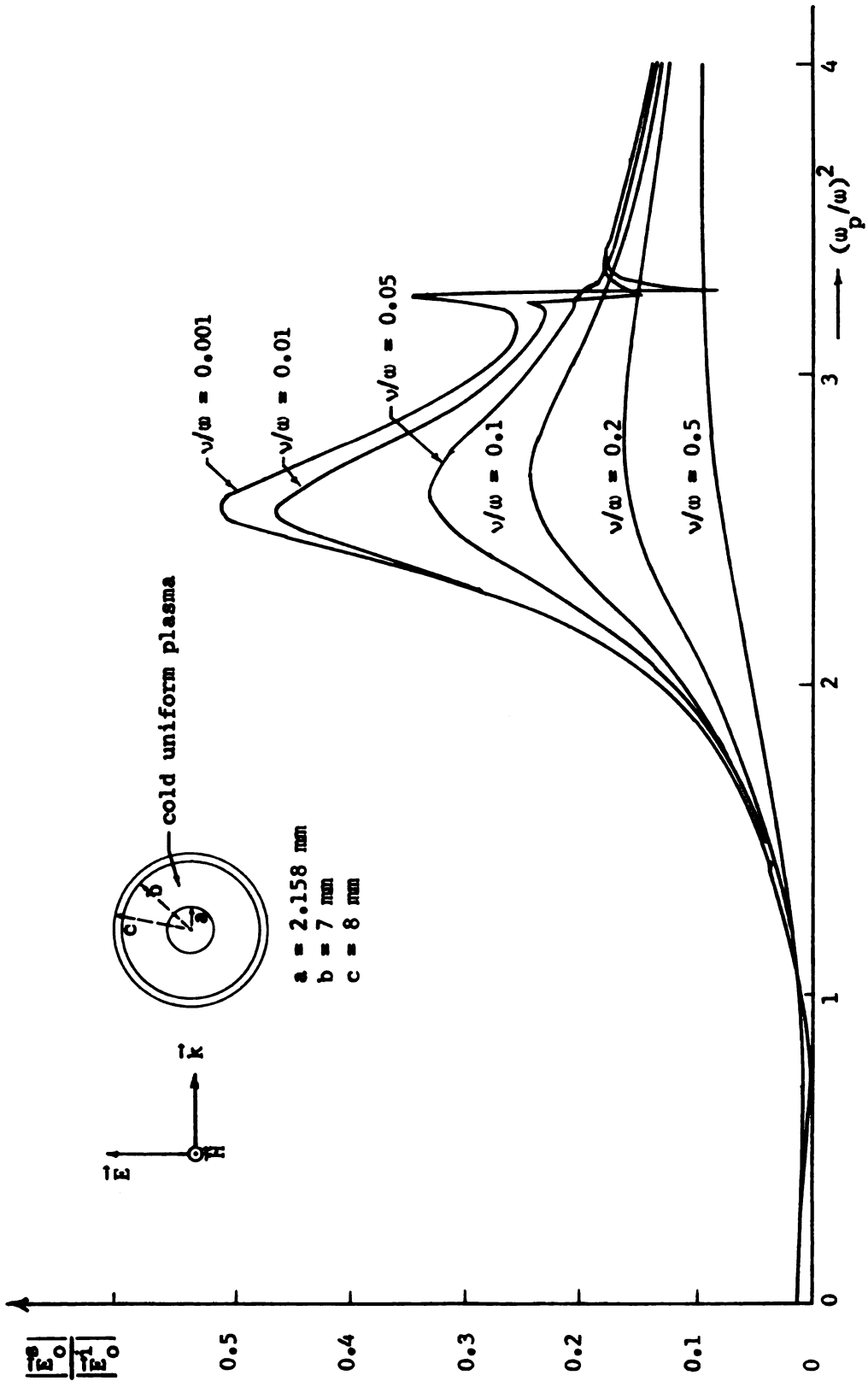

Fig. 2.2 Theoretical back scattered E field from a plasma-coated metallic cylinder as a function of $(\omega_p/\omega)^2$ for a uniform plasma density distribution. (f = 2.3 GHz, $\theta = 180^o$, $k_o r = 10$)

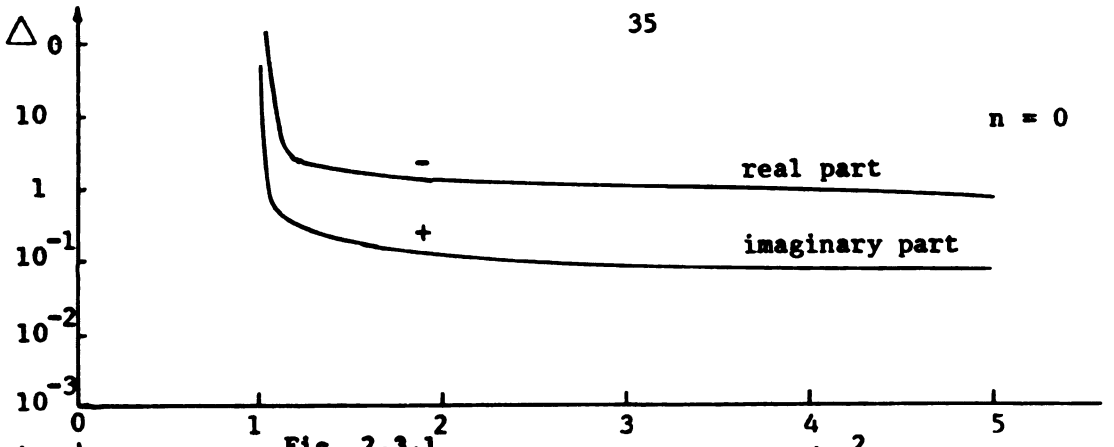

Fig. 2.3.1

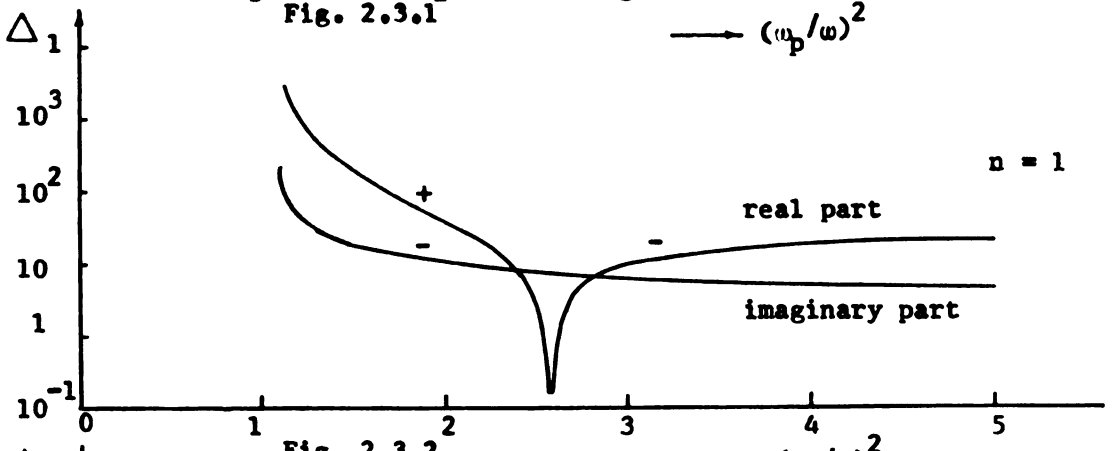

Fig. 2.3.2

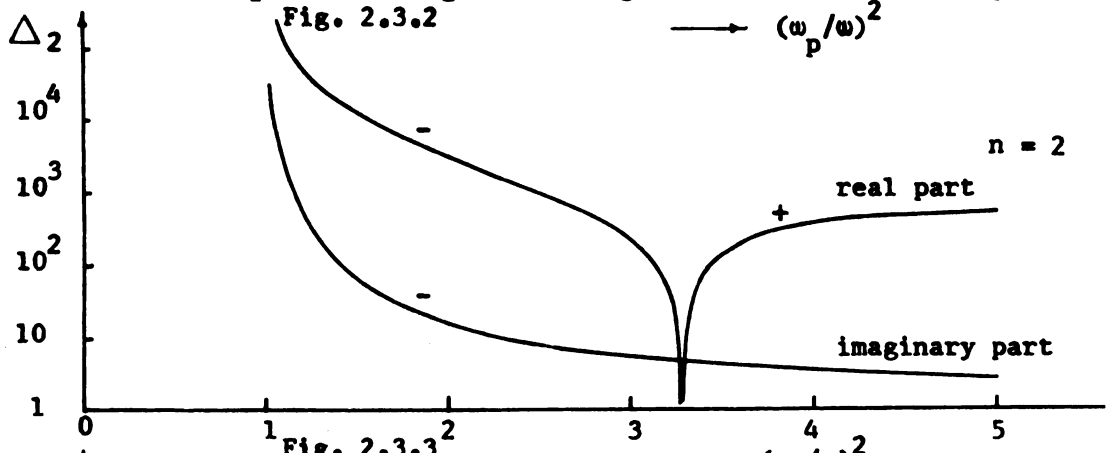

Fig. 2.3.3

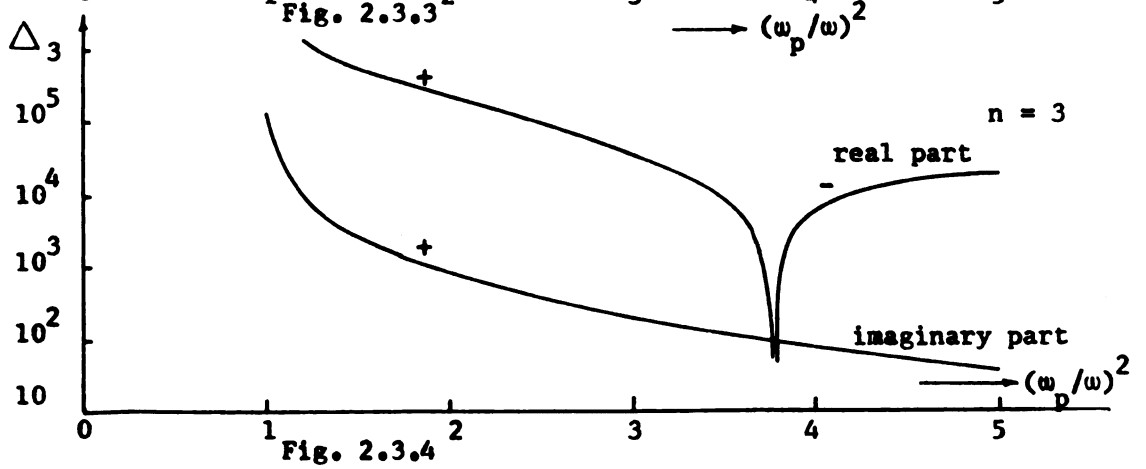

Fig. 2.3.4

Fig. 2.3 Values of Δ_n of Eq. (2.93) for various values of n as functions of $(\omega_p/\omega)^2$.

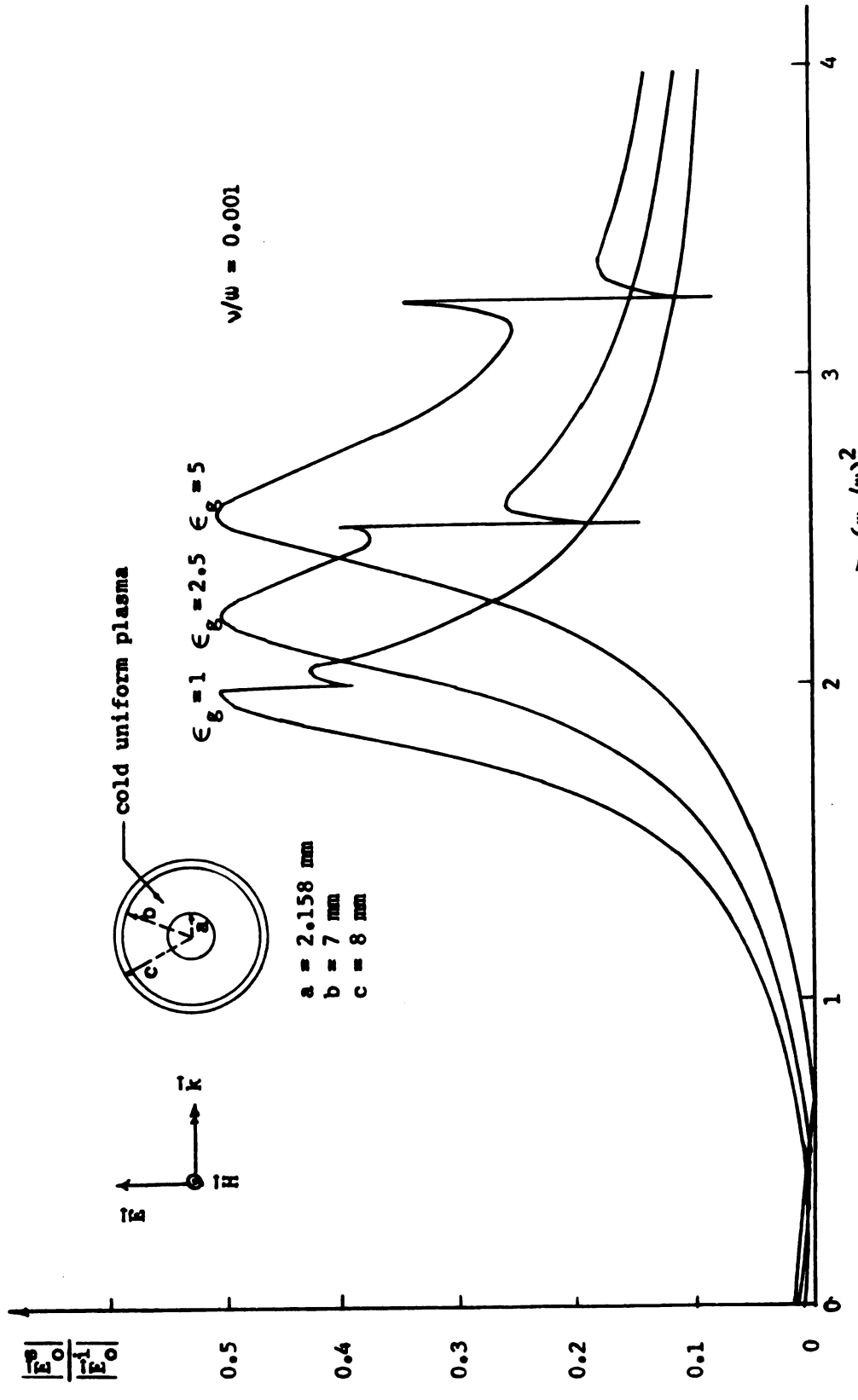

Fig. 2.4 Theoretical back scattered E field from a plasma-coated metallic cylinder as a function of $(\omega_p/\omega)^2$ with glass tubes of various dielectric constants and a uniform plasma density distribution. (f = 2.3 GHz, $\theta = 180^o$, $k_o r = 10$)

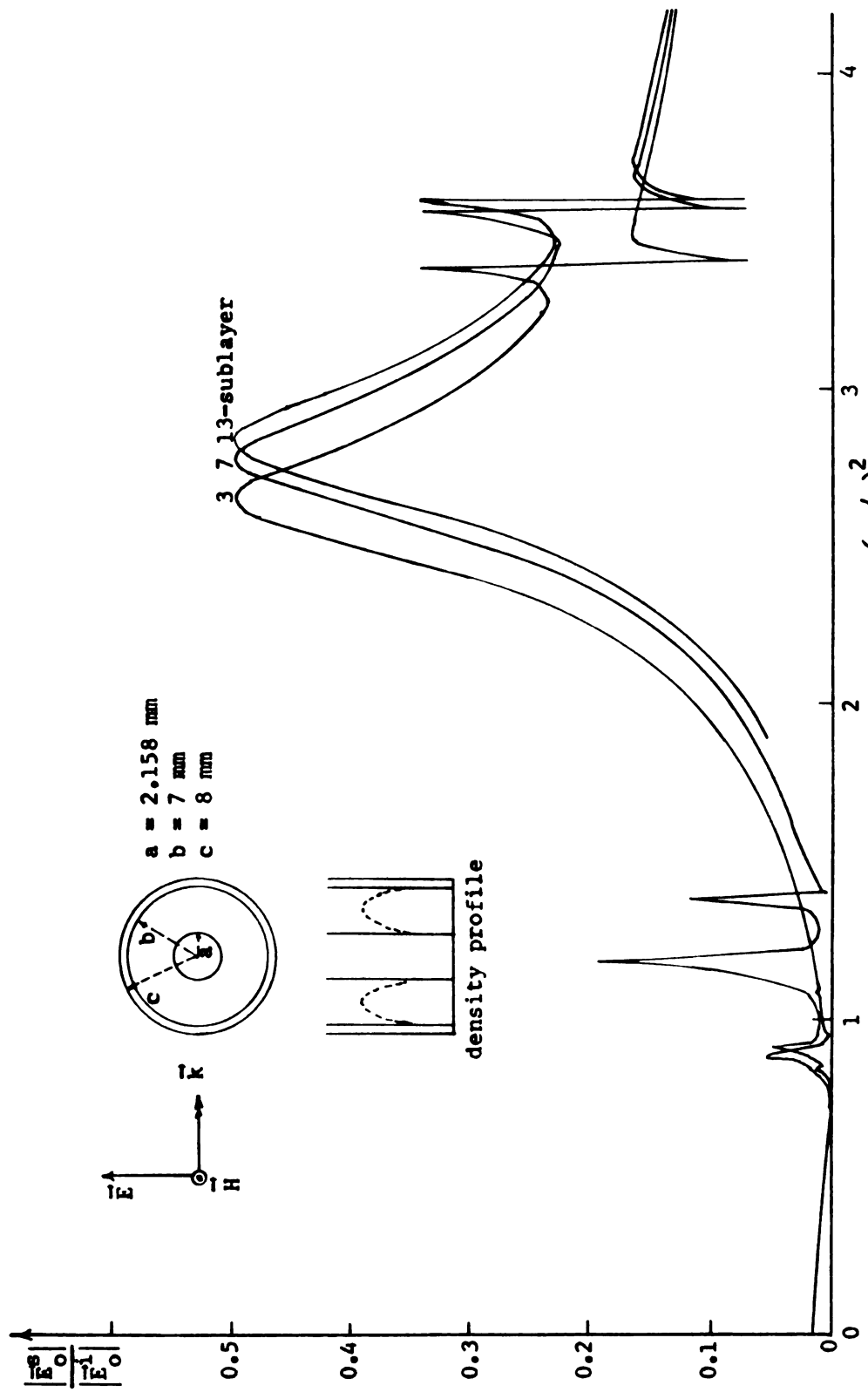

Fig. 2.5 Theoretical back scattered E field from a plasma-coated metallic cylinder as a function of $(\omega_p/\omega)^2_{ave.}$ for a parabolic plasma density distribution. (f = 2.3 GHz, $\theta = 180^o$, $k_o r = 10$, $\nu/\omega = 0.001$)

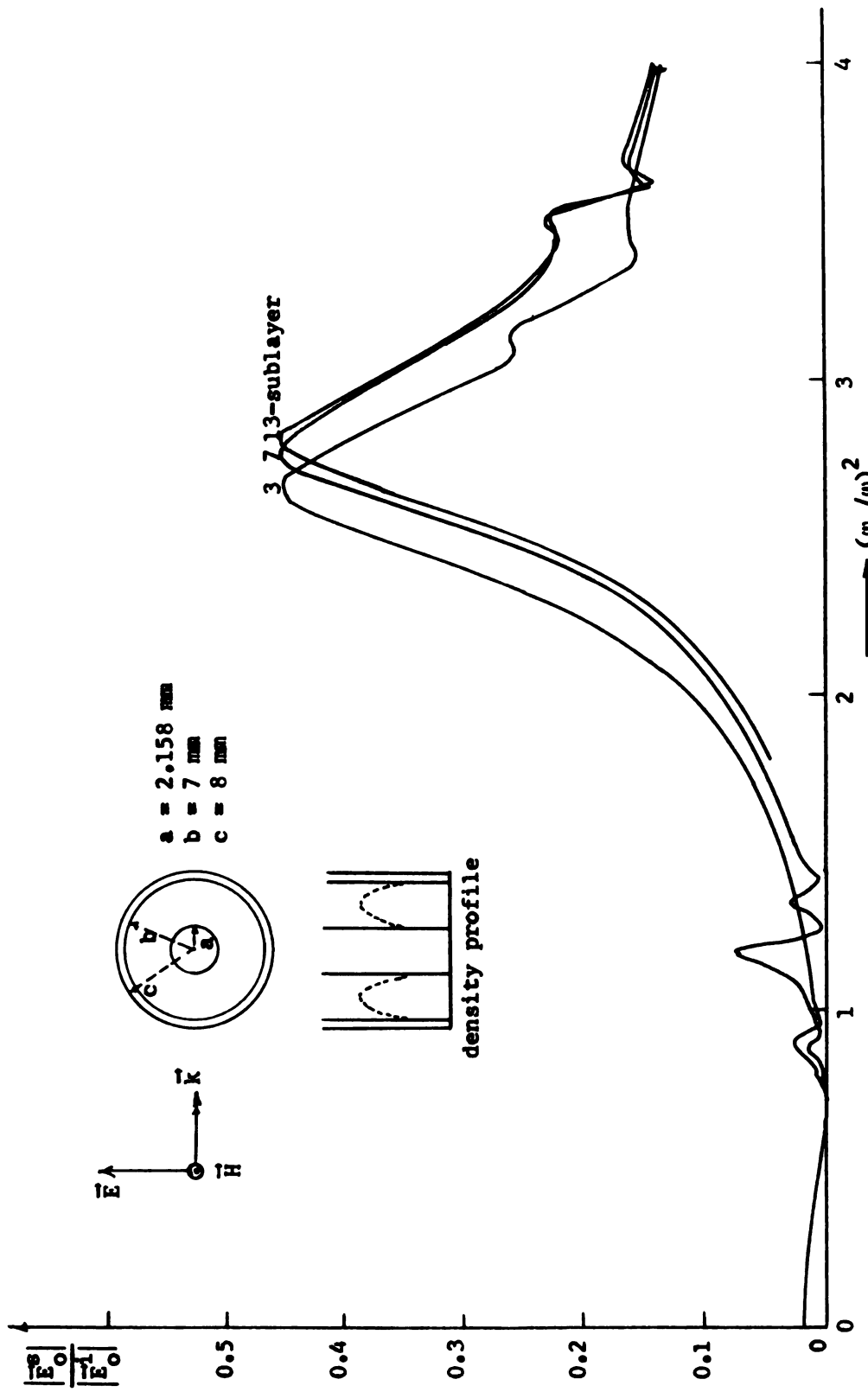

Fig. 2.6 Theoretical back scattered E field from a plasma-coated metallic cylinder as a function of $(\omega_p/\omega)^2_{ave.}$ for a parabolic plasma density distribution. (f = 2.3 GHz, $\theta = 180^0$, $k_o r = 10$, $\nu/\omega = 0.01$)

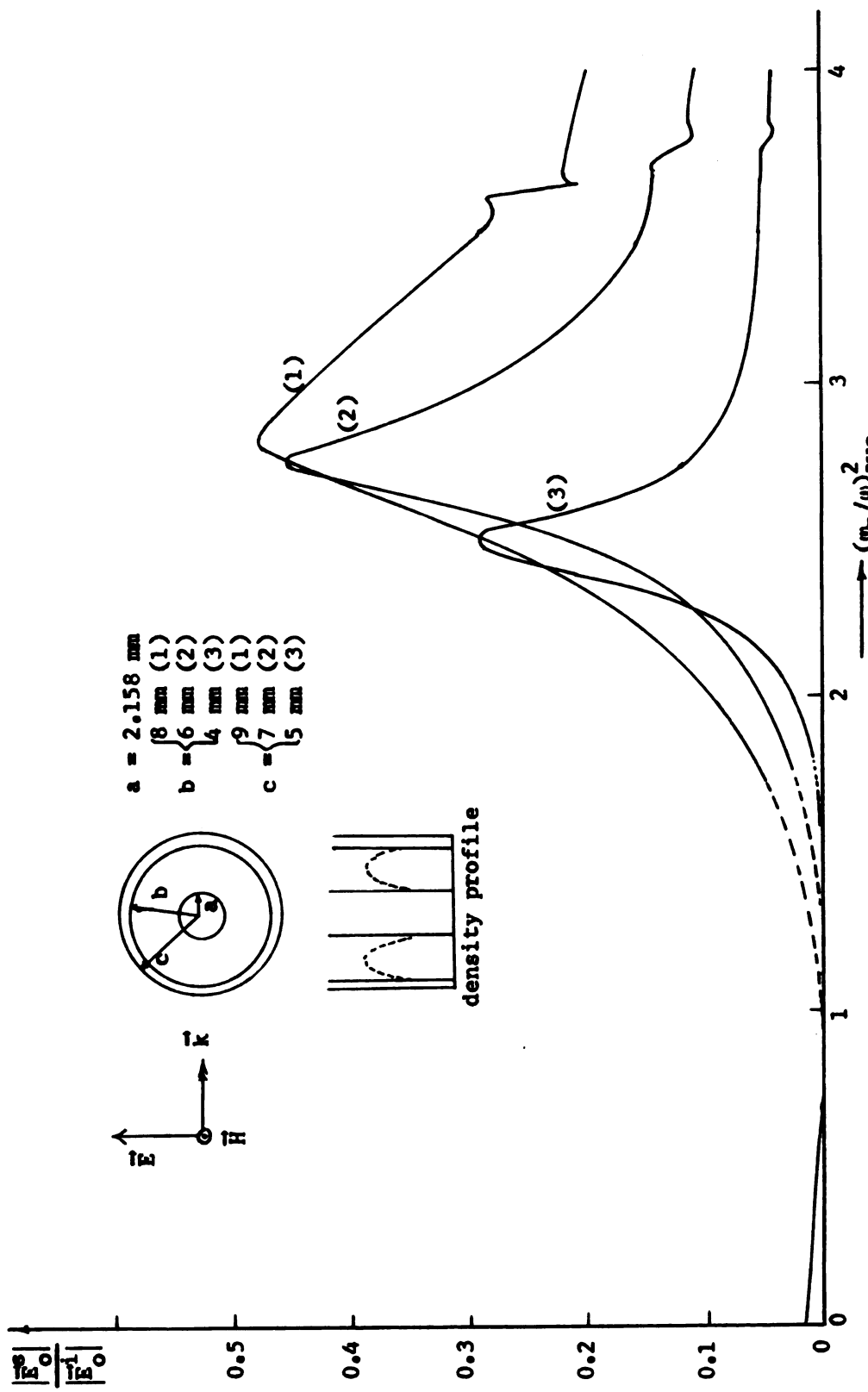

Fig. 2.7 Theoretical back scattered E field from a plasma-coated metallic cylinder as a function of $(\omega_p/\omega)^2_{ave.}$ for various thickness's of non-uniform plasma layer and a fixed conductor radius. ($f = 2.3$ GHz, $\theta = 180^0$, $k_0 r = 10$, $\nu/\omega = 0.01$)

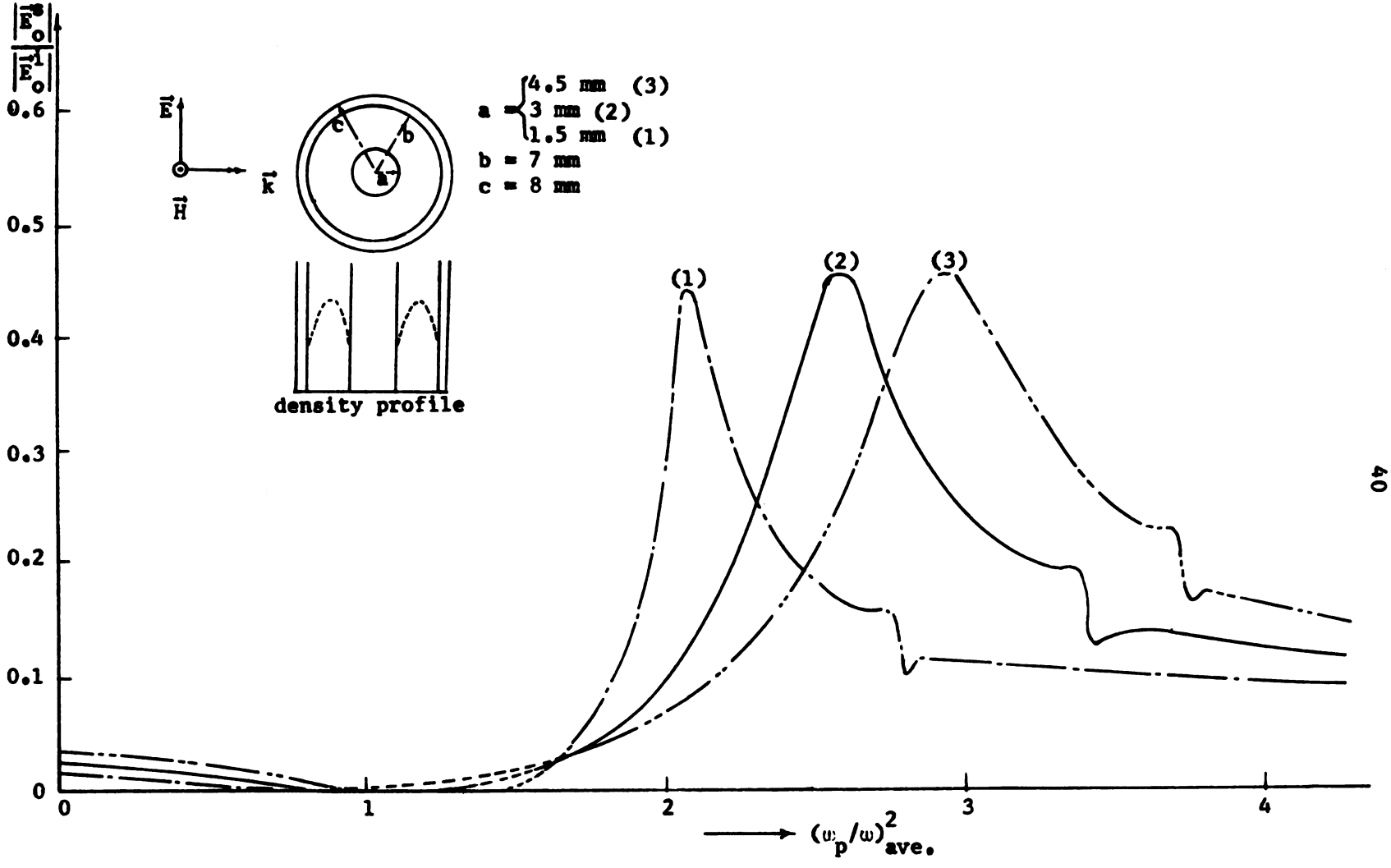

Fig. 2.8 Theoretical back scattered E field from a plasma-coated metallic cylinder as a function of $(\omega_p/\omega)^2_{ave.}$ for various radii of conductor and a fixed glass wall radius. (f =2.3 GHz, $\theta = 180^o$, $k_o r = 10$, $\nu/\omega = 0.01$)

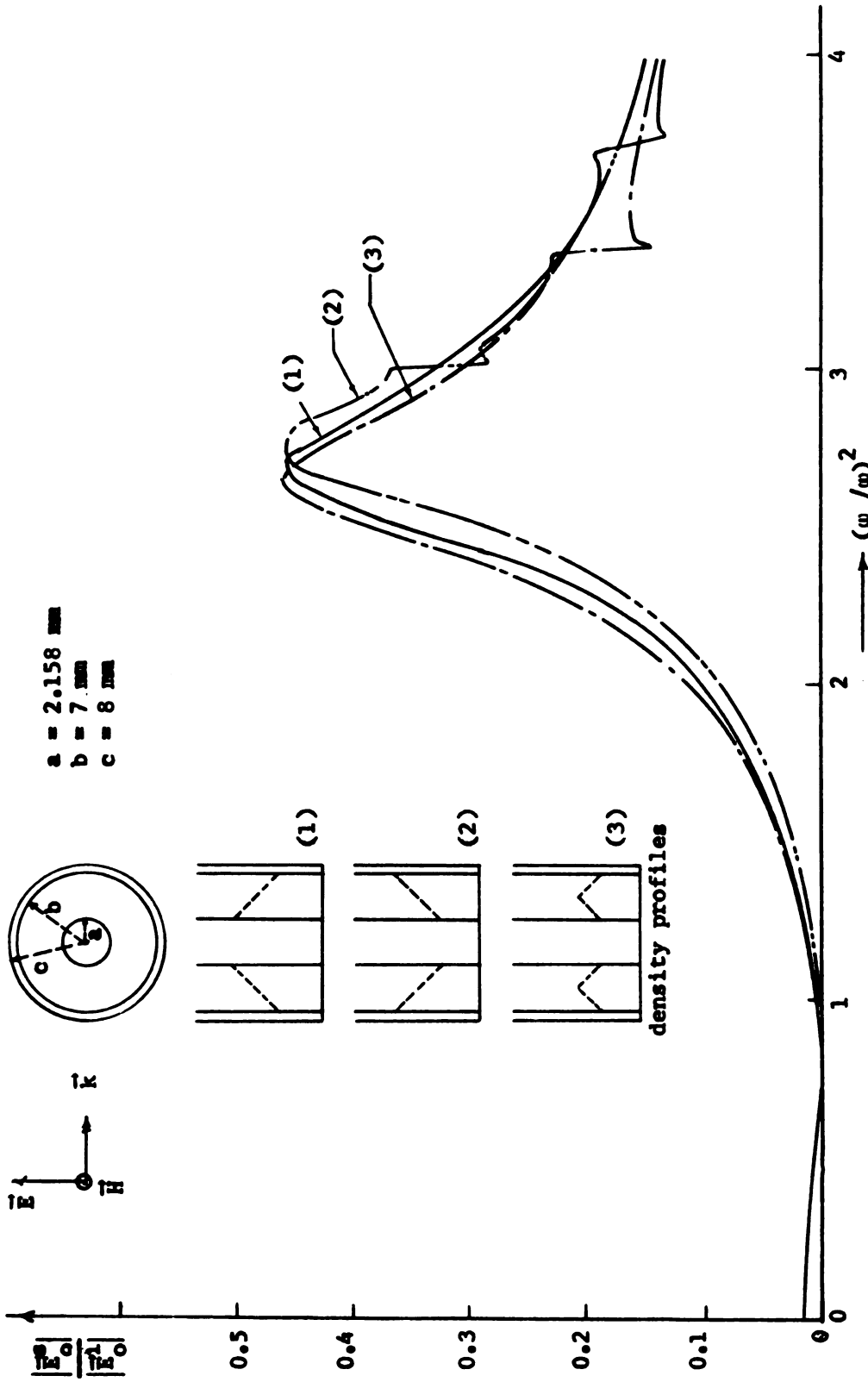

Fig. 2.9 Theoretical back scattered E field from a plasma-coated metallic cylinder as a function of $(\omega_p/\omega)^2_{ave.}$ for various density profiles. (f = 2.3 GHz, $\theta = 180^o$, $k_o r = 10$, $\nu/\omega = 0.01$)

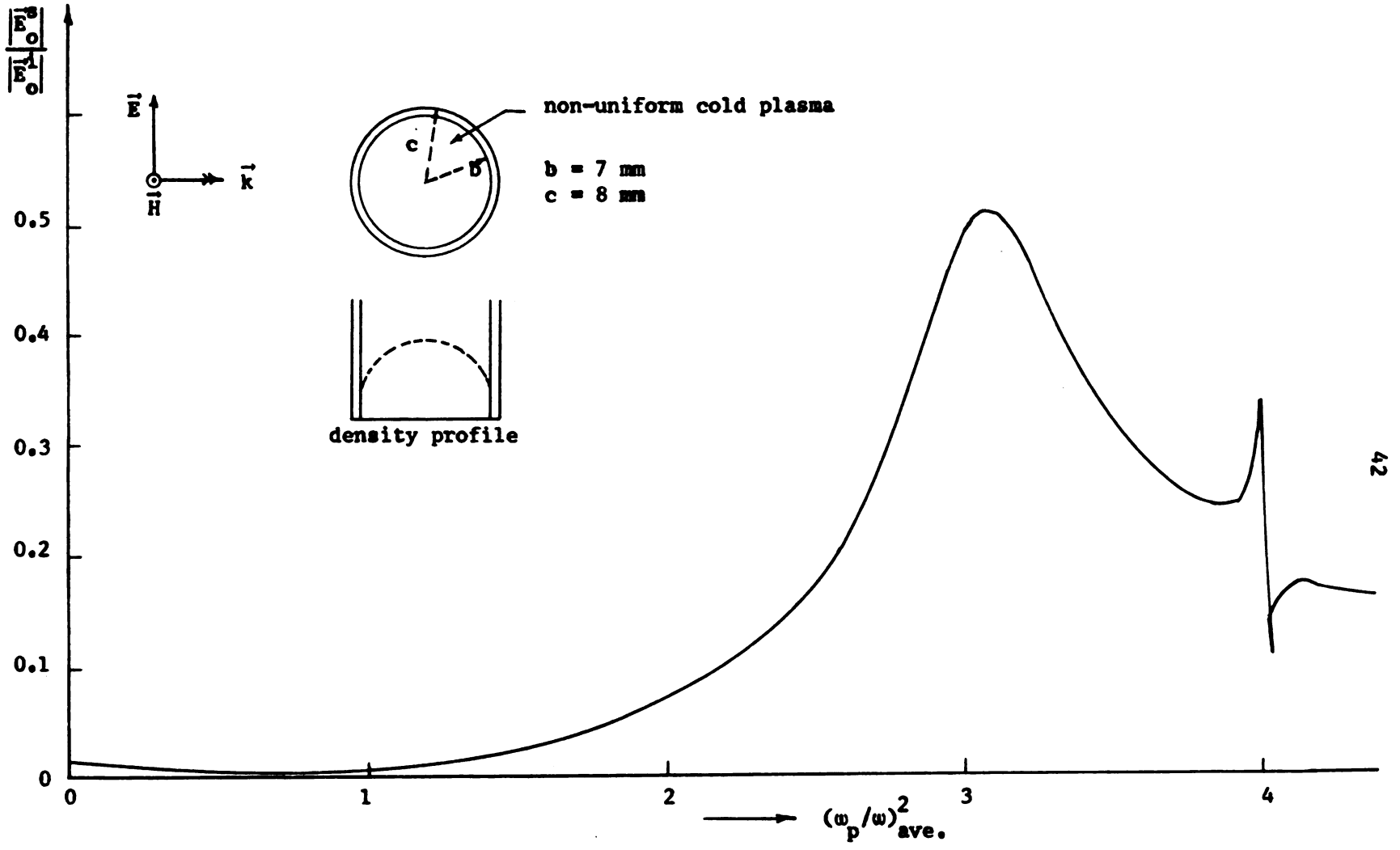

Fig. 2.10 Theoretical back scattered E field from a plain plasma cylinder as a function of $(\omega_p/\omega)^2_{ave.}$ for a parabolic plasma density distribution. (f = 2.3 GHz, θ = 180°, ν/ω = 0.001, $k_o r$ = 10)

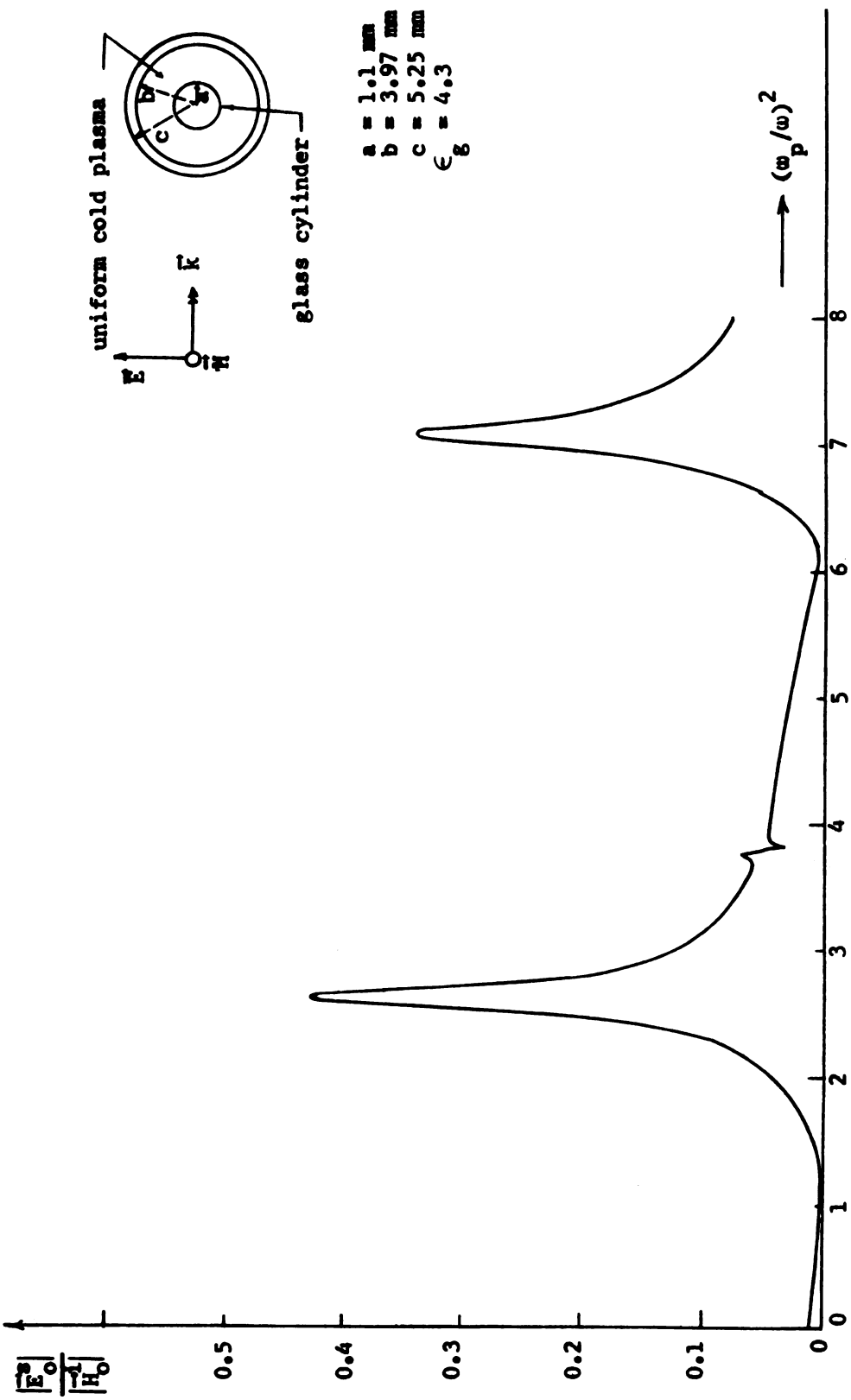

Fig. 2.11 Theoretical back scattered E field from a plasma-coated glass cylinder as a function of $(\omega_p/\omega)^2$ for a uniform plasma density distribution. (f = 2.7 GHz, $\theta = 180^0$, $k_o r = 10$, $\nu/\omega = 0.005$)

CHAPTER 3

SCATTERING FROM A METALLIC CYLINDER SURROUNDED BY A LAYER OF LOSSY, HOT PLASMA ILLUMINATED BY A TE WAVE

3.1 Introduction

In the previous chapter, using a cold plasma approximation we have developed a theory for the scattering of an electromagnetic wave from a plasma-coated metallic cylinder when it is illuminated by a normally incident plane wave with its $\vec{H}$ field parallel to the cylinder axis. In this chapter, the surrounding plasma medium is assumed to be hot and the temperature effect or the excitation of an electroacoustic wave will be considered. Also the plasma medium will be assumed to be non-uniform.

This temperature resonance, also known as Tonks-Dattner's resonance, has received attention from a number of investigators.[14, 15, 16] Some problems related to the present one have also been investigated. Crawford and Kino[17] studied the mechanism of Tonks-Dattner's resonances excited in a plain plasma discharge tube. Wait[18] studied the scattering of an electromagnetic wave by a cylindrical object in an infinite hot plasma. Fejer[19] studied the scattering of an electromagnetic wave by a plain plasma cylinder using a differential equation method. Vandenplas and Messian[11] studied the scattering of an electromagnetic wave from a plasma cylinder using a quasi-static approximation. There are other investigators who studied similar problems.

However, to our best knowledge, the problem of the electromagnetic scattering from a metallic cylinder covered by a layer of non-uniform, hot plasma has not been treated elsewhere.

In the development of theory, the collision loss, the excitation of an electroacoustic wave and the inhomogeneity of the surrounding plasma layer are all considered. The stratification method is used in the analysis. The plasma layer is subdivided into a number of concentric sublayers of sufficiently small thickness compared with the electromagnetic wave length. The plasma density is, then, assumed to be a constant within each sublayer so that a step function approximation of density profile is adopted. In each sublayer of plasma, one can find two electromagnetic and two electroacoustic cylindrical waves with unknown magnitudes propagating in opposite directions. These electromagnetic and electroacoustic waves are coupled at the interface of two adjacent sublayers. The magnitudes of these waves are determined by matching the boundary conditions at the interfaces. This boundary matching process will lead to the final determination of the scatted fields in free space.

In order to compare with experimental results, a glass wall is assumed to surround the plasma in the theoretical model.

3.2 Geometry of the Problem

An infinitely long metallic cylinder with a radius a and covered by a layer of non-uniform hot plasma is confined in a glass tube with inner radius b and outer radius c. The plasma-coated metallic cylinder is placed along the z axis and is illuminated normally by a plane electromagnetic wave with its $\vec{E}$ field perpendicular to the z axis and

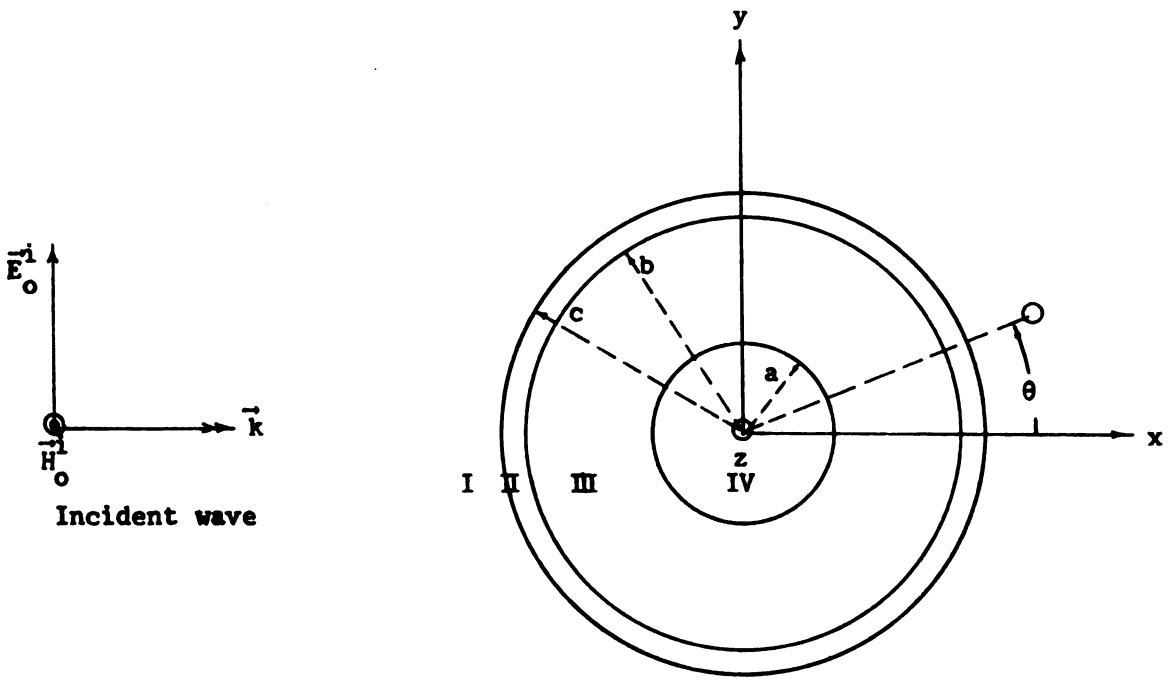

Region I: free space

Region II: glass wall

Region III: hot plasma

Region IV: metallic cylinder

Fig. 3.1.(a) A plasma-coated metallic cylinder illuminated by a TE wave from the left. (hot plasma model)

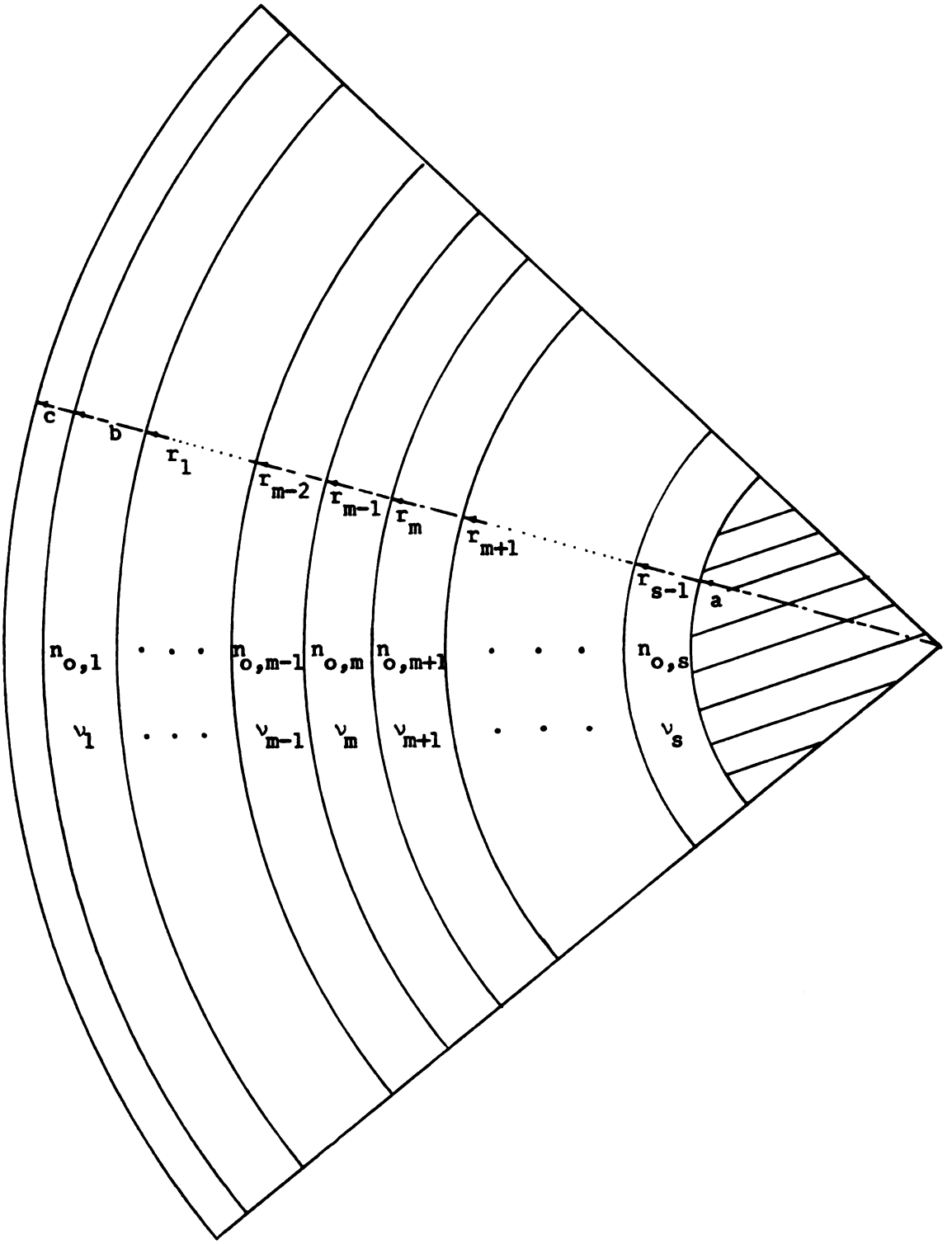

Fig. 3.1.(b) Stratified hot plasma medium.

$\vec{H}$ field parallel to the z axis (TE wave). The layer of non-uniform hot plasma is subdivided into a number of concentric sublayers as shown in Fig. 3.1 for the analysis. These sublayers are counted from outmost sublayer and inwardly. For example, the first sublayer is located immediately inside the glass wall and last sublayer is located immediately outside the metallic cylinder. The radius between two adjacent mth and (m+1)th sublayers is denoted as r_m. In the mth sublayer, we assume that the plasma density is $n_{o,m}$, the collision frequency is ν_m, the propagation constant of electromagnetic wave is $k_{e,m}$, the propagation constant of electroacoustic wave is $k_{p,m}$, and the equivalent complex permittivity is ξ_m.

The cylinder is assumed to be infinitely long in the analysis so that there is no field variation along the z direction. The angle of θ in cylindrical coordinates starts from x axis and increases in the counter clockwise direction. The time dependence of $\exp(j\omega t)$ is assumed and the fields of incident plane wave are the same as given in Chapter 2. They are

$$H_{oz}^{i} = \sum_{n=o}^{\infty} \epsilon_{on}(-j)^n \cos(n\theta)\, J_n(k_o r) \tag{3.1}$$

$$H_{or}^{i} = H_{o\theta}^{i} = 0 \tag{3.2}$$

$$E_{or}^{i} = -\frac{j}{\omega \epsilon_o r} \frac{\partial}{\partial \theta} H_{oz}^{i} = \frac{j}{\omega \epsilon_o r} \sum_{n=o}^{\infty} \epsilon_{on}(-j)^n n\sin(n\theta)\, J_n(k_o r) \tag{3.3}$$

$$E_{o\theta}^{i} = \frac{j}{\omega \epsilon_o} \frac{\partial}{\partial r} H_{oz}^{i} = j\zeta_o \sum_{n=o}^{\infty} \epsilon_{on}(-j)^n \cos(n\theta)\, J_n'(k_o r) \tag{3.4}$$

$$E_{oz}^{i} = 0 \,. \tag{3.5}$$

In this expression the superscript "i" represents the incident wave. k_o is the propagation constant of free space. ϵ_{on} is the Neumann factor defined as $\epsilon_{on} = 1$ when n=0 and $\epsilon_{on} = 2$ when n≠0. $J_n(k_o r)$ is Bessel function of first kind with integer order n and argument $k_o r$. $J_n'(k_o r)$ is the first derivative of $J_n(k_o r)$. ϵ_o is the permittivity of free space. ζ_o is the impedance of free space and is defined as $\zeta_o = \sqrt{\frac{\mu_o}{\epsilon_o}} = 120\pi$ ohms where μ_o is the permeability of free space.

3.3 Fields in the Regions of Free Space and Glass Wall

In these regions the Maxwell's equations are the same as those in the cold plasma case (Chapter 2) and thus, fields in these regions remain the same as that in Chapter 2. Appropriate solutions for the fields in these regions are reproduced from Chapter 2 as follows: The total fields in free space are

$$H_{oz}^t = \sum_{n=o}^{\infty} \cos(n\theta) \left[\epsilon_{on}(-j)^n J_n(k_o r) + H_n^{(2)}(k_o r)\, A_n\right] \tag{3.6}$$

$$H_{or}^t = H_{o\theta}^t = 0 \tag{3.7}$$

$$E_{or}^t = \frac{j}{\omega \epsilon_o r} \sum_{n=o}^{\infty} n\sin(n\theta) \left[\epsilon_{on}(-j)^n J_n(k_o r) + H_n^{(2)}(k_o r)\, A_n\right] \tag{3.8}$$

$$E_{o\theta}^t = j\zeta_o \sum_{n=o}^{\infty} \cos(n\theta) \left[\epsilon_{on}(-j)^n J_n'(k_o r) + H_n^{(2)'}(k_o r)\, A_n\right] \tag{3.9}$$

$$E_{oz}^t = 0 \ . \tag{3.10}$$

The superscript "t" represents the total fields (incident wave plus reflected wave). $H_n^{(2)}(k_o r)$ is Hankel function of second kind. $H_n^{(2)'}(k_o r)$ is the first derivative of $H_n^{(2)}(k_o r)$. A_n is a constant to be determined by boundary conditions.

The fields in the glass wall region are

$$H_{gz} = \sum_{n=o}^{\infty} \cos(n\theta)\left[H_n^{(1)}(k_g r)\, B_n + H_n^{(2)}(k_g r)\, C_n\right] \tag{3.11}$$

$$H_{gr} = H_{g\theta} = 0 \tag{3.12}$$

$$E_{gr} = \frac{j}{\omega \epsilon_o \epsilon_g r} \sum_{n=o}^{\infty} n\sin(n\theta)\left[H_n^{(1)}(k_g r)\, B_n + H_n^{(2)}(k_g r)\, C_n\right] \tag{3.13}$$

$$E_{g\theta} = j \frac{\zeta_o}{\sqrt{\epsilon_g}} \sum_{n=o}^{\infty} \cos(n\theta)\left[H_n^{(1)'}(k_g r)\, B_n + H_n^{(2)'}(k_g r)\, C_n\right] \tag{3.14}$$

$$E_{gz} = 0 \tag{3.15}$$

where k_g, the propagation constant of glass, is defined as $k_g = \omega\sqrt{\mu_o \epsilon_o \epsilon_g}$ with ϵ_g as the dielectric constant of glass. B_n and C_n are the constants to be determined by boundary conditions.

3.4 Fields in Hot Plasma Region

In the plasma region ($b \geq r \geq a$) the plasma is considered as an one-component electron fluid and the ions are neglected in the equations of motion. The presence of ions is, however, required to neutralize electrical charge in the plasma. The stratification method is used in the analysis. The inhomogeneous plasma layer is subdivided into a number of concentric sublayers with sufficiently small thickness. The plasma density is then considered to be a constant within each sublayer but it varies from sublayer to sublayer in the radial direction. In the mth sublayer the plasma density is assumed to be $n_{o,m}$. The collision frequency of a electron with neutral particles of gas is assumed to be ν_m. The density deviation of electrons from the mean $n_{o,m}$ is assumed to be $n_{1,m}$ and the velocity of electrons induced by the fields is assumed to be $\vec{V}_m$.

It is assumed that the perturbation of plasma due to the fields is sufficiently small that the linearized equations are applicable. No static magnetic field is present in the analysis. The time dependence of exp(jωt) is assumed and the Maxwell's equations in the mth sublayer of plasma region are

$$\nabla \times \vec{E}_m = - j\omega\mu_o \vec{H}_m \tag{3.16}$$

$$\nabla \times \vec{H}_m = -en_{o,m} \vec{V}_m + j\omega \epsilon_o \vec{E}_m \tag{3.17}$$

$$\nabla \cdot \vec{E}_m = - \frac{en_{1,m}}{\epsilon_o} \tag{3.18}$$

$$\nabla \cdot \vec{H}_m = 0 \ . \tag{3.19}$$

The linearized continuity and force equations are

$$n_{o,m} \nabla \cdot \vec{V}_m + j\omega n_{1,m} = 0 \tag{3.20}$$

$$(\nu_m + j\omega) \vec{V}_m = - \frac{e}{M} \vec{E}_m - \frac{v_o^2}{n_{o,m}} \nabla n_{1,m} \tag{3.21}$$

where e and M are the electron charge and mass respectively. v_o is the r. m. s. velocity of electrons which is considered to be constant throughout the plasma region and is defined as $v_o = \sqrt{3kT/M}$ where k is Boltzmann's constant and T is the electron temperature. The last term in Eq. (3.21) represents the force due to the pressure gradient, and $v_o = \sqrt{3kT/M}$ is valid on the assumption of adiabatic pressure variation and one dimensional compression.[20]

In our formulation of the problem there are four unknowns to be solved. They are $\vec{H}_m$, $n_{1,m}$, $\vec{E}_m$ and $\vec{V}_m$. We will determine $\vec{H}_m$ and $n_{1,m}$

first and then calculate $\vec{E}_m$ and $\vec{V}_m$.

From Eqs. (3.17) and (3.21), we obtain two expressions as

$$\nabla \times \nabla \times \vec{H}_m = - en_{o,m} \nabla \times \vec{V}_m + j\omega \epsilon_o \nabla \times \vec{E}_m \tag{3.22}$$

and

$$\nabla \times \vec{V}_m = - \frac{e}{M(\nu_m + j\omega)} \nabla \times \vec{E}_m \quad . \tag{3.23}$$

The substitution of Eq. (3.23) in Eq. (3.22) yields

$$\nabla \times \nabla \times \vec{H}_m = \left[\frac{e^2 n_{o,m}}{M(\nu_m + j\omega)} + j\omega \epsilon_o \right] \nabla \times \vec{E}_m \quad . \tag{3.24}$$

Expressing $\nabla \times \vec{E}_m$ in terms of $\vec{H}_m$ as in Eq. (3.16), Eq. (3.24) can be rewritten as

$$\nabla \times \nabla \times \vec{H}_m = \omega^2 \mu_o \epsilon_o \left[1 + \frac{\omega_{p,m}^2}{j\omega(\nu_m + j\omega)} \right] \vec{H}_m \tag{3.25}$$

where $\omega_{p,m}$ is the plasma frequency defined as

$$\omega_{p,m} = \sqrt{\frac{e^2 n_{o,m}}{M \epsilon_o}} \quad . \tag{3.26}$$

Equation (3.25) can be expressed as

$$\nabla \times \nabla \times \vec{H}_m = k_{e,m}^2 \vec{H}_m \tag{3.27}$$

where $k_{e,m}$ is the complex propagation constant of the electromagnetic wave in the mth sublayer and is given by

$$k_{e,m} = \omega \sqrt{\mu_o \xi_m} \tag{3.28}$$

with ξ_m, the equivalent complex permittivity, defined as

$$\xi_m = \epsilon_o \left[\left(1 - \frac{\omega_{p,m}^2}{\omega^2+\nu_m^2}\right) - \frac{j\omega_{p,m}^2 \nu_m}{\omega(\omega^2+\nu_m^2)} \right] . \tag{3.29}$$

If we express $k_{e,m}$ as

$$k_{e,m} = \beta_{e,m} - j\,\alpha_{e,m} \tag{3.30}$$

$\beta_{e,m}$ and $\alpha_{e,m}$ can be determined to be

$$\beta_{e,m} = \frac{\beta_o}{\sqrt{2}} \left\{ 1 - \frac{\omega_{p,m}^2}{\omega^2+\nu_m^2} + \left[1 - \frac{2\omega_{p,m}^2}{\omega^2+\nu_m^2} + \frac{\omega_{p,m}^4}{\omega^2(\omega^2+\nu_m^2)} \right]^{\frac{1}{2}} \right\}^{\frac{1}{2}} \tag{3.31}$$

$$\alpha_{e,m} = \frac{\beta_o}{\sqrt{2}} \left\{ -1 + \frac{\omega_{p,m}^2}{\omega^2+\nu_m^2} + \left[1 - \frac{2\omega_{p,m}^2}{\omega^2+\nu_m^2} + \frac{\omega_{p,m}^4}{\omega^2(\omega^2+\nu_m^2)} \right]^{\frac{1}{2}} \right\}^{\frac{1}{2}} . \tag{3.32}$$

$\beta_{e,m}$ and $\alpha_{e,m}$ are the wave number and the attenuation constant of the electromagnetic wave in the mth sublayer of the plasma and β_o is the wave number of free space defined as $\beta_o = \omega\sqrt{\mu_o \epsilon_o}$.

In the mth sublayer both incoming and outgoing (reflected) waves can exist. Before solving Eq. (3.27) the $\vec{H}$ fields of incoming and reflected waves will be assumed to have z component only. This assumption can be justified from Maxwell's equation and the symmetry of geometry. Since the incident $\vec{E}$ field has no z component and the symmetry of geometry provides no variation along z direction such that $\frac{\partial}{\partial z} = 0$, Eq. (3.16) can be reduced to

$$\frac{1}{r}\left[\frac{\partial}{\partial r}(r\, E_{m\theta}) - \frac{\partial E_{mr}}{\partial \theta} \right] \hat{z} = -j\omega\mu_o \vec{H}_m . \tag{3.33}$$

Equation (3.33) shows that $\vec{H}_m$ is allowed to have a z component only.

Thus, we assume that

$$\vec{H}_m = H_{mz}\hat{z} \quad . \tag{3.34}$$

Equation (3.27) can now, be reduced to

$$\frac{\partial^2 H_{mz}}{\partial r^2} + \frac{1}{r}\frac{\partial H_{mz}}{\partial r} + \frac{1}{r^2}\frac{\partial^2 H_{mz}}{\partial \theta^2} + k_{e,m}^2 H_{mz} = 0 \quad . \tag{3.35}$$

Equation (3.35) can be solved by the method of separation of variables. We assume that

$$H_{mz} = H(r)\, H(\theta) \tag{3.36}$$

where $H_m(r)$ and $H_m(\theta)$ are functions of r and θ respectively. The substitution of Eq. (3.36) in Eq. (3.35) leads to

$$\frac{r^2}{H(r)}\frac{\partial^2 H(r)}{\partial r^2} + \frac{r}{H(r)}\frac{\partial H(r)}{\partial r} + k_{e,m}^2 r^2 = n^2 \tag{3.37}$$

$$\frac{1}{H(\theta)}\frac{\partial^2 H(\theta)}{\partial \theta^2} = n^2 \quad . \tag{3.38}$$

Considering the symmetry of the problem and the degeneracy of angle θ, the solution for $H(\theta)$ is

$$H(\theta) = \cos(n\theta) \tag{3.39}$$

where n is an integer. Equation (3.37) can be rearranged to

$$\frac{\partial^2 H(r)}{\partial (k_{e,m} r)^2} + \frac{1}{(k_{e,m} r)}\frac{\partial H(r)}{\partial (k_{e,m} r)} + \left(1 - \frac{n^2}{(k_{e,m} r)^2}\right) H(r) = 0 \tag{3.40}$$

which is a Bessel equation.

Since both incoming and outgoing waves are expected to exist the proper solutions for H(r) are Hankel function of first kind and second kind. Therefore, the final solution for H_{mz} can be written as

$$H_{mz} = \sum_{n=o}^{\infty} \cos(n\theta)\left[H_n^{(1)}(k_{e,m}r)D_{m,n} + H_n^{(2)}(k_{e,m}r)\, F_{m,n}\right] \quad (3.41)$$

where $D_{m,n}$ and $F_{m,n}$ are constants in the mth sublayer and will be determined by boundary conditions. It is noted that in the expressions of $D_{m,n}$ and $F_{m,n}$ the first subscript m specified the sublayer and the second subcript n specifies the index of summation.

Up to this point, the magnetic field $\vec{H}_m$ has been determined and the next quantity to be solved is the density deviation, $n_{1,m}$, of electrons from the mean. Taking the divergence of Eq. (3.21), we obtain

$$(\nu_m + j\omega)\nabla\cdot\vec{V}_m = -\frac{e}{M}\nabla\cdot\vec{E}_m - \frac{v_{o,m}^2}{n_o}\nabla^2 n_{1,m} \quad . \quad (3.42)$$

From Eq. (3.20), $\nabla\cdot\vec{V}_m$ can be represented in terms of $n_{1,m}$ as

$$\nabla\cdot\vec{V}_m = -\frac{j\omega n_{1,m}}{n_{o,m}} \quad . \quad (3.43)$$

Substituting the quantities, $\nabla\cdot\vec{V}_m$ and $\nabla\cdot\vec{E}_m$ from Eqs. (3.43) and (3.18), into Eq. (3.42), we obtain a homogeneous wave equation for $n_{1,m}$ as

$$\nabla^2 n_{1,m} + k_{p,m}^2\, n_{1,m} = 0 \quad (3.44)$$

where $k_{p,m}$ is the complex propagation constant of the electroacoustic wave and is expressed by

$$k_{p,m}^2 = \frac{1}{v_o^2}\left[(\omega^2 - \omega_{p,m}^2) - j\omega\nu_m\right] \quad . \quad (3.45)$$

If we express $k_{p,m}$ as

$$k_{p,m} = \beta_{p,m} - j\alpha_{p,m} \quad , \quad (3.46)$$

$\beta_{p,m}$ and $\alpha_{p,m}$ can be determined to be

$$\beta_{p,m} = \frac{1}{\sqrt{2}v_o}\left\{\omega^2 - \omega_{p,m}^2 + \left[(\omega^2 - \omega_{p,m}^2)^2 + \omega^2\nu_m^2\right]^{\frac{1}{2}}\right\}^{\frac{1}{2}} \tag{3.47}$$

$$\alpha_{p,m} = \frac{1}{\sqrt{2}v_o}\left\{-\omega^2 + \omega_{p,m}^2 + \left[(\omega^2 - \omega_{p,m}^2)^2 + \omega^2\nu_m^2\right]^{\frac{1}{2}}\right\}^{\frac{1}{2}} \tag{3.48}$$

where $\beta_{p,m}$ and $\alpha_{p,m}$ are the wave number and the attenuation constant of the electroacoustic wave in the mth sublayer of plasma medium respectively.

With the symmetry condition of $\frac{\partial}{\partial z} = 0$, Eq. (3.44) can be reduced to

$$\frac{\partial^2 n_{1,m}}{\partial r^2} + \frac{1}{r}\frac{\partial n_{1,m}}{\partial r} + \frac{1}{r^2}\frac{\partial^2 n_{1,m}}{\partial \theta^2} + k_{p,m}^2 n_{1,m} = 0 \quad . \tag{3.49}$$

Equation (3.49) has the same form as Eq. (3.35). Following the same procedures as we used in solving Eq. (3.35), the proper solution of $n_{1,m}$ can be expressed as

$$n_{1,m} = \sum_{n=0}^{\infty} \sin(n\theta)\left[H_n^{(1)}(k_{p,m}\, r)\, G_{m,n} + H_n^{(2)}(k_{p,m}\, r)\, I_{m,n}\right] \tag{3.50}$$

where $G_{m,n}$ and $I_{m,n}$ are constants to be determined by boundary conditions.

The density deviation of electron is completely determined. The next quantities to be determined are the induced velocity of electrons, $\vec{V}_m$, and the electric field, $\vec{E}_m$. From Eq. (3.17), the $\vec{E}$ field can be expressed in terms of $\nabla \times \vec{H}_m$ and $\vec{V}_m$ as

$$\vec{E}_m = \frac{1}{j\omega\epsilon_o}\nabla \times \vec{H}_m + \frac{en_{o,m}}{j\omega\epsilon_o}\vec{V}_m \quad . \tag{3.51}$$

Substituting Eq. (3.51) in Eq. (3.21) and after rearrangement, it yields

$$\vec{V}_m = -\frac{e}{j\omega(\nu_m + j\omega)\xi_m M}\nabla \times \vec{H}_m - \frac{v_o^2\epsilon_o}{n_{o,m}\xi_m(\nu_m + j\omega)}\nabla n_{1,m} \quad . \tag{3.52}$$

In Eq. (3.52), the quantities $\vec{H}_m$ and $n_{1,m}$ have been determined before. Taking the curl of the magnetic field $\vec{H}_m$ as expressed in Eq. (3.41) and using the symmetry of geometry, $\nabla \times \vec{H}_m$ can be obtained as

$$\nabla \times \vec{H}_m = -\frac{1}{r}\left\{ \sum_{n=o}^{\infty} n\sin(n\theta)\left[H_n^{(1)}(k_{e,m}r)D_{m,n} + H_n^{(2)}(k_{e,m}r)F_{m,n}\right]\right\} \hat{r}$$

$$- k_{e,m}\left\{ \sum_{n=o}^{\infty} \cos(n\theta)\left[H_n^{(1)'}(k_{e,m}r)\, D_{m,n} + H_n^{(2)'}(k_{e,m}r)F_{m,n}\right]\right\} \hat{\theta} \tag{3.53}$$

Similarly, the quantity $\nabla n_{1,m}$ can be derived from Eq. (3.50) as

$$\nabla n_{1,m} = k_{p,m}\left\{ \sum_{n=o}^{\infty} \sin(n\theta)\left[H_n^{(1)'}(k_{p,m}r)\, G_{m,n} + H_n^{(2)'}(k_{p,m}r)I_{m,n}\right]\right\} \hat{r}$$

$$+ \frac{1}{r}\left\{ \sum_{n=o}^{\infty} n\cos(n\theta)\left[H_n^{(1)}(k_{p,m}r)\, G_{m,n} + H_n^{(2)}(k_{p,m}r)I_{m,n}\right]\right\} \hat{\theta} \tag{3.54}$$

Substituting Eqs. (3.53) and (3.54) into Eq. (3.52), the induced velocity of electrons, $\vec{V}_m$, can be obtained explicitly. The components of $\vec{V}_m$ vector are

$$V_{mr} = \frac{-je}{\omega\xi_m M(\nu_m+j\omega)r} \sum_{n=o}^{\infty} n\sin(n\theta)\left[R_{m,n}(k_e r,\, D,F)\right]$$

$$- \frac{v_o^2 \epsilon_o k_{p,m}}{n_{o,m}\xi_m(\nu_m+j\omega)} \sum_{n=o}^{\infty} \sin(n\theta)\left[R'_{m,n}(k_p r,\, G,\, I)\right] \tag{3.55}$$

$$V_{m\theta} = \frac{-jek_{e,m}}{\omega\xi_m M(\nu_m+j\omega)} \sum_{n=o}^{\infty} \cos(n\theta)\left[R'_{m,n}(k_e r,\, D,\, F)\right]$$

$$- \frac{v_o^2 \epsilon_o}{n_{o,m}\xi_m(\nu_m+j\omega)r} \sum_{n=o}^{\infty} n\cos(n\theta)\left[R_{m,n}(k_p r,\, G,\, I)\right] \tag{3.56}$$

$$V_{mz} = 0 \tag{3.57}$$

where

$$R_{m,n}(k_e r, D, F) = H_n^{(1)}(k_{e,m} r)\, D_{m,n} + H_n^{(2)}(k_{e,m} r)\, F_{m,n} \tag{3.58}$$

$$R'_{m,n}(k_p r, G, I) = H_n^{(1)'}(k_{p,m} r)\, G_{m,n} + H_n^{(2)'}(k_{p,m} r)\, I_{m,n} \tag{3.59}$$

$$R'_{m,n}(k_e r, D, F) = H_n^{(1)'}(k_{e,m} r)\, D_{m,n} + H_n^{(2)'}(k_{e,m} r)\, F_{m,n} \tag{3.60}$$

$$R_{m,n}(k_p r, G, I) = H_n^{(1)}(k_{p,m} r)\, G_{m,n} + H_n^{(2)}(k_{p,m} r)\, I_{m,n} \quad . \tag{3.61}$$

The last quantity to be determined is the electric field $\vec{E}_m$. From Eqs. (3.51) and (3.21), the electric field $\vec{E}_m$ can be expressed as

$$\vec{E}_m = \frac{1}{j\omega\xi_m} \nabla \times \vec{H}_m + \frac{jev_o^2}{\omega\xi_m(\nu_m + j\omega)} \nabla n_{1,m} \quad . \tag{3.62}$$

Substituting Eqs.(3.53) and (3.54), into Eq. (3.62), the components of $\vec{E}_m$ field can be obtained as

$$E_{mr} = \frac{j}{\omega\xi_m r} \sum_{n=o}^{\infty} n\sin(n\theta)\left[R_{m,n}(k_e r, D, F)\right] + \frac{jev_o^2 k_{p,m}}{\omega\xi_m(\nu_m + j\omega)} \sum_{n=o}^{\infty} \sin(n\theta)\left[R'_{m,n}(k_p r, G, I)\right] \tag{3.63}$$

$$E_{m\theta} = \frac{jk_{e,m}}{\omega\xi_m} \sum_{n=o}^{\infty} \cos(n\theta)\left[R'_{m,n}(k_e r, D, F)\right] + \frac{jev_o^2}{\omega\xi_m(\nu_m + j\omega)r} \sum_{n=o}^{\infty} n\cos(n\theta)\left[R_{m,n}(k_p r, G, I)\right] \tag{3.64}$$

$$E_{mz} = 0 \tag{3.65}$$

where the expression for those $\left[R_n(k r)\right]'$s are given in Eqs. (3.58) to (3.61). Up to this point, all the relevant quantities, $\vec{H}_m$, $n_{1,m}$, $\vec{V}_m$ and $\vec{E}_m$, have been explicitly determined. Those unknown constants associated with these four quantities will be determined by matching boundary conditions in the next section.

3.5 Matching Boundary Conditions at Interfaces

Four relevant field quantities in the mth sublayer of the plasma medium are $\vec{E}_m$, $\vec{H}_m$, $n_{1,m}$ and $\vec{V}_m$. Associated with these field quantities, there are four unknown constants, $D_{m,n}$, $F_{m,n}$, $G_{m,n}$, $I_{m,n}$. In applying the stratification method, the field quantities are matched at the interface of two adjacent sublayers and the four unknown constants in a sublayer are expressed in terms of the corresponding four unknown constants in the adjacent sublayer. Since there are four unknown constants to be determined, four independent boundary conditions are needed at the interface. We will derive four independent boundary conditions from four basic equations used in Section 3.4.

For the needed four boundary conditions, three of them are rather conventional. They are the continuity of the tangential components of electric field and magnetic field and the continuity of the particle flux. The fourth boundary condition is not a trivial one and is not uniquely known since various forms are used by various workers.[18,21, 22, 23, 7] In our study, the fourth boundary condition will be directly derived from the force equation.

Let us consider the boundary condition at $r = r_m$ which is the interface between the mth and (m+1)th sublayers.

Equation (3.16) will readily lead to a boundary condition of

tangential component of $\vec{E}$ field is continuous.

In the present study, this implies that

$$E_{m\theta} = E_{(m+1)\theta} \quad \text{at } r = r_m \quad . \tag{3.66}$$

Equation (3.17) can be used to derive a boundary condition of

tangential component of $\vec{H}$ field is continuous

if no surface current is assumed on the interface. In the present study, this condition gives

$$H_{mz} = H_{(m+1)z} \qquad \text{at } r = r_m \ . \tag{3.67}$$

The third boundary condition will be derived from the original form of Eq. (3.20). The original equation for the continuity of particles is

$$\nabla\cdot(n_e \vec{V}) + \frac{\partial n_e}{\partial t} = 0 \tag{3.68}$$

where n_e is the total electron density which is the sum of the average electron density n_o and the density deviation n_1 . Integrating Eq. (3.68) over the pill box as shown in Fig. 3.2, we have

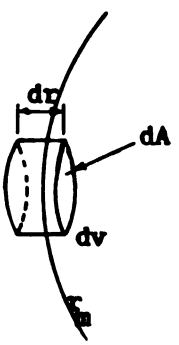

Fig. 3.2 The interface at $r = r_m$

$$\int \nabla\cdot(n_e\vec{V})\, dv + \int \frac{\partial n_e}{\partial t}\, dv = 0 \ . \tag{3.69}$$

If we let the increment dr approach to zero, the limiting case will be

$$\lim_{dr\to o} \int \nabla\cdot(n_e\vec{V})\, drdA + \frac{\partial}{\partial t} \lim_{dr\to o} \int n_e drdA = 0 \ . \tag{3.70}$$

The last term of the above equation approaches zero, provided n_e is finite accross the boundary. Thus, using the divergence theorem, the above equation can be written as

$$\lim_{dr\to o} \int (n_e\vec{V})\cdot\hat{n}\, ds = 0 \tag{3.71}$$

where $\hat{n}$ is the unit vector pointing outward of the surface of pill box. This equation then leads to

$$n_{e,m} V_{mr} - n_{e,m+1} V_{(m+1)r} = 0 \qquad \text{at } r = r_m \tag{3.72}$$

where subscripts m and m+1 identify the sublayers and subscript r denotes the radial component. Since the total electron density $n_{e,m}$ is

$$n_{e,m} = n_{o,m} + n_{1,m} \approx n_{o,m} , \tag{3.73}$$

under the linearized assumption, Eq. (3.72) can be reduced to

$$n_{o,m} V_{mr} - n_{o,m+1} V_{(m+1)r} = 0 \qquad \text{at } r = r_m . \tag{3.74}$$

Equation (3.74) is the third boundary condition to be used in our analysis.

The fourth boundary condition will be derived from the original form of the force equation. The force equation as expressed in Eq. (3.21) is a linearized form containing only a.c. component. The original force equation contains both a.c. and d.c. components and can be expressed as

$$\frac{\partial \vec{V}}{\partial t} + \nu \vec{V} = - \frac{e}{M} \vec{E}_t - \frac{1}{n_e M} \nabla P \approx - \frac{e}{M} \vec{E}_t - \frac{1}{n_o M} \nabla P \tag{3.75}$$

where ν is the collision frequency, P is the pressure and $\vec{E}_t$ is the total $\vec{E}$ field including both a.c. and d.c. components. Mathematically we write

$$\vec{E}_t = \vec{E}_{d.c.} + \vec{E} . \tag{3.76}$$

The gradient of pressure can be shown in Appendix A to be

$$\nabla P = kT \nabla n_o + 3\, kT \nabla n_1 \tag{3.77}$$

where the term, ∇n_o, gives d.c. component and ∇n_1 gives a.c. component. Substituting Eq. (3.77) in Eq. (3.75) and taking d.c. component out of Eq. (3.75) we have

$$0 = - \frac{e}{M} \vec{E}_{d.c.} - \frac{kT}{n_o M} \nabla n_o . \tag{3.78}$$

Equation (3.78) implies that there exists a static $\vec{E}$ field if the

stationary plasma is non-uniform. Physically, it means that the stationary density variation is maintained by a static electric force acting on the electrons. In our analysis using the stratification method, step density discontinuities are assumed to approximate a non-uniform density profile. Therefore, delta function type of static $\vec{E}$ fields should exist theoretically at the points of step discontinuities or the interfaces between sublayers. This phenomenon is explained graphically in Fig. 3.3.

The a.c. component of Eq. (3.75) is

$$(\nu + j\omega)\,\vec{V} = -\frac{e}{M}\vec{E} - \frac{v_o^2}{n_o}\nabla n_1 \tag{3.79}$$

for the $\exp(j\omega t)$ time dependence. Integrating Eq. (3.79) over the pill box shown in Fig. 3.2, we obtain

$$\int (\nu+j\omega)\,\vec{V}\,dv = -\frac{e}{M}\int \vec{E}\,dv - v_o^2 \int \frac{1}{n_o}\nabla n_1 dv. \tag{3.80}$$

The limting case of Eq. (3.80) as dr approaching zero is

$$\lim_{dr\to o}\int (\nu+j\omega)\,\vec{V}\,drdA = -\lim_{dr\to o}\frac{e}{M}\int \vec{E}\,drdA - v_o^2 \int \frac{1}{n_o}\nabla n_1\,drdA. \tag{3.81}$$

In Eq. (3.81) the first two terms approach zero since the volume goes to zero and the quantities in the integrands, $\vec{V}$ and $\vec{E}$, are finite accross the boundary. Thus Eq. (3.81) becomes

$$\lim_{dr\to o} v_o^2 \int \frac{1}{n_o}\nabla n_1\,drdA = 0\ . \tag{3.82}$$

Since the step discontinuity of density is balanced out by the static $\vec{E}$ field and the density is constant within each sublayer, Eq. (3.82) can be expressed as

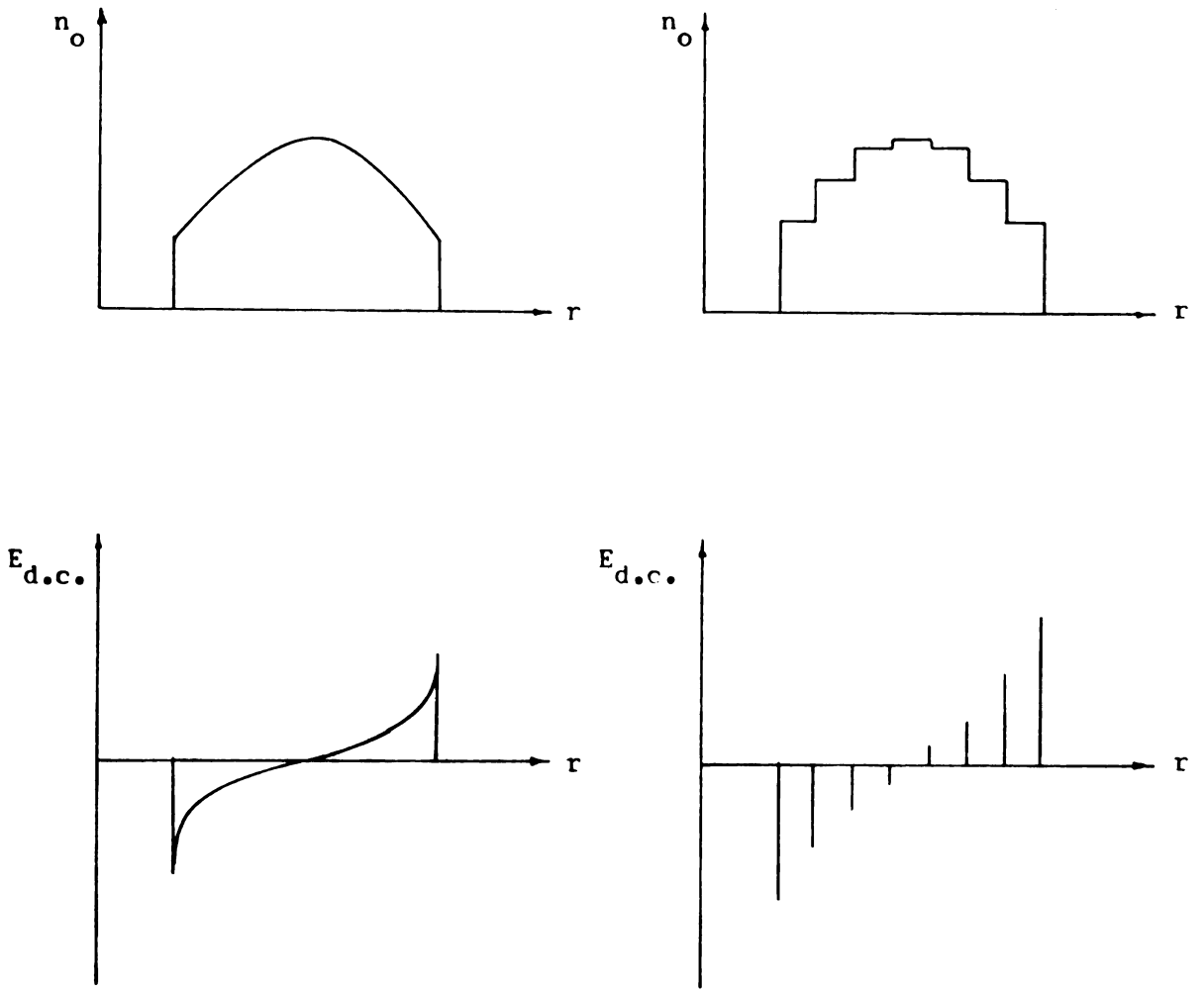

Fig. 3.3 Stationary electron density profiles and associated static $E_{d.c.}$ fields.

$$\lim_{dr\to o} \int \nabla \frac{n_1}{n_o} \, drdA = 0 \quad . \tag{3.83}$$

This step is justified because the singular part of ∇n_o has been taken into account in Eq. (3.78). Applying the gradient theorem, we have at the boundary of $r = r_m$

$$\frac{n_{1,m}}{n_{o,m}} - \frac{n_{1,m+1}}{n_{o,m+1}} = 0 \qquad \text{at } r = r_m \quad . \tag{3.84}$$

Up to this point, four independent boundary conditions have been derived in Eqs. (3.66), (3.67), (3.74) and (3.84). Applying the boundary condition of Eq. (3.67), we have

$$\sum_{n=o}^{\infty} \cos(n\theta) \; R_{m,n}(k_e r_m, D, F) = \sum_{n=o}^{\infty} \cos(n\theta) \; R_{m+1,n}(k_e r_m, D, F) \quad . \tag{3.85}$$

Due to the orthogonality of $\cos(n\theta)$ function, Eq. (3.85) leads to

$$H_n^{(1)}(k_{e,m} r_m) \, D_{m,n} + H_n^{(2)}(k_{e,m} r_m) \, F_{m,n} = H_n^{(1)}(k_{e,m+1} r_m) \, D_{m+1,n} + H_n^{(2)}(k_{e,m+1} r_m) \, F_{m+1,n} \quad . \tag{3.86}$$

The boundary condition of Eq. (3.66) can be used to derive an expression such as

$$\frac{k_{e,m}}{\xi_m} H_n^{(1)'}(k_{e,m} r_m) \, D_{m,n} + \frac{k_{e,m}}{\xi_m} H_n^{(2)'}(k_{e,m} r_m) \, F_{m,n} + \frac{ev_o^2 n \, H_n^{(1)}(k_{p,m} r_m)}{\xi_m (\nu_m + j\omega) \, r_m} G_{m,n} + \frac{ev_o^2 n \, H_n^{(2)}(k_{p,m} r_m)}{\xi_m (\nu_m + j\omega) \, r_m} I_{m,n} = \frac{k_{e,m+1}}{\xi_{m+1}} H_n^{(1)'}(k_{e,m+1} r_m) \, D_{m+1,n} + \frac{k_{e,m+1}}{\xi_{m+1}} H_n^{(2)'}(k_{e,m+1} r_m) \, F_{m+1,n}$$

$$+\frac{\epsilon v_o^2 n H_n^{(1)}(k_{p,m+1} r_m)}{\xi_{m+1}(\nu_{m+1}+j\omega)\, r_m} G_{m+1,n} + \frac{\epsilon v_o^2 n H_n^{(2)}(k_{p,m+1} r_m)}{\xi_{m+1}(\nu_{m+1}+j\omega)\, r_m} I_{m+1,n} \quad . \tag{3.87}$$

From the boundary condition of Eq. (3.74), we obtain

$$\frac{jen_{o,m}}{\omega\xi_m M(\nu_m+j\omega)\, r_m} \sum_{n=o}^{\infty} n\sin(n\theta)\left[R_{m,n}(k_e r_m, D, F)\right]$$

$$+\frac{v_o^2 \epsilon_o k_{p,m}}{\xi_m(\nu_m+j\omega)} \sum_{n=o}^{\infty} \sin(n\theta)\left[R'_{m,n}(k_p r_m, G, I)\right]$$

$$= \frac{jen_{o,m+1}}{\omega\xi_{m+1} M(\nu_{m+1}+j\omega)\, r_m} \sum_{n=o}^{\infty} n\sin(n\theta)\left[R_{m+1,n}(k_e r_m, D, F)\right]$$

$$+\frac{v_o^2 \epsilon_o k_{p,m+1}}{\xi_{m+1}(\nu_{m+1}+j\omega)} \sum_{n=o}^{\infty} \sin(n\theta)\left[R'_{m+1,n}(k_p r_m, G, I)\right] \quad . \tag{3.88}$$

Due to the orthogonality of $\sin(n\theta)$ function, it yields

$$\frac{jen_{o,m}\, n\, H_n^{(1)}(k_{e,m} r_m)}{\xi_m \omega\, M(\nu_m+j\omega)\, r_m} D_{m,n} + \frac{jen_{o,m}\, n\, H_n^{(2)}(k_{e,m} r_m)}{\xi_m \omega\, M(\nu_m+j\omega)\, r_m} F_{m,n}$$

$$+\frac{v_o^2 \epsilon_o k_{p,m}\, H_n^{(1)'}(k_{p,m} r_m)}{\xi_m(\nu_m+j\omega)} G_{m,n} + \frac{v_o^2 \epsilon_o k_{p,m}\, H_n^{(2)'}(k_{p,m} r_m)}{\xi_m(\nu_m+j\omega)} I_{m,n}$$

$$= \frac{jen_{o,m+1}\, n\, H_n^{(1)}(k_{e,m+1} r_m)}{\xi_{m+1} \omega\, M(\nu_{m+1}+j\omega)\, r_m} D_{m+1,n} + \frac{jen_{o,m+1}\, n\, H_n^{(2)}(k_{e,m+1} r_m)}{\xi_{m+1} \omega\, M(\nu_{m+1}+j\omega)\, r_m} F_{m+1,n}$$

$$+\frac{v_o^2 \epsilon_o k_{p,m+1}\, H_n^{(1)'}(k_{p,m+1} r_m)}{\xi_{m+1}(\nu_{m+1}+j\omega)} G_{m+1,n} + \frac{v_o^2 \epsilon_o k_{p,m+1}\, H_n^{(2)'}(k_{p,m+1} r_m)}{\xi_{m+1}(\nu_{m+1}+j\omega)} I_{m+1,n} \quad . \tag{3.89}$$

From the boundary condition of Eq. (3.84), we obtain

$$\frac{H_n^{(1)}(k_{p,m}r_m)}{n_{o,m}} G_{m,n} + \frac{H_n^{(2)}(k_{p,m}r_m)}{n_{o,m}} I_{m,n}$$

$$= \frac{H_n^{(1)}(k_{p,m+1}r_m)}{n_{o,m+1}} G_{m+1,n} + \frac{H_n^{(2)}(k_{p,m+1}r_m)}{n_{o,m+1}} I_{m+1,n} \quad . \tag{3.90}$$

Equation (3.86), (3.87), (3.89) and (3.90) can be written in a matrix form and after rearrangement we obtain a matrix equation as

$$\begin{bmatrix} D_{m,n} \\ F_{m,n} \\ G_{m,n} \\ I_{m,n} \end{bmatrix} = \left[L_n(k_{e,m},k_{p,m},r_m) \right]^{-1} \left[L_n(k_{e,m+1},k_{p,m+1},r_m) \right] \begin{bmatrix} D_{m+1,n} \\ F_{m+1,n} \\ G_{m+1,n} \\ I_{m+1,n} \end{bmatrix} \tag{3.91}$$

where

$$\left[L_n(k_{e,m},k_{p,m},r_m) \right]^{-1} =$$

$$\begin{bmatrix} L_{m,n}(1,1) & L_{m,n}(1,2) & L_{m,n}(1,3) & L_{m,n}(1,4) \\ L_{m,n}(2,1) & L_{m,n}(2,2) & L_{m,n}(2,3) & L_{m,n}(2,4) \\ L_{m,n}(3,1) & L_{m,n}(3,2) & L_{m,n}(3,3) & L_{m,n}(3,4) \\ L_{m,n}(4,1) & L_{m,n}(4,2) & L_{m,n}(4,3) & L_{m,n}(4,4) \end{bmatrix} \tag{3.92}$$

and

$$\left[L_n(k_{e,m+1},k_{p,m+1},r_m) \right] =$$

$$\begin{bmatrix} L_{m+1,n}(1,1) & L_{m+1,n}(1,2) & L_{m+1,n}(1,3) & L_{m+1,n}(1,4) \\ L_{m+1,n}(2,1) & L_{m+1,n}(2,2) & L_{m+1,n}(2,3) & L_{m+1,n}(2,4) \\ L_{m+1,n}(3,1) & L_{m+1,n}(3,2) & L_{m+1,n}(3,3) & L_{m+1,n}(3,4) \\ L_{m+1,n}(4,1) & L_{m+1,n}(4,2) & L_{m+1,n}(4,3) & L_{m+1,n}(4,4) \end{bmatrix} \tag{3.93}$$

with

$$L_{m,n}(1,1) = H_n^{(1)}(k_{e,m}r_m) \tag{3.94}$$

$$L_{m,n}(1,2) = H_n^{(2)}(k_{e,m}r_m) \tag{3.95}$$

$$L_{m,n}(1,3) = 0 \tag{3.96}$$

$$L_{m,n}(1,4) = 0 \tag{3.97}$$

$$L_{m,n}(2,1) = \frac{k_{e,m}}{\xi_m} H_n^{(1)'}(k_{e,m}r_m) \tag{3.98}$$

$$L_{m,n}(2,2) = \frac{k_{e,m}}{\xi_m} H_n^{(2)'}(k_{e,m}r_m) \tag{3.99}$$

$$L_{m,n}(2,3) = \frac{ev_o^2 n\, H_n^{(1)}(k_{p,m}r_m)}{\xi_m(\nu_m+j\omega)\, r_m} \tag{3.100}$$

$$L_{m,n}(2,4) = \frac{ev_o^2 n\, H_n^{(2)}(k_{p,m}r_m)}{\xi_m(\nu_m+j\omega)\, r_m} \tag{3.101}$$

$$L_{m,n}(3,1) = \frac{jen_{o,m} n\, H_n^{(1)}(k_{e,m}r_m)}{\xi_m \omega\, M(\nu_m+j\omega)\, r_m} \tag{3.102}$$

$$L_{m,n}(3,2) = \frac{jen_{o,m} n\, H_n^{(2)}(k_{e,m}r_m)}{\xi_m \omega\, M(\nu_m+j\omega)\, r_m} \tag{3.103}$$

$$L_{m,n}(3,3) = \frac{v_o^2 \epsilon_o k_{p,m} H_n^{(1)'}(k_{p,m} r_m)}{\xi_m(\nu_m + j\omega)} \tag{3.104}$$

$$L_{m,n}(3,4) = \frac{v_o^2 \epsilon_o k_{p,m} H_n^{(2)'}(k_{p,m} r_m)}{\xi_m(\nu_m + j\omega)} \tag{3.105}$$

$$L_{m,n}(4,1) = 0 \tag{3.106}$$

$$L_{m,n}(4,2) = 0 \tag{3.107}$$

$$L_{m,n}(4,3) = \frac{H_n^{(1)}(k_{p,m} r_m)}{n_{o,m}} \tag{3.108}$$

$$L_{m,n}(4,4) = \frac{H_n^{(2)}(k_{p,m} r_m)}{n_{o,m}} \tag{3.109}$$

$$L_{m+1,n}(1,1) = H_n^{(1)}(k_{e,m+1} r_m) \tag{3.110}$$

$$L_{m+1,n}(1,2) = H_n^{(2)}(k_{e,m+1} r_m) \tag{3.111}$$

$$L_{m+1,n}(1,3) = 0 \tag{3.112}$$

$$L_{m+1,n}(1,4) = 0 \tag{3.113}$$

$$L_{m+1,n}(2,1) = \frac{k_{e,m+1}}{\xi_{m+1}} H_n^{(1)'}(k_{e,m+1} r_m) \tag{3.114}$$

$$L_{m+1,n}(2,2) = \frac{k_{e,m+1}}{\xi_{m+1}} H_n^{(2)'}(k_{e,m+1} r_m) \tag{3.115}$$

$$L_{m+1,n}(2,3) = \frac{ev_o^2 n\, H_n^{(1)}(k_{p,m+1} r_m)}{\xi_{m+1}(\nu_{m+1}+j\omega)\, r_m} \tag{3.116}$$

$$L_{m+1,n}(2,4) = \frac{ev_o^2 n\, H_n^{(2)}(k_{p,m+1} r_m)}{\xi_{m+1}(\nu_{m+1}+j\omega)\, r_m} \tag{3.117}$$

$$L_{m+1,n}(3,1) = \frac{jen_{o,m+1} n\, H_n^{(1)}(k_{e,m+1} r_m)}{\xi_{m+1}\omega\, M(\nu_{m+1}+j\omega)\, r_m} \tag{3.118}$$

$$L_{m+1,n}(3,2) = \frac{jen_{o,m+1} n\, H_n^{(2)}(k_{e,m+1} r_m)}{\xi_{m+1}\omega\, M(\nu_{m+1}+j\omega)\, r_m} \tag{3.119}$$

$$L_{m+1,n}(3,3) = \frac{v_o^2 \epsilon_o k_{p,m+1}\, H_n^{(1)'}(k_{p,m+1} r_m)}{\xi_{m+1}(\nu_{m+1}+j\omega)} \tag{3.120}$$

$$L_{m+1,n}(3,4) = \frac{v_o^2 \epsilon_o k_{p,m+1}\, H_n^{(2)'}(k_{p,m+1} r_m)}{\xi_{m+1}(\nu_{m+1}+j\omega)} \tag{3.121}$$

$$L_{m+1,n}(4,1) = 0 \tag{3.122}$$

$$L_{m+1,n}(4,2) = 0 \tag{3.123}$$

$$L_{m+1,n}(4,3) = \frac{H_n^{(1)}(k_{p,m+1} r_m)}{n_{o,m+1}} \tag{3.124}$$

$$L_{m+1,n}(4,4) = \frac{H_n^{(2)}(k_{p,m+1} r_m)}{n_{o,m+1}} \,. \tag{3.125}$$

Up to this point, it is possible to express four unknown constants of the mth sublayer in terms of the corresponding four unknown constants of the (m+1)th sublayer. By applying the same boundary conditions at the interface of $r = r_{m+1}$ between the (m+1)th sublayer and the (m+2)th sublayer and following the same procedure, we can obtain a relation between the unknown constants in the (m+1)th and the (m+2)th sublayers as

$$\begin{bmatrix} D_{m+1,n} \\ F_{m+1,n} \\ G_{m+1,n} \\ I_{m+1,n} \end{bmatrix} = \left[L_n(k_{e,m+1}, k_{p,m+1}, r_{m+1}) \right]^{-1} \left[L_n(k_{e,m+2}, k_{p,m+2}, r_{m+1}) \right] \begin{bmatrix} D_{m+2,n} \\ F_{m+2,n} \\ G_{m+2,n} \\ I_{m+2,n} \end{bmatrix} . \tag{3.126}$$

Substituting $D_{m+1,n}$, $F_{m+1,n}$, $G_{m+1,n}$ and $I_{m+1,n}$ as expressed in Eq.(3.126) into Eq. (3.91), we can express $D_{m,n}$, $F_{m,n}$, $G_{m,n}$ and $I_{m,n}$ in terms of $D_{m+2,n}$, $F_{m+2,n}$, $G_{m+2,n}$ and $I_{m+2,n}$ as

$$\begin{bmatrix} D_{m,n} \\ F_{m,n} \\ G_{m,n} \\ I_{m,n} \end{bmatrix} = \left[L_n(k_{e,m}, k_{p,m}, r_m) \right]^{-1} \left[L_n(k_{e,m+1}, k_{p,m+1}, r_m) \right]$$

$$\left[L_n(k_{e,m+1}, k_{p,m+1}, r_{m+1}) \right]^{-1} \left[L_n(k_{e,m+2}, k_{p,m+2}, r_{m+1}) \right] \begin{bmatrix} D_{m+2,n} \\ F_{m+2,n} \\ G_{m+2,n} \\ I_{m+2,n} \end{bmatrix} . \tag{3.127}$$

Following the same procedure of matching the boundary conditions at the interfaces of sublayers successively, it is possible to express the unknown constants of $D_{1,n}$, $F_{1,n}$, $G_{1,n}$ and $I_{1,n}$ in the first sublayer in terms of the unknown constants of $D_{s,n}$, $F_{s,n}$, $G_{s,n}$ and $I_{s,n}$ in the last inmost sublayer as

$$\begin{bmatrix} D_{1,n} \\ F_{1,n} \\ G_{1,n} \\ I_{1,n} \end{bmatrix} = \left[L_n(k_{e,1},k_{p,1},r_1)\right]^{-1}\left[L_n(k_{e,2},k_{p,2},r_1)\right]$$

$$\left[L_n(k_{e,2},k_{p,2},r_2)\right]^{-1}\left[L_n(k_{e,3},k_{p,3},r_2)\right] \cdots$$

$$\cdots \left[L_n(k_{e,s-1},k_{p,s-1},r_{s-1})\right]^{-1}\left[L_n(k_{e,s},k_{p,s},r_{s-1})\right]\begin{bmatrix} D_{s,n} \\ F_{s,n} \\ G_{s,n} \\ I_{s,n} \end{bmatrix} . \tag{3.128}$$

Equation (3.128) can be expressed in shorthand as

$$\begin{bmatrix} D_{1,n} \\ F_{1,n} \\ G_{1,n} \\ I_{1,n} \end{bmatrix} = \begin{bmatrix} M_n(1,1) & M_n(1,2) & M_n(1,3) & M_n(1,4) \\ M_n(2,1) & M_n(2,2) & M_n(2,3) & M_n(2,4) \\ M_n(3,1) & M_n(3,2) & M_n(3,3) & M_n(3,4) \\ M_n(4,1) & M_n(4,2) & M_n(4,3) & M_n(4,4) \end{bmatrix}\begin{bmatrix} D_{s,n} \\ F_{s,n} \\ G_{s,n} \\ I_{s,n} \end{bmatrix} \tag{3.129}$$

where $M_n(i,j)$'s are the entries of the matrix which is the product of those $[L_n]$matrices in Eq. (3.128).

Let's now consider the interface between free space and the

glass wall at r = c. The continuity of the tangential components of $\vec{E}$ and $\vec{H}$ fields leads to

$$H_{oz}^{t} = H_{gz} \qquad \text{at } r = c \tag{3.130}$$

and

$$E_{o\theta}^{t} = E_{g\theta} \qquad \text{at } r = c \tag{3.131}$$

where H_{oz}^{t} amd $E_{o\theta}^{t}$ are given in Eqs. (3.6) and (3.9) and H_{gz}, $E_{g\theta}$ are given in Eqs. (3.11) and (3.14) respectively. The substitution of H_{oz}^{t}, $E_{o\theta}^{t}$, H_{gz} and $E_{g\theta}$ in Eqs. (3.130) and (3.131) leads to

$$- H_n^{(2)}(k_o c)\, A_n + H_n^{(1)}(k_g c)\, B_n + H_n^{(2)}(k_g c)\, C_n = \epsilon_{on}(-j)^n J_n(k_o c) \tag{3.132}$$

$$- H_n^{(2)'}(k_o c)\, A_n + \frac{1}{\sqrt{\epsilon_g}} H_n^{(1)'}(k_g c)\, B_n + \frac{1}{\sqrt{\epsilon_g}} H_n^{(2)'}(k_g c)\, C_n = \epsilon_{on}(-j)^n J_n'(k_o c) \ . \tag{3.133}$$

Next, we consider the interface between the glass wall and the first sublayer of plasma at r = b. The continuity of the tangential components of $\vec{H}$ and $\vec{E}$ fields lead to

$$- H_n^{(1)}(k_g b)\, B_n - H_n^{(2)}(k_g b)\, C_n + H_n^{(1)}(k_{e,1} b)\, D_{1,n} + H_n^{(2)}(k_{e,1} b)\, F_{1,n} = 0 \tag{3.134}$$

$$-\frac{\zeta_o}{\sqrt{\epsilon_g}} H_n^{(1)'}(k_g b)\, B_n - \frac{\zeta_o}{\sqrt{\epsilon_g}} H_n^{(2)'}(k_g b)\, C_n + \sqrt{\frac{\mu_o}{\xi_1}} H_n^{(1)'}(k_{e,1} b)\, D_{1,n}$$

$$+\sqrt{\frac{\mu_o}{\xi_1}} H_n^{(2)'}(k_{e,1} b)\, F_{1,n} + \frac{ev_o^2 n}{\omega\xi_1(\nu_1+j\omega)b} H_n^{(1)}(k_{p,1} b)\, G_{1,n}$$

$$+\frac{ev_o^2 n}{\omega\xi_1(\nu_1+j\omega)b} H_n^{(2)}(k_{p,1} b)\, I_{1,n} = 0 \quad . \tag{3.135}$$

Two additional boundary conditions for the induced electron velocity on the rigid surfaces of the glass wall and the metallic cylinder can be used. Assuming that the surfaces of the glass wall and the metallic cylinder are rigid, the normal component of the induced electron velocity at those surfaces can be required to vanish. This boundary condition has been used by numerous workers.[18, 24] Applying this boundary condition to the r component of induced electron velocity, v_r, at r = b and r = a and using Eq. (3.55), we obtain

$$\frac{jen}{\omega Mb} H_n^{(1)}(k_{e,1} b)\, D_{1,n} + \frac{jen}{\omega Mb} H_n^{(2)}(k_{e,1} b)\, F_{1,n}$$

$$+\frac{v_o^2 \epsilon_o k_{p,1}}{n_{o,1}} H_n^{(1)'}(k_{p,1} b)\, G_{1,n} + \frac{v_o^2 \epsilon_o k_{p,1}}{n_{o,1}} H_n^{(2)'}(k_{p,1} b)\, I_{1,n} = 0 \tag{3.136}$$

and

$$\frac{jen}{\omega Ma} H_n^{(1)}(k_{e,s} a)\, D_{s,n} + \frac{jen}{\omega Ma} H_n^{(2)}(k_{e,s} a)\, F_{s,n}$$

$$+\frac{v_o^2 \epsilon_o k_{p,s}}{n_{o,s}} H_n^{(1)'}(k_{p,s} b)\, G_{s,n} + \frac{v_o^2 \epsilon_o k_{p,s}}{n_{o,s}} H_n^{(2)'}(k_{p,s} a)\, I_{s,n} = 0 \quad . \tag{3.137}$$

Since the metallic cylinder is assumed to be perfectly conducting, the tangential component of $\vec{E}$ field is required to vanish at its surface. This boundary condition will lead to

$$k_{e,s} H_n^{(1)'}(k_{e,s}a) D_{s,n} + K_{e,s} H_n^{(2)'}(k_{e,s}a) F_{s,n}$$

$$+ \frac{ev_o^2 n}{(\nu_s+j\omega)a} H_n^{(1)}(k_{p,s}a) G_{s,n} + \frac{ev_o^2 n}{(\nu_s+j\omega)a} H_n^{(2)}(k_{p,s}a) I_{s,n} = 0 \quad (3.138)$$

Seven boundary conditions as expressed in Eqs. (3.132) to (3.138) contain eleven unknown constants, A_n, B_n, C_n, $D_{l,n}$, $F_{l,n}$, $G_{l,n}$, $I_{l,n}$, $D_{s,n}$, $F_{s,n}$, $G_{s,n}$, and $I_{s,n}$. However, the constants, $D_{l,n}$, $F_{l,n}$, $G_{l,n}$, $I_{l,n}$ can be expressed in terms of the constants, $D_{s,n}$, $F_{s,n}$, $G_{s,n}$, $I_{s,n}$ in a manner as indicated by Eq. (3.129). With this substitution, we obtain a set of seven independent equations with seven unknown constants, A_n, B_n, C_n, $D_{s,n}$, $F_{s,n}$, $G_{s,n}$ and $I_{s,n}$. This set of simultaneous equation can be expressed in a matrix form as

$$[Q_n] \begin{bmatrix} A_n \\ B_n \\ C_n \\ D_{s,n} \\ F_{s,n} \\ G_{s,n} \\ I_{s,n} \end{bmatrix} = \begin{bmatrix} Q_n(1,8) \\ Q_n(2,8) \\ 0 \\ 0 \\ 0 \\ 0 \\ 0 \end{bmatrix} \quad (3.139)$$

where $[Q_n]$ is the matrix given by

$$[Q_n] = \begin{bmatrix} Q_n(1,1) & Q_n(1,2) & Q_n(1,3) & 0 & 0 & 0 & 0 \\ Q_n(2,1) & Q_n(2,2) & Q_n(2,3) & 0 & 0 & 0 & 0 \\ 0 & Q_n(3,2) & Q_n(3,3) & Q_n(3,4) & Q_n(3,5) & Q_n(3,6) & Q_n(3,7) \\ 0 & Q_n(4,2) & Q_n(4,3) & Q_n(4,4) & Q_n(4,5) & Q_n(4,6) & Q_n(4,7) \\ 0 & 0 & 0 & Q_n(5,4) & Q_n(5,5) & Q_n(5,6) & Q_n(5,7) \\ 0 & 0 & 0 & Q_n(6,4) & Q_n(6,5) & Q_n(6,6) & Q_n(6,7) \\ 0 & 0 & 0 & Q_n(7,4) & Q_n(7,5) & Q_n(7,6) & Q_n(7,7) \end{bmatrix} . \tag{3.140}$$

The matrix entries $Q_n(i,j)$'s are expressed explicitly as follows:

$$Q_n(1,1) = - H_n^{(2)}(k_o c) \tag{3.141}$$

$$Q_n(1,2) = H_n^{(1)}(k_g c) \tag{3.142}$$

$$Q_n(1,3) = H_n^{(2)}(k_g c) \tag{3.143}$$

$$Q_n(1,8) = \epsilon_{on}(-j)^n J_n(k_o c) \tag{3.144}$$

$$Q_n(2,1) = -H_n^{(2)'}(k_o c) \tag{3.145}$$

$$Q_n(2,2) = \frac{1}{\sqrt{\epsilon_g}} H_n^{(1)'}(k_g c) \tag{3.146}$$

$$Q_n(2,3) = \frac{1}{\sqrt{\epsilon_g}} H_n^{(2)'}(k_g c) \tag{3.147}$$

$$Q_n(2,8) = \epsilon_{on}(-j)^n J_n'(k_o c) \tag{3.148}$$

$$Q_n(3,2) = -H_n^{(1)}(k_g b) \tag{3.149}$$

$$Q_n(3,3) = -H_n^{(2)}(k_g b) \tag{3.150}$$

$$Q_n(3,4) = H_n^{(1)}(k_{e,1}b)\, M_n(1,1) + H_n^{(2)}(k_{e,1}b)\, M_n(2,1) \tag{3.151}$$

$$Q_n(3,5) = H_n^{(1)}(k_{e,1}b)\, M_n(1,2) + H_n^{(2)}(k_{e,1}b)\, M_n(2,2) \tag{3.152}$$

$$Q_n(3,6) = H_n^{(1)}(k_{e,1}b)\, M_n(1,3) + H_n^{(2)}(k_{e,1}b)\, M_n(2,3) \tag{3.153}$$

$$Q_n(3,7) = H_n^{(1)}(k_{e,1}b)\, M_n(1,4) + H_n^{(2)}(k_{e,1}b)\, M_n(2,4) \tag{3.154}$$

$$Q_n(4,2) = -\frac{\zeta_o}{\sqrt{\epsilon_g}} H_n^{(1)'}(k_g b) \tag{3.155}$$

$$Q_n(4,3) = -\frac{\zeta_o}{\sqrt{\epsilon_g}} H_n^{(2)'}(k_g b) \tag{3.156}$$

$$\begin{aligned} Q_n(4,4) = {} & \sqrt{\frac{\mu_o}{\xi_1}}\, H_n^{(1)'}(k_{e,1}b)\, M_n(1,1) + \sqrt{\frac{\mu_o}{\xi_1}}\, H_n^{(2)'}(k_{e,1}b)\, M_n(2,1) \\ & + \frac{ev_o^2 n\, H_n^{(1)}(k_{p,1}b)}{\omega\xi_1(\nu_1+j\omega)b} M_n(3,1) + \frac{ev_o^2 n\, H_n^{(2)}(k_{p,1}b)}{\omega\xi_1(\nu_1+j\omega)b} M_n(4,1) \end{aligned} \tag{3.157}$$

$$\begin{aligned} Q_n(4,5) = {} & \sqrt{\frac{\mu_o}{\xi_1}}\, H_n^{(1)'}(k_{e,1}b)\, M_n(1,2) + \sqrt{\frac{\mu_o}{\xi_1}}\, H_n^{(2)'}(k_{e,1}b)\, M_n(2,2) \\ & + \frac{ev_o^2 n\, H_n^{(1)}(k_{p,1}b)}{\omega\xi_1(\nu_1+j\omega)b} M_n(3,2) + \frac{ev_o^2 n\, H_n^{(2)}(k_{p,1}b)}{\omega\xi_1(\nu_1+j\omega)b} M_n(4,2) \end{aligned} \tag{3.158}$$

$$\begin{aligned} Q_n(4,6) = {} & \sqrt{\frac{\mu_o}{\xi_1}}\, H_n^{(1)'}(k_{e,1}b)\, M_n(1,3) + \sqrt{\frac{\mu_o}{\xi_1}}\, H_n^{(2)'}(k_{e,1}b)\, M_n(2,3) \\ & + \frac{ev_o^2 n\, H_n^{(1)}(k_{p,1}b)}{\omega\xi_1(\nu_1+j\omega)b} M_n(3,3) + \frac{ev_o^2 n\, H_n^{(2)}(k_{p,1}b)}{\omega\xi_1(\nu_1+j\omega)b} M_n(4,3) \end{aligned} \tag{3.159}$$

$$Q_n(4,7) = \sqrt{\frac{\mu_o}{\xi_1}}\, H_n^{(1)'}(k_{e,1}b)\, M_n(1,4) + \sqrt{\frac{\mu_o}{\xi_1}}\, H_n^{(2)'}(k_{e,1}b)\, M_n(2,4)$$

$$+ \frac{ev_o^2 n\, H_n^{(1)}(k_{p,1}b)}{\omega\xi_1(\nu_1+j\omega)\, b}\, M_n(3,4) + \frac{ev_o^2 n\, H_n^{(2)}(k_{p,1}b)}{\omega\xi_1(\nu_1+j\omega)\, b}\, M_n(4,4) \tag{3.160}$$

$$Q_n(5,4) = \frac{jen\, H_n^{(1)}(k_{e,1}b)}{\omega Mb}\, M_n(1,1) + \frac{jen\, H_n^{(2)}(k_{e,1}b)}{\omega Mb}\, M_n(2,1)$$

$$+ \frac{v_o^2 \epsilon_o k_{p,1}\, H_n^{(1)'}(k_{p,1}b)}{n_{o,1}}\, M_n(3,1) + \frac{v_o^2 \epsilon_o k_{p,1}\, H_n^{(2)'}(k_{p,1}b)}{n_{o,1}}\, M_n(4,1) \tag{3.161}$$

$$Q_n(5,5) = \frac{jen\, H_n^{(1)}(k_{e,1}b)}{\omega Mb}\, M_n(1,2) + \frac{jen\, H_n^{(2)}(k_{e,1}b)}{\omega Mb}\, M_n(2,2)$$

$$+ \frac{v_o^2 \epsilon_o k_{p,1}\, H_n^{(1)'}(k_{p,1}b)}{n_{o,1}}\, M_n(3,2) + \frac{v_o^2 \epsilon_o k_{p,1}\, H_n^{(2)'}(k_{p,1}b)}{n_{o,1}}\, M_n(4,2) \tag{3.162}$$

$$Q_n(5,6) = \frac{jen\, H_n^{(1)}(k_{e,1}b)}{\omega Mb}\, M_n(1,3) + \frac{jen\, H_n^{(2)}(k_{e,1}b)}{\omega Mb}\, M_n(2,3)$$

$$+ \frac{v_o^2 \epsilon_o k_{p,1}\, H_n^{(1)'}(k_{p,1}b)}{n_{o,1}}\, M_n(3,3) + \frac{v_o^2 \epsilon_o k_{p,1}\, H_n^{(2)'}(k_{p,1}b)}{n_{o,1}}\, M_n(4,3) \tag{3.163}$$

$$Q_n(5,7) = \frac{jen\, H_n^{(1)}(k_{e,1}b)}{\omega Mb}\, M_n(1,4) + \frac{jen\, H_n^{(2)}(k_{e,1}b)}{\omega Mb}\, M_n(2,4)$$

$$+ \frac{v_o^2 \epsilon_o k_{p,1}\, H_n^{(1)'}(k_{p,1}b)}{n_{o,1}}\, M_n(3,4) + \frac{v_o^2 \epsilon_o k_{p,1}\, H_n^{(2)'}(k_{p,1}b)}{n_{o,1}}\, M_n(4,4) \tag{3.164}$$

$$Q_n(6,4) = \frac{jen\, H_n^{(1)}(k_{e,s}a)}{\omega Ma} \tag{3.165}$$

$$Q_n(6,5) = \frac{jen\, H_n^{(2)}(k_{e,s}a)}{\omega Ma} \tag{3.166}$$

$$Q_n(6,6) = \frac{v_o^2 \epsilon_o k_{p,s}\, H_n^{(1)'}(k_{p,s}a)}{n_{o,s}} \tag{3.167}$$

$$Q_n(6,7) = \frac{v_o^2 \epsilon_o k_{p,s}\, H_n^{(2)'}(k_{p,s}a)}{n_{o,s}} \tag{3.168}$$

$$Q_n(7,4) = k_{e,s}\, H_n^{(1)'}(k_{e,s}a) \tag{3.169}$$

$$Q_n(7,5) = k_{e,s}\, H_n^{(2)'}(k_{e,s}a) \tag{3.170}$$

$$Q_n(7,6) = \frac{ev_o^2 n\, H_n^{(1)}(k_{p,s}a)}{(\nu_s + j\omega)\, a} \tag{3.171}$$

$$Q_n(7,7) = \frac{ev_o^2 n\, H_n^{(2)}(k_{p,s}a)}{(\nu_s + j\omega)\, a} \quad . \tag{3.172}$$

In Eq. (3.139), the first two rows represent the continuity of H_z and E_θ at r = c respectively, the third and the fourth rows represent the continuity of H_z and E_θ at r = b respectively, the fifth and the sixth rows indicate zero normal component of induced electron velocity at r = b and r = a, respectively, and the seventh row represents zero

tangential electric field at the conductor surface at r = a. The seven linear simultaneous equations as expressed in Eq. (3.139) can be solved numerically using a computer or by any other method.

3.6 Scattered Fields in Free Space Region

The quantities of main interest in this study are the scattered fields in free space region. To calculate these quantities, the constant A_n is solved from Eq. (3.139) by Cramer's Rule as

$$A_n = \frac{\Delta_{n1}}{\Delta_n} \quad . \tag{3.173}$$

The two determinants, Δ_n and Δ_{n1}, are given as

$$\Delta_n = \begin{vmatrix} Q_n(1,1) & Q_n(1,2) & Q_n(1,3) & 0 & 0 & 0 & 0 \\ Q_n(2,1) & Q_n(2,2) & Q_n(2,3) & 0 & 0 & 0 & 0 \\ 0 & Q_n(3,2) & Q_n(3,3) & Q_n(3,4) & Q_n(3,5) & Q_n(3,6) & Q_n(3,7) \\ 0 & Q_n(4,2) & Q_n(4,3) & Q_n(4,4) & Q_n(4,5) & Q_n(4,6) & Q_n(4,7) \\ 0 & 0 & 0 & Q_n(5,4) & Q_n(5,5) & Q_n(5,6) & Q_n(5,7) \\ 0 & 0 & 0 & Q_n(6,4) & Q_n(6,5) & Q_n(6,6) & Q_n(6,7) \\ 0 & 0 & 0 & Q_n(7,4) & Q_n(7,5) & Q_n(7,6) & Q_n(7,7) \end{vmatrix} \tag{3.174}$$

and

$$\Delta_{n1} = \begin{vmatrix} Q_n(1,8) & Q_n(1,2) & Q_n(1,3) & 0 & 0 & 0 & 0 \\ Q_n(2,8) & Q_n(2,2) & Q_n(2,3) & 0 & 0 & 0 & 0 \\ 0 & Q_n(3,2) & Q_n(3,3) & Q_n(3,4) & Q_n(3,5) & Q_n(3,6) & Q_n(3,7) \\ 0 & Q_n(4,2) & Q_n(4,3) & Q_n(4,4) & Q_n(4,5) & Q_n(4,6) & Q_n(4,7) \\ 0 & 0 & 0 & Q_n(5,4) & Q_n(5,5) & Q_n(5,6) & Q_n(5,7) \\ 0 & 0 & 0 & Q_n(6,4) & Q_n(6,5) & Q_n(6,6) & Q_n(6,7) \\ 0 & 0 & 0 & Q_n(7,4) & Q_n(7,5) & Q_n(7,6) & Q_n(7,7) \end{vmatrix} \tag{3.175}$$

where the expressions for $Q_n(i,j)$'s have been given in the previous section.

After the constant A_n is determined, the scattered fields in free space region are obtained as

$$H_{oz}^s = \sum_{n=0}^{\infty} \cos(n\theta)\, H_n^{(2)}(k_o r)\, A_n \tag{3.176}$$

$$H_{or}^s = H_{o\theta}^s = 0 \tag{3.177}$$

$$E_{or}^s = \frac{j}{\omega \epsilon_o r} \sum_{n=0}^{\infty} n\sin(n\theta)\, H_n^{(2)}(k_o r)\, A_n \tag{3.178}$$

$$E_{o\theta}^s = j\zeta_o \sum_{n=0}^{\infty} \cos(n\theta)\, H_n^{(2)'}(k_o r)\, A_n \tag{3.179}$$

$$E_{oz}^s = 0 \tag{3.180}$$

where r is the distance between the observation point and the cylinder axis. If the scattered fields are observed at a large distance, Hankel function can be expressed in its asymptotic form as

$$H_n^{(2)}(k_o r) \approx \sqrt{\frac{2}{\pi k_o r}}\, e^{-j(k_o r - \frac{1}{2}n\pi - \frac{1}{4}\pi)}, \tag{3.181}$$

and the scattered fields at a large distance are then obtained as

$$H_{oz}^s = \sqrt{\frac{2}{\pi k_o r}}\, e^{-j(k_o r - \frac{1}{4}\pi)} \sum_{n=0}^{\infty} \cos(n\theta)\, e^{j\frac{1}{2}n\pi}\, A_n \tag{3.182}$$

$$H_{or}^s = H_{o\theta}^s = 0 \tag{3.183}$$

$$E_{or}^s = j\sqrt{\frac{2}{\pi k_o r}}\, \frac{1}{\omega \epsilon_o r}\, e^{-j(k_o r - \frac{1}{4}\pi)} \sum_{n=0}^{\infty} n\sin(n\theta)\, e^{j\frac{1}{2}n\pi}\, A_n$$

$$\doteq 0 \tag{3.184}$$

$$E^s_{o\theta} = j\zeta_o\sqrt{\frac{2}{\pi k_o r}} \sum_{n=0}^{\infty} \cos(n\theta)\left[-e^{-j(k_o r-\frac{1}{2}(n+1)\pi-\frac{1}{4}\pi)}\right.$$

$$\left. + \frac{n}{k_o r} e^{-j(k_o r-\frac{1}{2}n\pi-\frac{1}{4}\pi)}\right] A_n$$

$$\approx \zeta_o\sqrt{\frac{2}{\pi k_o r}} e^{-j(k_o r-\frac{1}{4}\pi)} \sum_{n=0}^{\infty} \cos(n\theta)\, e^{j\frac{1}{2}n\pi} A_n \qquad (3.185)$$

after neglecting the $r^{-\frac{3}{2}}$ term.

$$E^s_{oz} = 0 \ . \qquad (3.186)$$

To derive Eq. (3.185) the relation of

$$H_n^{(2)'}(k_o r) = -H_{n+1}^{(2)}(k_o r) + \frac{n}{k_o r} H_n^{(2)}(k_o r) \qquad (3.187)$$

has been used.

It is also observed that the only significant scattered fields in the far zone of the plasma-coated cylinder are $E^s_{o\theta}$ and H^s_{oz} and the ratio between these two fields is simply the impedance of free space ζ_o.

3.7 Some Special Cases

There are two special cases, namely: a plain plasma cylinder and a plasma-coated dielectric cylinder which are quite interesting from a practical viewpoint. These two cases can be solved by modifying the procedure and solutions obtained in the previous section.

3.7.1 Scattered Fields by a Plain Plasma Cylinder

In this case, the whole cylinder is filled with a plasma in the absence of a metallic cylinder. If we let the inmost sublayer be a plasma cylinder with an extremely small radius and located along the z

axis, the whole plasma cylinder is subdivided into an extremely thin plasma cylinder at the center and a number of concentric sublayers extended from radius r = 0 to radius r = b up to glass wall (Refer to Fig. 3.1). Since the Bessel functions of the second kind, $Y_n(k_{e,s}r)$ and $Y_n(k_{p,s}r)$, have a singularity at r = 0, the proper solutions in the inmost sublayer are Bessel functions of the first kind. This condition can be achieved by setting the constants $D_{s,n}$ and $F_{s,n}$, $G_{s,n}$ and $I_{s,n}$, to be equal respectively, because

$$J_n(k_{e,s}r) = \frac{1}{2}\left[H_n^{(1)}(k_{e,s}r) + H_n^{(2)}(k_{e,s}r)\right] \qquad (3.188)$$

and

$$J_n(k_{p,s}r) = \frac{1}{2}\left[H_n^{(1)}(k_{p,s}r) + H_n^{(2)}(k_{p,s}r)\right] \quad . \qquad (3.189)$$

Thus, the simultaneous equations which give solutions to the scattered fields from a plain plasma cylinder are Eqs. (3.132), (3.133), (3.134), (3.135), (3.136) and the following two equations

$$D_{s,n} - F_{s,n} = 0 \qquad (3.190)$$

$$G_{s,n} - I_{s,n} = 0 \quad . \qquad (3.191)$$

With the set of equations, A_n can be solved and consequently the scattered field.

3.7.2 Scattered Fields by a Plasma-Coated Dielectric Cylinder

In this case a dielectric cylinder instead of a metallic cylinder is located in the center of the plasma cylinder. The tangential component of $\vec{E}$ field will not vanish on the surface of

the dielectric cylinder as it did in the metallic cylinder case. The fields inside the dielectric cylinder are purely electromagnetic and their amplitude remain finite. Because of the singularity of the Bessel function of the second kind at r = 0, the proper solution inside the dielectric cylinder is the Bessel function of the first kind. Thus, one additional constant is introduced to describe the fields inside the dielectric cylinder compared to the metallic cylinder case. However, the continuity of tangential components of $\vec{E}$ and $\vec{H}$ fields provides two boundary conditions at r = a. Using these two boundary conditions instead of the boundary condition of zero tangential electric field at r = a as previously used for the case of a metallic cylinder, we obtain a set of eight simultaneous equations with eight unknown constants. The scattered fields from a plasma-coated dielectric cylinder can then be obtained by solving this set of equations.

3.8 Numerical Results

The back scattered E fields from a plasma-coated metallic cylinder and from a plain plasma cylinder have been calculated as a function of $(\omega_p/\omega)^2$. In the numerical calculation, the collision frequency ν is assumed to be constant for all sublayers for simplicity (Reason for this assumption has been given in Sec. 2.9, Chapter 2). The series solutions are produced by summing up the first four terms only because of the rapid convergence of series. The scattered fields are calculated at a distance from the z axis with $k_o r = 10$ for convenience. The asymptotic from of Hankel function is used whenever the argument with real part or imaginary part becomes greater than 10. The dimensions for the glass

tube, plasma layer and central cylindrical conductor are based on the actual dimensions of the experimental model. These dimensions and the dielectric constant of glass and the operating frequency are given in Table 3.1.

Operating frequency	a (mm)	b (mm)	c (mm)	ϵ_g
f = 2.3 GHz	2.158	7	8	5

Table 3.1 Physical dimension of plasma tube, dielectric constant of glass and operating frequency of a plasma-coated metallic cylinder.

All the numerical results of the back scattered E field are plotted with the normalized value, E_o^s/E_o^i , where E_o^s is the scattered E field and E_o^i is the incident wave as a function of $(\omega_p/\omega)^2$.

Figure 3.4 shows the back scattered E field of a plasma-coated metallic cylinder in the direction of $\theta = 180^o$ as a function of $(\omega_p/\omega)^2$ for various collision frequencies and for the case of a uniform density distribution in plasma region ($b \geq r \geq a$). The ratio of the r.m.s. electron velocity to the velocity of light in free space, v_o/c, is assumed to be 0.01. This is equivalent to a electron temperature of approximately equal to $200{,}000^o$ K. The main resonance, also known as the dipolar resonance, occurs at the value of $(\omega_p/\omega)^2 = 2.34$. This resonance corresponds to the resonance due to n=1 term of series solution. The sharp peak at the right of the main resonance is a quadrupolar resonance corresponding to the resonance due to n=2 term in series solution. Three small peaks occured in the region of $0<(\omega_p/\omega)^2<1$ are the so called temperature resonances due to an electroacoustic wave.

These resonances are set up when an electroacoustic wave sets up a standing wave pattern between the metallic cylinder and the glass wall. It is observed that when the collision frequency is increased to a value in the order of $\nu/\omega = 0.5$ all resonances disappear. Also the quadrupolar resonance seems to be damped out by the collision more strongly than the dipolar resonance.

Figure 3.5 is also a plot of the back scattered E field of a plasma-coated metallic cylinder as a function of $(\omega_p/\omega)^2$ for various collision frequencies. The plasma layer is assumed to have a uniform density distribution. The ratio v_o/c is assumed to be $(4/3) \times 10^{-2}$ which is slightly greater than the value of v_o/c in Fig. 3.4. It is observed that the effect of collision frequency is to damp out the resonances and the over all picture is approximately the same as that in Fig. 3.4. Due to the change of v_o and consequently k_p, the number of temperature resonances reduces to two compared to three in Figure 3.4. The locations of main resonance and quadrupolar resonance in Figs. 3.4 and 3.5 are slightly different.

Figure 3.6 is a plot of the propagation constant, k_e, of an electromagnetic wave as a function of $(\omega_p/\omega)^2$. The expression of k_e is given by Eqs. (3.30), (3.31) and (3.32). The abrupt change of real part β_e and imaginary part α_e in the neighborhood of $(\omega_p/\omega)^2 = 1$ is clearly shown in the figure. The slopes of curves are greater for the case of lower collision freqnency.

Figure 3.7 is a plot of the propagation constant, k_p, of an electroacoustic wave as a function of $(\omega_p/\omega)^2$ with $v_o/c = 0.01$ and $\nu/\omega = 0.001$. The expression for k_p is given by Eqs. (3.46), (3.47)

and (3.48). It is observed that in the region near $(\omega_p/\omega)^2 = 1$ the real part of k_p changes from the order of 10^3 to the order of 1 while the imaginary part changes from the order of 1 to the order of 10^3. The real part, β_p, represents the wave number and it determines the wave length of an electroacoustic wave. The imaginary part, α_p, represents the attenuation constant and consequently it produces a cut off phenomenon for an electroaccoustic wave when $(\omega_p/\omega)^2$ becomes greater than 1.

Figures 3.8 and 3.9 are the plots of the back scattered E fields of a plasma-coated metallic cylinder with a uniform density distritution as a function of $(\omega_p/\omega)^2$. The collision frequency is assumed to be $\nu/\omega = 0.001$. Various values of r.m.s. electron velocity are assumed. It is observed that smaller value of v_o/c will lead to more temperature resonances appearing in the region of $0 < (\omega_p/\omega)^2 < 1$. This is resonable since a smaller value of v_o/c implies a larger value of k_p or a shorter wave length of an electroacoustic wave. Consequently, an electroacoustic wave can set up more standing wave modes between a finite distance between the boundaries. It is also shown that a higher value of v_o/c produces greater amplitudes for the temperature resonances.

Figures 3.10 and 3.11 are the plots of the back scattered E field of a plasma-coated metallic cylinder with a non-uniform plasma density distribution as a function of $(\omega_p/\omega)^2_{ave.}$ which is the average value of $(\omega_p/\omega)^2$. The collision frequency is assumed to be $\nu/\omega = 0.001$. The ratio of v_o/c is assumed to be 0.01 and 0.0133 in Figs. 3.10 and 3.11, respectively. The non-uniform plasma density distribution is assumed to be the same as that used in the cold plasma case which is mathematically expressed as

$$n_{o,r} = n_{o,c}\left[1 - 0.6\left(\frac{2r-b-a}{b+a}\right)^2\right] \qquad (3.192)$$

where $n_{o,c}$ is the plasma density at $r = \frac{b+a}{2}$. It is noted that the value of $(\omega_p/\omega)^2$ is directly proportional to the density $n_{o,r}$ under a fixed operating frequency. The stratification method is used and a 3-sublayer model is assumed. A great care has been taken when performing the numerical calculation. Due to a great difference between the magnitude of an electromagnetic wave and that of an electroacoustic wave, the matrix $[L_n]$ as expressed in Eqs. (3.92) and (3.93) becomes nearly singular. In our calculation, the matrix inversion and multiplication have been performed by a double precision technique to avoid run off error. Without this technique, a single precision method would have led to a complete false result. It is noted that there are mathematical resonances inherently associated with the stratification method being used (Details of mathematical resonances, refer to page 29, Chapter 2). It is possible to identify the mathematical resonances when Figs. 3.10 and 3.11 are compared with the corresponding cold plasma cases where no temperature resonances are possible. Since as we have discussed in Chapter 2, mathematical resonances bear no physical meaning, they are to be overlooked. For example, the peak located at the value of $(\omega_p/\omega)^2_{ave.} = 0.94$ in Fig. 3.10 is a mathematical resonance. For the cases of uniform plasma density distribution, the temperature resonances are all shown to be located in the region where $(\omega_p/\omega)^2$ is less than 1. However, for a non-uniform plasma density distribution, temperature resonances can be set up in the plasma layer in the region where $(\omega_p/\omega)^2_{ave.}$ is greater than 1. The reason is rather evident. Because

even $(\omega_p/\omega)^2_{ave.}$ is greater than 1, there are regions of plasma near the boundaries where the local $(\omega_p/\omega)^2$ is still smaller than 1. Thus, a standing electroacoustic wave can be set up in these underdense plasma regions. This mechanism has been discussed by Crawford.[17] The main resonance of the 3-sublayer model of a non-uniform density distribution is located at a slightly higher value of $(\omega_p/\omega)^2_{ave.}$ compared with the case of uniform density distribution. The 5-sublayer model has also been calculated. Unfortunately, the asymptotic form of Hankel function gives a discontinuity in the region where mathematical resonances and temperature resonances occur. This discontinuity causes the identification of temperature resonances from mathematical resonances becoming a very difficult task. This difficulty will be solved if a computer subroutine for calculating Hankel functions with a large complex argument becomes available.

Figure 3.12 is a plot of the back scattered E field of a plain plasma cylinder with b = 7 mm and c = 8 mm as a function of $(\omega_p/\omega)^2_{ave.}$. Both cases of uniform and non-uniform density distributions are shown in Fig. 3.12. The 3-sublayer model is used for the non-uniform density distribution with a density distribution of

$$n_{o,r} = n_{o,c}\left[1 - 0.6\left(\frac{r}{b}\right)^2\right] \tag{3.193}$$

being assumed. The resonance located at $(\omega_p/\omega)^2_{ave.} = 0.94$ is a mathematical resonance and should be ignored. The general behavior of a plain plasma cylinder is similar to that of a plasma-coated metallic cylinder. However, the locations of temperature resonances are quite different and also the dipolar and quadrupolar resonances are moved to

higher values of $(\omega_p/\omega)^2_{ave.}$ for the case of a plain plasma cylinder.

The numerical calculations are performed by a CDC 6500 computer.

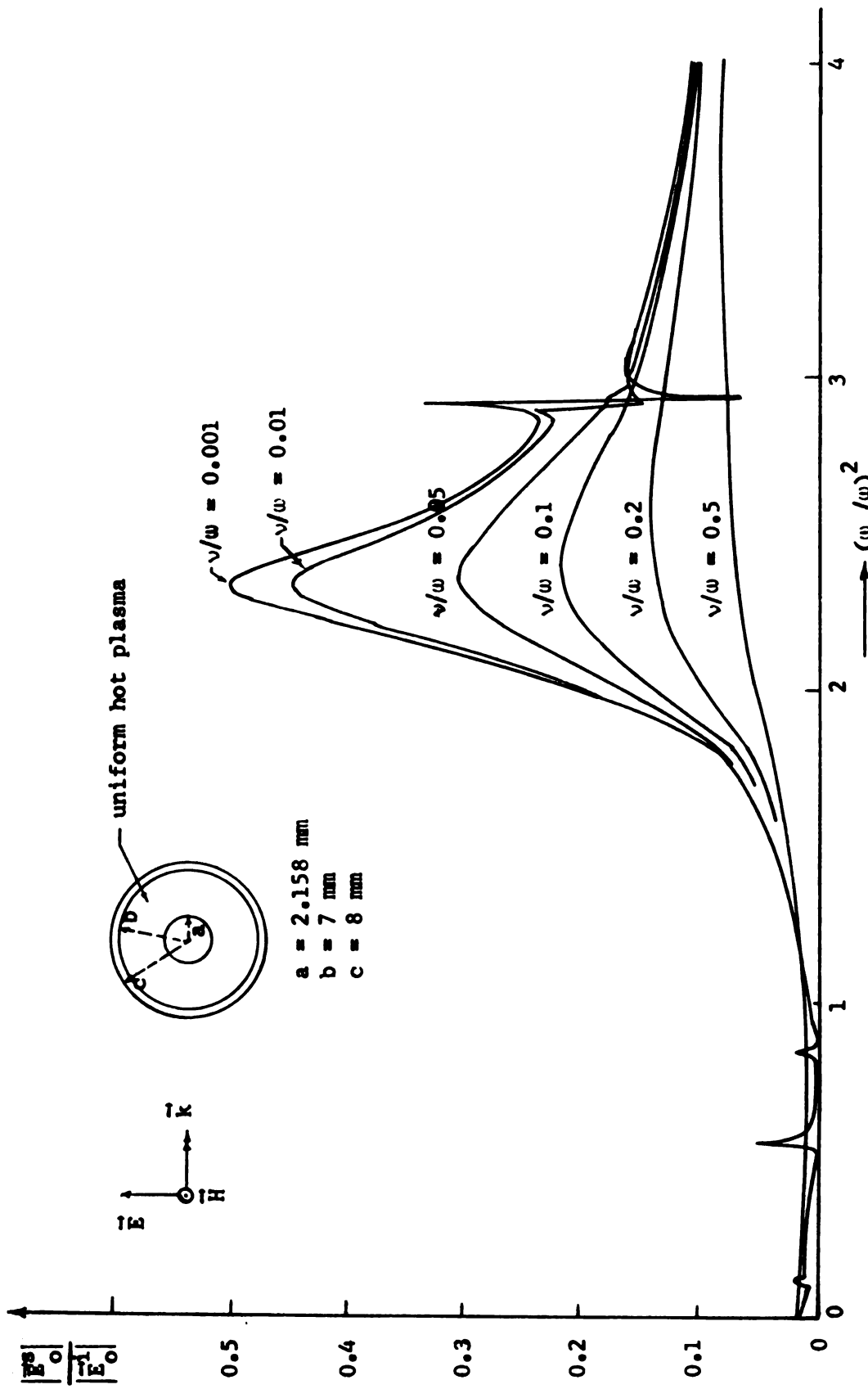

Fig. 3.4 Theoretical back scattered E field from a plasma-coated metallic cylinder as a function of $(\omega_p/\omega)^2$ for a uniform plasma density distribution. (f = 2.3 GHz, $\nu_o/c = 0.01$, $\theta = 180^o$, $k_o r = 10$)

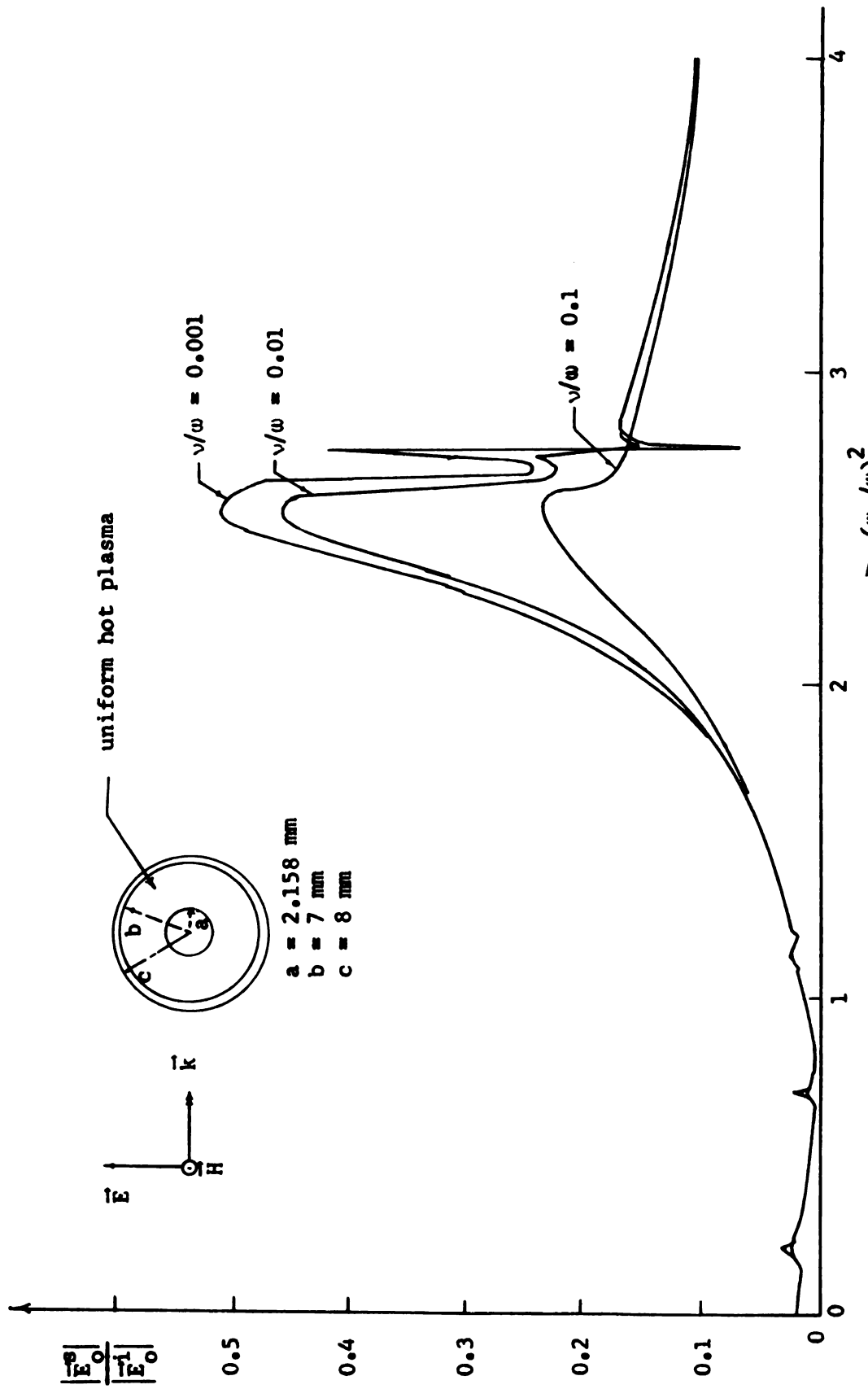

Fig. 3.5 Theoretical back scattered E field from a plasma-coated metallic cylinder as a function of $(\omega_p/\omega)^2$ for a uniform plasma density distribution. (f = 2.3 GHz, $v_o/c = 0.0133$, $\theta = 180^o$, $k_o r = 10$)

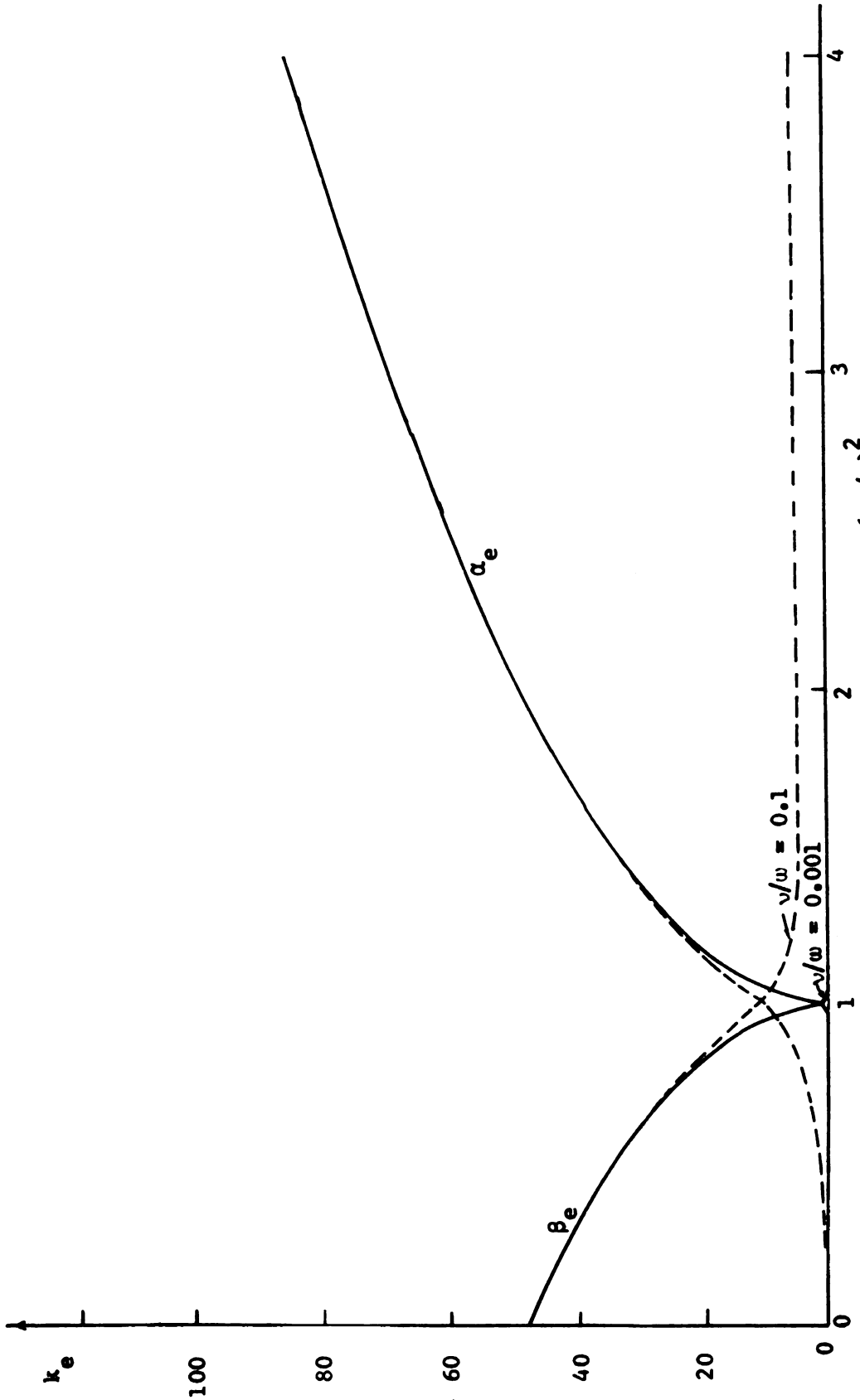

Fig. 3.6 Theoretical propagation constant, $k_e = \beta_e - j\alpha_e$, of electromagnetic wave as a function of $(\omega_p/\omega)^2$ for various collision frequencies. (f = 2.3 GHz)

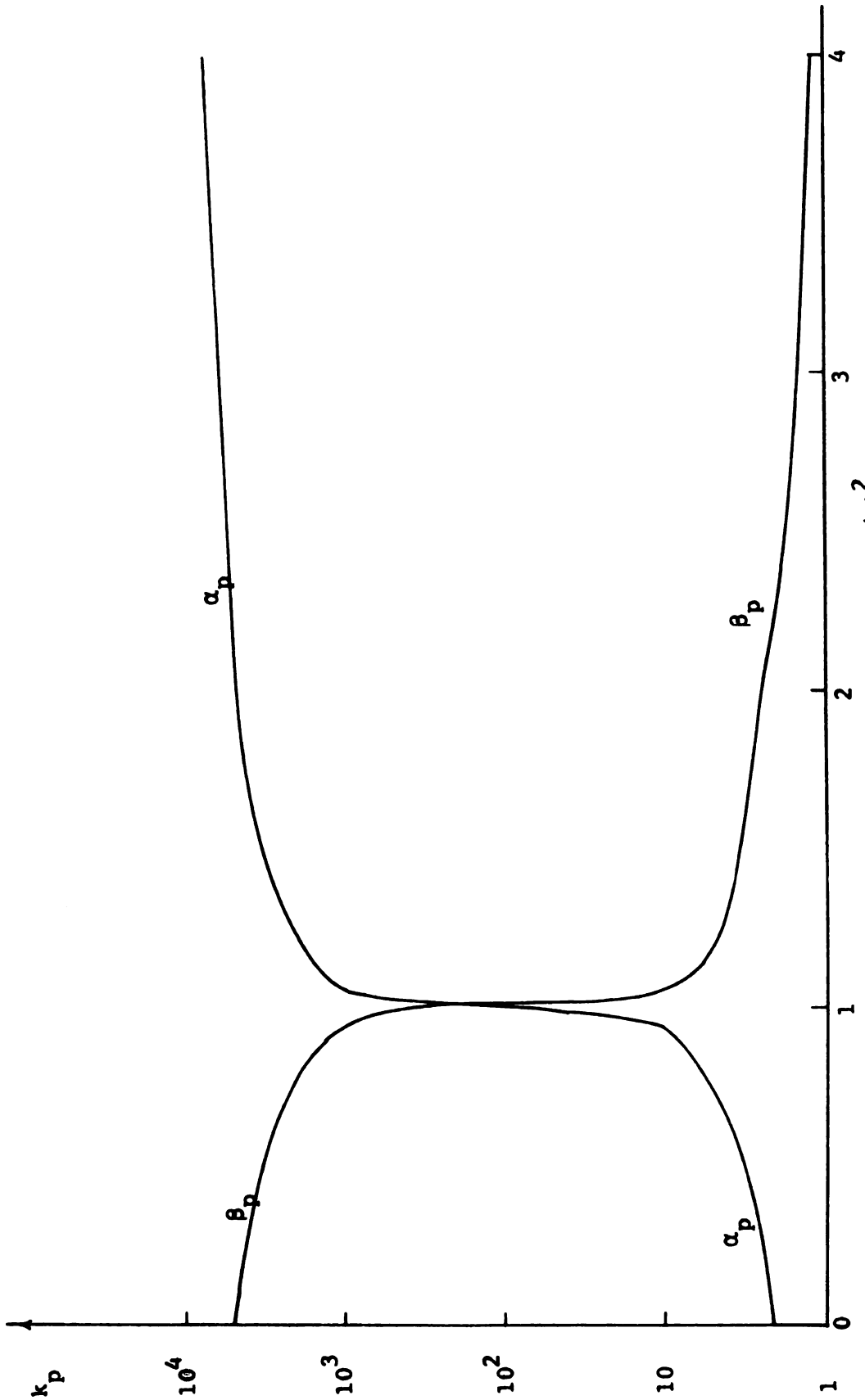

Fig. 3.7 Theoretical propagation constant, $k_p = \beta_p - j\alpha_p$, of electroacoustic wave as a function of $(\omega_p/\omega)^2$ with $v_o/c = 0.01$ and $\nu/\omega = 0.001$. (f =2.3 GHz)

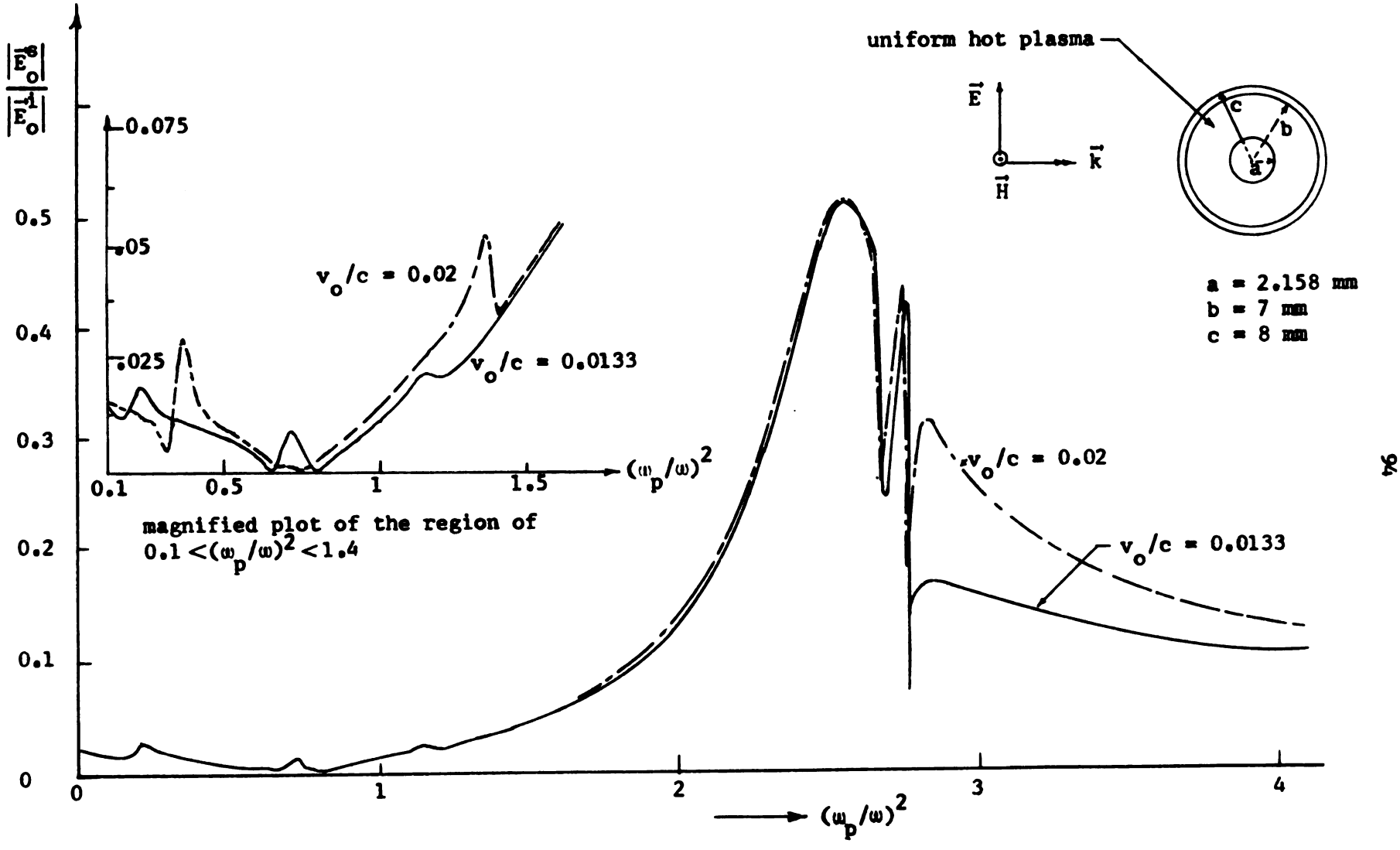

Fig. 3.8 Theoretical back scattered E field from a plasma-coated metallic cylinder as a function of $(\omega_p/\omega)^2$ for a uniform plasma density distribution and for various values of v_o/c. (f = 2.3 GHz, $\theta = 180^o$, $k_o r = 10$, $\nu/\omega = 0.001$)

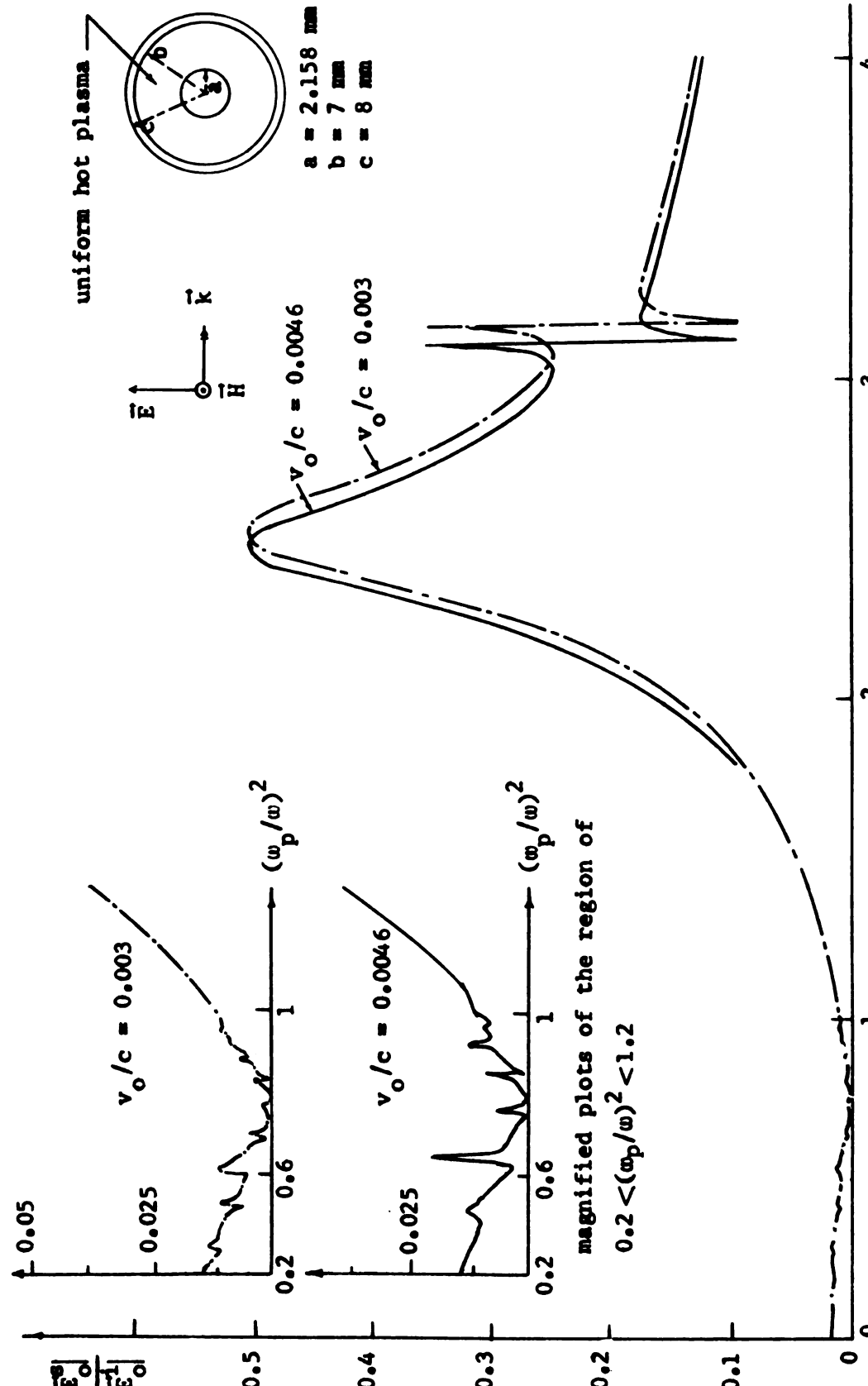

Fig. 3.9 Theoretical back scattered E field from a plasma-coated metallic cylinder as a function of $(\omega_p/\omega)^2$ for a uniform plasma density distribution and for various values of v_o/c. (f =2.3 GHz, $\theta = 180^0$, $k_o r = 10$, $\nu/\omega = 0.001$)

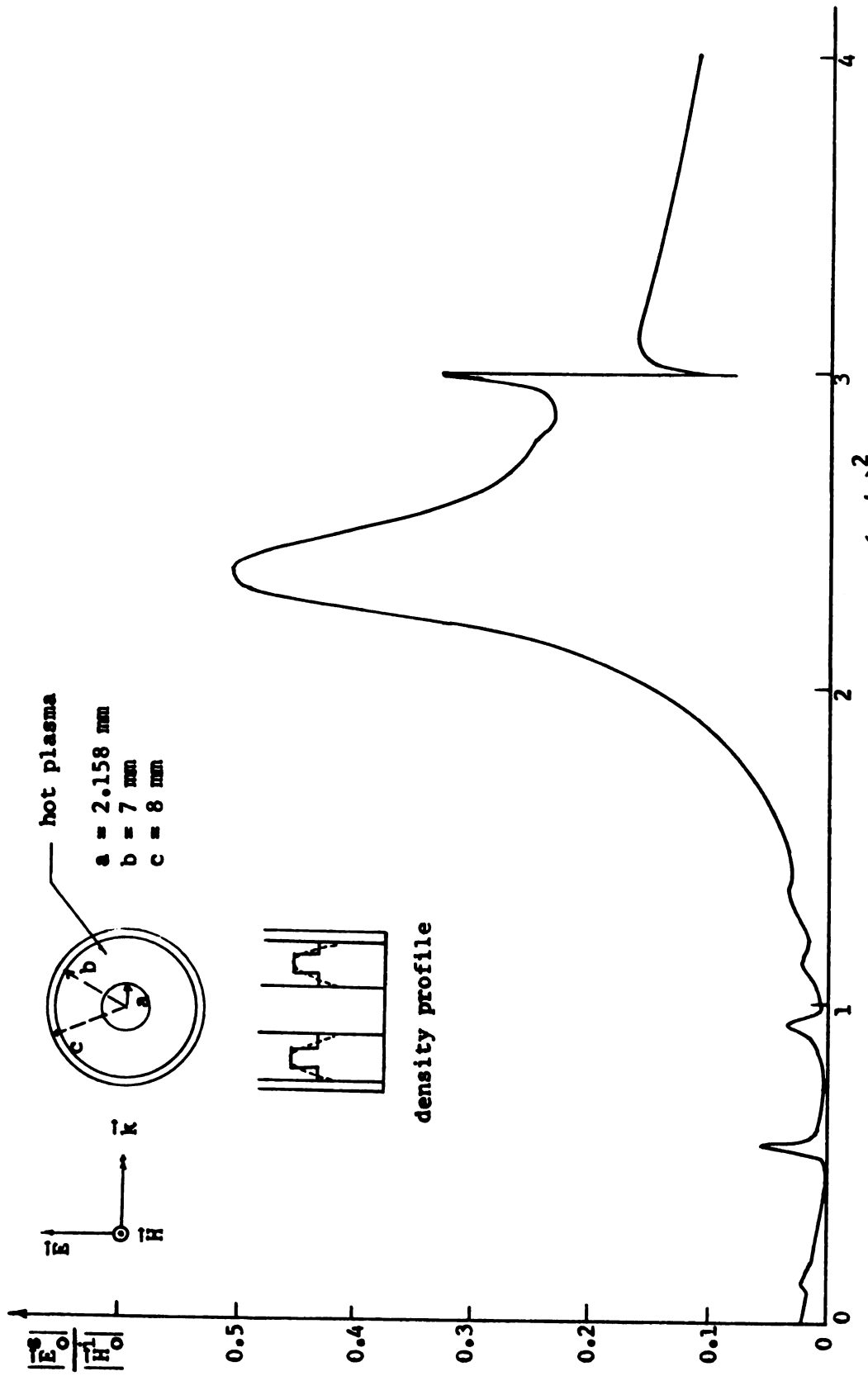

Fig 3.10 Theoretical back scattered E field from a plasma-coated metallic cylinder as a function of $(\omega_p/\omega)^2_{ave}$ for a parabolic plasma density distribution with a 3-sublayer model. ($f = 2.3$ GHz, $\nu_o/c = 0.01$, $\theta = 180^o$, $k_o r = 10$, $\nu/\omega = 0.001$)

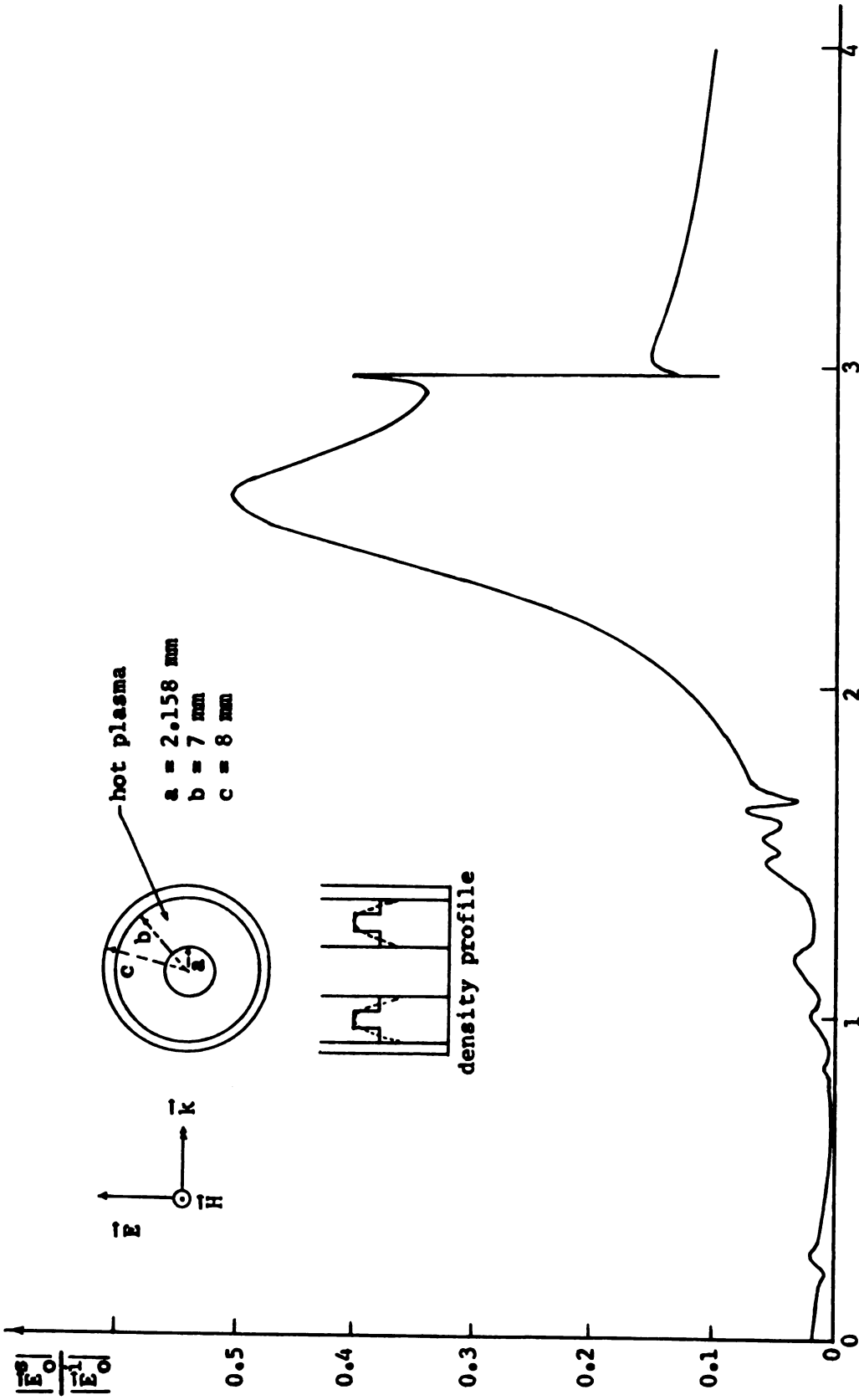

Fig. 3.11 Theoretical back scattered E field from a plasma-coated metallic cylinder as a function of $(\omega_p/\omega)^2_{ave.}$ for a parabolic plasma density distribution with a 3-sublayer model. ($f = 2.3$ GHz, $v_o/c = 0.0133$, $\theta = 180^0$, $k_o r = 10$, $\nu/\omega = 0.001$)

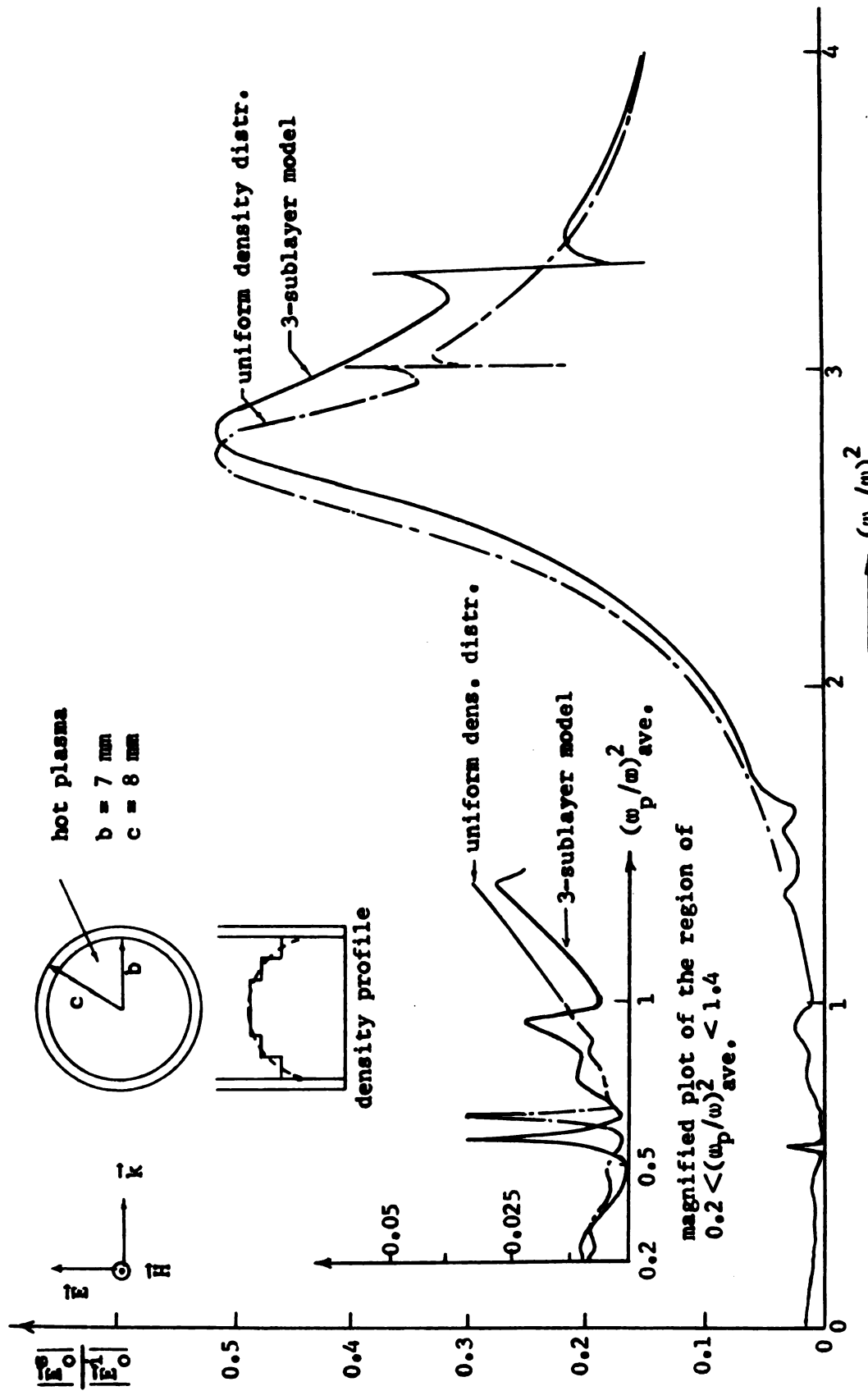

Fig. 3.12 Theoretical back scattered E field from a plain plasma cylinder as a function of $(\omega_p/\omega)^2_{ave.}$ for a parabolic plasma density distribution with a 3-sublayer model. ($f = 2.3$ GHz, $\nu_o/c = 0.0133$, $\theta = 180^o$, $k_o r = 10$, $\nu/\omega = 0.001$)

CHAPTER 4

SCATTERING FROM A METALLIC CYLINDER SURROUNDED BY A LAYER OF LOSSY PLASMA ILLUMINATED BY A TM WAVE

4.1 Introduction

In the preceding chapters, the scattered field from a plasma-coated metallic cylinder when illuminated by a TE wave at normal incidence has been studied. In general, the incident plane wave may have an arbitrary polarization. In order to study the scattered field from a plasma-coated cylinder illuminated by a plane wave of arbitrary polarization, it is necessary to consider the scattering from the same cylinder when it is illuminated by a TM wave. A TM wave is defined as a plane wave with its $\vec{H}$ field perpendicular to the cylinder axis and its $\vec{E}$ field parallel to the cylinder axis. The superposition of a TE and a TM wave can yield a plane wave of arbitrary polarization.

The analysis in this chapter is similar to that of preceding two chapters. The stratification method is again used. Also a glass wall is assumed to surround the plasma in the theoretical model. The surrounding plasma is assumed to be hot and non-uniform in the analysis. It is shown in a later section that under the assumed geometry and boundary conditions it is impossible to excite an electroacoustic wave in the hot plasma. Thus, the solutions obtained for the case of a cylinder covered by a cold plasma can also be applied to the hot plasma case.

4.2 Geometry of the Problem

The geometry of the problem and the notations of stratified plasma medium are the same as that described in Sec. 3.2 of Chapter 3. However, the incident fields are different from that of the previous chapters. The indicent plane wave in this chapter is assumed to have a $\vec{E}$ field paralled to the z axis and a $\vec{H}$ field perpendicular to the z axis as shown in Fig. 4.1. The fields of the incident plane wave are given by

$$E_{oz}^{i} = e^{-jk_o x} = e^{-jk_o r\cos\theta}$$

$$= \sum_{n=o}^{\infty} \epsilon_{on}(-j)^n \cos(n\theta)\, J_n(k_o r) \tag{4.1}$$

$$E_{or}^{i} = E_{o\theta}^{i} = 0 \tag{4.2}$$

$$H_{or}^{i} = -\frac{j}{\omega\mu_o r} \sum_{n=o}^{\infty} \epsilon_{on}(-j)^n n\sin(n\theta)\, J_n(k_o r) \tag{4.3}$$

$$H_{o\theta}^{i} = -\frac{j}{\zeta_o} \sum_{n=o}^{\infty} \epsilon_{on}(-j)^n \cos(n\theta)\, J_n'(k_o r) \tag{4.4}$$

$$H_{oz}^{i} = 0 \ . \tag{4.5}$$

Mathematical symbols used in Eqs. (4.1) to (4.5) have been explained in the preceding chapters.

4.3 Fields in Free space Region

In the free space region Maxwell's equations are

$$\nabla \times \vec{E}_o^s = -j\omega\mu_o \vec{H}_o^s \tag{4.6}$$

$$\nabla \times \vec{H}_o^s = j\omega\epsilon_o \vec{E}_o^s \tag{4.7}$$

where $\vec{E}_o^s$ and $\vec{H}_o^s$ are the scattered electric and magnetic fields.

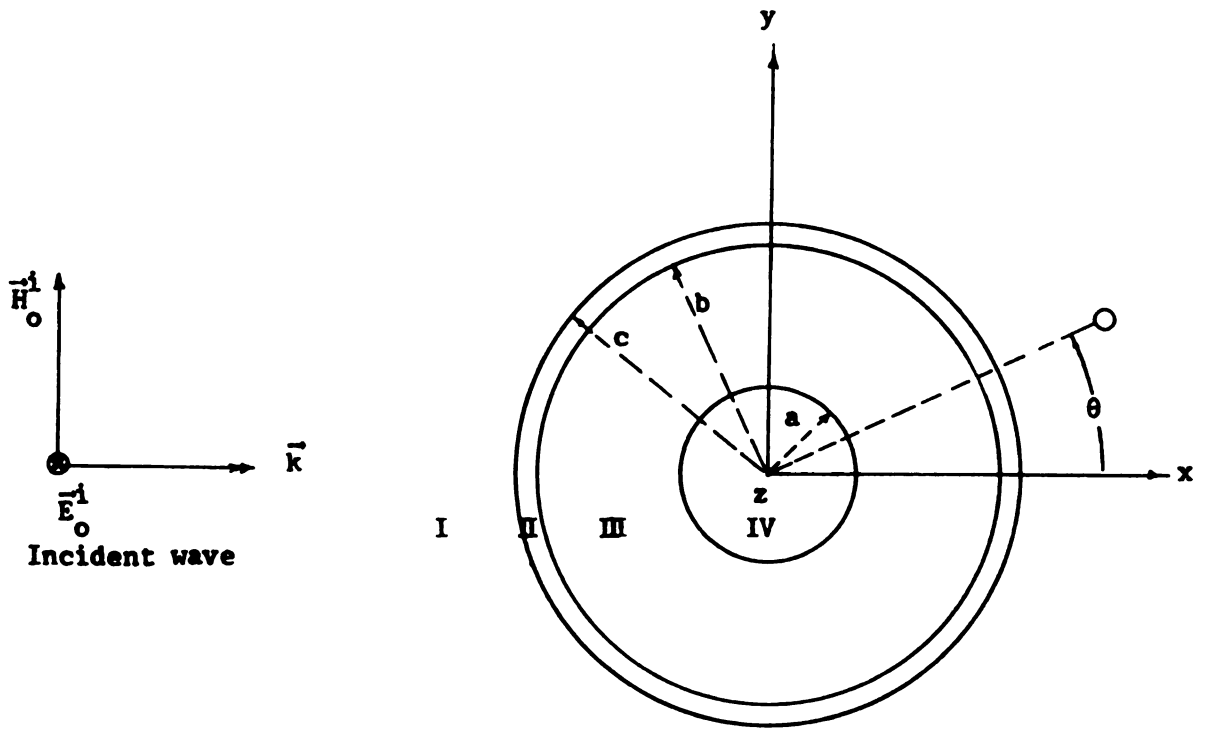

Region I: free space

Region II: glass wall

Region III: plasma

Region IV: metallic cylinder

Fig. 4.1 A plasma-coated metallic cylinder illuminated by a TM wave from the left.

Due to geometrical symmetry, all fields are symmetrical with respect to the $\theta = 0$ axis. Since the $\vec{H}$ field of the incident wave does not have a z component, it is reasonable to assume that the scattered $\vec{H}$ field possesses no z component and it is independent of z variable because of geometry. Thus, the Eq. (4.7) yields

$$\frac{1}{r}\left[\frac{\partial}{\partial r}(r\, H^s_{o\theta}) - \frac{\partial H^s_{or}}{\partial \theta}\right]\hat{z} = j\omega\epsilon_o\, \vec{E}^s_o \quad . \tag{4.8}$$

Equation (4.8) implies that $\vec{E}^s_o$ is allowed to have a z component only. We can assume that

$$\vec{E}^s_o = E^s_{oz}\,\hat{z} \quad . \tag{4.9}$$

From Eqs. (4.6) and (4.7),we obtain a wave equation as

$$\nabla \times \nabla \times \vec{E}^s_o = k_o^2 \vec{E}^s_o \quad . \tag{4.10}$$

Substituting Eq. (4.9) in (4.10), it yields

$$\frac{\partial^2 E^s_{oz}}{\partial r^2} + \frac{1}{r}\frac{\partial E^s_{oz}}{\partial r} + \frac{1}{r^2}\frac{\partial^2 E^s_{oz}}{\partial \theta^2} + k_o^2\, E^s_{oz} = 0 \quad . \tag{4.11}$$

Equation (4.11) can be solved by the method of separation of variables. Since Eq. (4.11) is the same equation as Eq. (2.10) in Chapter 2, the solution of Eq. (4.11) can be written as

$$E^s_{oz} = \sum_{n=o}^{\infty} \cos(n\theta)\, H^{(2)}_n(k_o r)\, A_n \tag{4.12}$$

where A_n is a constant to be determined by the boundary conditions. The corresponding $\vec{H}^s_o$ field can be found from Eq. (4.6) to have components such as

$$H_{or}^{s} = -\frac{j}{\omega\mu_o r}\sum_{n=o}^{\infty} n\sin(n\theta)\, H_n^{(2)}(k_o r)\, A_n \tag{4.13}$$

$$H_{o\theta}^{s} = -\frac{j}{\zeta_o}\sum_{n=o}^{\infty} \cos(n\theta)\, H_n^{(2)'}(k_o r)\, A_n \tag{4.14}$$

$$H_{oz}^{s} = 0 \ . \tag{4.15}$$

The total fields in the free space region can be obtained by summing the incident and the scattered fields to be

$$E_{oz}^{t} = \sum_{n=o}^{\infty} \cos(n\theta)\left[\epsilon_{on}(-j)^n J_n(k_o r) + H_n^{(2)}(k_o r)\, A_n\right] \tag{4.16}$$

$$E_{or}^{t} = E_{o\theta}^{t} = 0 \tag{4.17}$$

$$H_{or}^{t} = -\frac{j}{\omega\mu_o r}\sum_{n=o}^{\infty} n\sin(n\theta)\left[\epsilon_{on}(-j)^n J_n(k_o r) + H_n^{(2)}(k_o r)\, A_n\right] \tag{4.18}$$

$$H_{o\theta}^{t} = -\frac{j}{\zeta_o}\sum_{n=o}^{\infty} \cos(n\theta)\left[\epsilon_{on}(-j)^n J_n'(k_o r) + H_n^{(2)'}(k_o r)\, A_n\right] \tag{4.19}$$

$$H_{oz}^{t} = 0 \ . \tag{4.20}$$

4.4 Fields in Glass Wall Region

In the glass wall region Maxwell's equations are

$$\nabla \times \vec{E}_g = -j\omega\mu_o \vec{H}_g \tag{4.21}$$

$$\nabla \times \vec{H}_g = j\omega\epsilon_o\epsilon_g \vec{E}_g \tag{4.22}$$

where ϵ_g is the dielectric constant of glass.

If we allow an incoming and an outgoing (reflected) wave to exist in the glass wall region, the solution for $\vec{E}_g$ field can be expressed as

$$\vec{E}_g = E_{gz}\hat{z} \tag{4.23}$$

where

$$E_{gz} = \sum_{n=o}^{\infty} \cos(n\theta) \left[H_n^{(1)}(k_g r)\, B_n + H_n^{(2)}(k_g r)\, C_n \right] . \qquad (4.24)$$

In Eq. (4.24), B_n and C_n are the constants to be determined by the boundary conditions and k_g is the propagation constant of the electromagnetic wave in the glass defined as $k_g = k_o\sqrt{\epsilon_g}$. The corresponding $\vec{H}_g$ field has components given by

$$H_{gr} = -\frac{j}{\omega\mu_o r} \sum_{n=o}^{\infty} n\sin(n\theta) \left[H_n^{(1)}(k_g r)\, B_n + H_n^{(2)}(k_g r)\, C_n \right] \qquad (4.25)$$

$$H_{g\theta} = -\frac{j\sqrt{\epsilon_g}}{\zeta_o} \sum_{n=o}^{\infty} \cos(n\theta) \left[H_n^{(1)'}(k_g r)\, B_n + H_n^{(2)'}(k_g r)\, C_n \right] \qquad (4.26)$$

$$H_{gz} = 0 . \qquad (4.27)$$

4.5 Fields in Plasma Region

In the analysis, the plasma is assumed to be hot. The possible excitation of an electroacoustic wave is considered and the density of plasma is assumed to vary in the radial direction only. As the result of analysis, with the assumed geometry and the polarization of the incident wave, it is shown that no electroacoustic wave can be excited. Thus, the hot plasma case reduces to the cold plasma case for this particular polarization of the incident wave. As in the preceding chapters, the stratification method is used and the same geometry as that shown in Fig.3.1.(b) of Chapter 3 is adopted.

Maxwell's equations in the mth sublayer of plasma region are

$$\nabla \times \vec{E}_m = -j\omega\mu_o \vec{H}_m \qquad (4.28)$$

$$\nabla \times \vec{H}_m = -en_{o,m} \vec{V}_m + j\omega \epsilon_o \vec{E}_m \qquad (4.29)$$

$$\nabla \cdot \vec{E}_m = -\frac{en_{1,m}}{\epsilon_o} \tag{4.30}$$

$$\nabla \cdot \vec{H}_m = 0 \ . \tag{4.31}$$

The linearized continuity and force equations are

$$n_{o,m} \nabla \cdot \vec{V}_m + j\omega n_{1,m} = 0 \tag{4.32}$$

$$(\nu_m + j\omega)\vec{V}_m = -\frac{e}{M}\vec{E}_m - \frac{v_o^2}{n_{o,m}} \nabla n_{1,m} \tag{4.33}$$

where

$$v_o = \sqrt{\frac{3kT}{M}} \tag{4.34}$$

and all other mathematical symbols have been defined in the preceding chapters.

From Eq. (4.28), we obtain

$$\nabla \times \nabla \times \vec{E}_m = -j\omega\mu_o \nabla \times \vec{H}_m \ . \tag{4.35}$$

The term, $\nabla \times \vec{H}_m$, can be expressed in terms of $\vec{V}_m$ and $\vec{E}_m$ as given by Eq. (4.29). Thus, Eq. (4.35) can be rewritten as

$$\nabla \times \nabla \times \vec{E}_m = j\omega\mu_o e n_{o,m} \vec{V}_m + k_o^2 \vec{E}_m \ . \tag{4.36}$$

From Eq. (4.33), the induced electron velocity, $\vec{V}_m$, can be written explicitly as

$$\vec{V}_m = -\frac{e}{(\nu_m + j\omega) M}\vec{E}_m - \frac{v_o^2}{(\nu_m + j\omega) n_{o,m}} \nabla n_{1,m} \ . \tag{4.37}$$

Substituting Eq. (4.37) in Eq. (4.36), we obtain

$$\nabla \times \nabla \times \vec{E}_m = \omega^2 \mu_o \epsilon_o \left[1 + \frac{\omega_{p,m}^2}{j\omega(\nu_m + j\omega)}\right] \vec{E}_m + \frac{\omega^2 \mu_o e\, v_o^2}{j\omega(\nu_m + j\omega)} \nabla n_{1,m} \ . \tag{4.38}$$

Equation (4.38) can be expressed as

$$\nabla \times \nabla \times \vec{E}_m = k_{e,m}^2 \vec{E}_m + R_m \nabla n_{1,m} \quad . \tag{4.39}$$

In Eq. (4.39) the term, R_m, is defined as

$$R_m = \frac{\omega^2 \mu_o e v_o^2}{j\omega(\nu_m + j\omega)} \tag{4.40}$$

for convenience. $k_{e,m}$ is the propagation constant of the electromagnetic wave in the plasma in the mth sublayer. Equation (4.39) can be reduced to three coupled scalar equations. After that, effort will be made to decouple the equations. In order to do this, we consider the magnetic field, $\vec{H}_m$, first. The incident $\vec{H}$ field has no z component and the plasma density is assumed to vary in r direction only. Thus, in the mth sublayer of the plasma the magnetic field, $\vec{H}_m$, will not have a z component. We can assume that

$$\vec{H}_m = H_{mr} \hat{r} + H_{m\theta} \hat{\theta} \quad . \tag{4.41}$$

Substituting Eq. (4.41) in Eq. (4.28), we have

$$\nabla \times \vec{E}_m = -j\omega\mu_o \left[H_{mr} \hat{r} + H_{m\theta} \hat{\theta} \right] \quad . \tag{4.42}$$

Equation (4.42) implies the vanishing of z component of vector quantity, $\nabla \times \vec{E}_m$. Also, due to the geometry of the problem, no variation of the fields along the z axis is assumed, i.e. $\frac{\partial}{\partial z} = 0$. The vector quantity, $\nabla \times \nabla \times \vec{E}_m$, can then be expressed as

$$\nabla \times \nabla \times \vec{E}_m = -\frac{1}{r}\left[\frac{\partial}{\partial r} \left(r \frac{\partial E_{mz}}{\partial r} \right) + \frac{1}{r} \frac{\partial^2 E_{mz}}{\partial \theta^2} \right] \hat{z} \quad . \tag{4.43}$$

With Eq. (4.43), Eq. (4.39) can be divided into three components to yield three scalar equations as

$$k_{e,m}^2 E_{mr} + \frac{R_m}{r} \frac{\partial n_{1,m}}{\partial r} = 0 \qquad (4.44)$$

$$k_{e,m}^2 E_{m\theta} + \frac{R_m}{r} \frac{n_{1,m}}{\partial \theta} = 0 \qquad (4.45)$$

$$\frac{\partial^2 E_{mz}}{\partial r^2} + \frac{1}{r} \frac{\partial E_{mz}}{\partial r} + \frac{1}{r^2} \frac{\partial^2 E_{mz}}{\partial \theta^2} + k_{e,m}^2 E_{mz} = 0 \ . \qquad (4.46)$$

Equation (4.46) is a homogeneous wave equation for the z component of $\vec{E}_m$ field and its solution is

$$E_{mz} = \sum_{n=0}^{\infty} \cos(n\theta) \left[H_n^{(1)}(k_{e,m} r) D_{m,n} + H_n^{(2)}(k_{e,m} r) F_{m,n} \right] \qquad (4.47)$$

where $D_{m,n}$ and $F_{m,n}$ are the constants to be determined by the boundary conditions. For the components of E_{mr} and $E_{m\theta}$, they are coupled with electroacoustic term, $n_{1,m}$, as shown in Eqs. (4.44) and (4.45). Before determining E_{mr} and $E_{m\theta}$, we seek the solution for $n_{1,m}$.

From Eq. (4.33), we have

$$(\nu_m + j\omega) \nabla \cdot \vec{V}_m = - \frac{e}{M} \nabla \cdot \vec{E}_m - \frac{v_o^2}{n_{o,m}} \nabla^2 n_{1,m} \ . \qquad (4.48)$$

The substitution of the quantities $\nabla \cdot \vec{V}_m$ and $\nabla \cdot \vec{E}_m$ expressed in Eqs. (4.32) and (4.30) in Eq. (4.48) gives a wave equation for $n_{1,m}$ as

$$\nabla^2 n_{1,m} + k_{p,m}^2 n_{1,m} = 0 \qquad (4.49)$$

where $k_{p,m}$ is the propagation constant of the electroacoustic wave and its expression has been given in Chapter 3. The solution for Eq. (4.49) is

$$n_{1,m} = \sum_{n=0}^{\infty} \left[H_n^{(1)}(k_{p,m}r)\, G_{m,n} + H_n^{(2)}(k_{p,m}r)\, I_{m,n} \right] \begin{Bmatrix} \cos(n\theta) \\ \sin(n\theta) \end{Bmatrix} \quad (4.50)$$

where $G_{m,n}$ and $I_{m,n}$ are constants to be determined by boundary conditions. With Eqs. (4.50), (4.44) and (4.45), the r and θ components of $\vec{E}_m$ field can be determined theoretically. Up to this point, $\vec{E}$ field and n_1 in any sublayer can be written down explicitly with appropriate labeling the quantities k_e, k_p, n_o, n_1, ν, etc. Before finding the final solutions for the $\vec{E}$ and n_1, let us consider the boundary conditons at the inmost sublayer of the plasma layer, i.e. the sth sublayer. This will lead to an interesting result and the solutions can be simplified greatly. Since the metallic cylinder is assumed to be perfectly conducting, the tangential components of $\vec{E}$ field at the surface of cylinder vanish. This give,

$$E_{s\theta} = 0 \qquad \text{at } r = a \quad (4.51)$$

and

$$E_{sz} = 0 \qquad \text{at } r = a. \quad (4.52)$$

The θ component of $\vec{E}_s$ field in the sth sublayer can be expressed from Eq. (4.45) as

$$E_{s\theta} = -\frac{R_s}{k_{e,s}^2 r} \frac{\partial n_{1,s}}{\partial \theta} . \quad (4.53)$$

The substitution of Eq. (4.53) in the boundary condition, Eq. (4.51), leads to

$$H_n^{(1)}(k_{p,s}a)\, G_{s,n} + H_n^{(2)}(k_{p,s}a)\, I_{s,n} = 0 . \quad (4.54)$$

This is one of the two equations which determine the constants $G_{s,n}$ and $I_{s,n}$. We now aim to find the other equation in order to completely specify $G_{s,n}$ and $I_{s,n}$. From Maxwell's equations in the sth sublayer, we obtain

$$-\frac{1}{j\omega\mu_o}\nabla \times \nabla \times \vec{E}_s = -en_{o,s}\vec{V}_s + j\omega\epsilon_o\vec{E}_s \quad . \tag{4.55}$$

The r component of Eq. (4.55) is

$$-en_{o,s}V_{sr} + j\omega\epsilon_o E_{sr} = 0 \quad , \tag{4.56}$$

since no r component can be obtained from $\nabla \times \nabla \times \vec{E}_s$ as explained in Eq. (4.43). If E_{sr} is expressed in terms of $n_{1,s}$ according to Eq. (4.44), the radial component of the induced velocity of electrons, V_{sr}, in the sth sublayer can be expressed as

$$V_{sr} = \frac{j\omega\epsilon_o R_s}{en_{o,s}k_{e,s}^2 r}\frac{\partial n_{1,s}}{\partial r} \quad . \tag{4.57}$$

If the rigid boundary of metallic cylinder is assumed as before, it requires the normal component of the induced velocity of electrons, V_{sr}, to vanish at r = a. This leads to

$$\frac{\partial n_{1,s}}{\partial r} = 0 \qquad \text{at } r = a \quad . \tag{4.58}$$

Substituting Eq. (4.50) in Eq. (4.58), we have

$$H_n^{(1)'}(k_{p,s}a)\,G_{s,n} + H_n^{(2)'}(k_{p,s}a)\,I_{s,n} = 0 \quad . \tag{4.59}$$

Equations (4.59) and (4.54) are the two simultaneous equations needed to determine the constants, $G_{s,n}$ and $I_{s,n}$. These two equations yield trivial solutions of

$$G_{s,n} = I_{s,n} = 0 \tag{4.60}$$

with the exception that when the determinant ,

$$\Delta_{sn} = \begin{vmatrix} H_n^{(1)}(k_{p,s}a) & H_n^{(2)}(k_{p,s}a) \\ H_n^{(1)'}(k_{p,s}a) & H_n^{(2)'}(k_{p,s}a) \end{vmatrix} , \tag{4.61}$$

becomes zero.

The determinant expressed in Eq. (4.61) can be written as

$$\Delta_{sn} = H_n^{(1)}(k_{p,s}a)\, H_n^{(2)'}(k_{p,s}a) - H_n^{(2)}(k_{p,s}a)\, H_n^{(1)'}(k_{p,s}a) \ . \tag{4.62}$$

Using the relation between Hankel function and its derivative such as

$$H_n^{(1)'}(z) = - H_{n+1}^{(1)}(z) + \frac{n}{z} H_n^{(1)}(z) \tag{4.63}$$

and

$$H_n^{(2)'}(z) = - H_{n+1}^{(2)}(z) + \frac{n}{z} H_n^{(2)}(z) \ , \tag{4.64}$$

Eq. (4.62) can be rewritten as

$$\Delta_{sn} = H_n^{(2)}(k_{p,s}a)\, H_{n+1}^{(1)}(k_{p,s}a) - H_n^{(1)}(k_{p,s}a)\, H_{n+1}^{(2)}(k_{p,s}a) \tag{4.65}$$

which is a Wronskian and is equal to[25]

$$\Delta_{sn} = - 4j/\pi(k_{p,s}a) \neq 0 \ . \tag{4.66}$$

Since Eq. (4.66) implies that the determinant of Eq. (4.61) is not equal to zero, Eq. (4.60) are the only valid solutions for $G_{s,n}$ and $I_{s,n}$.

Therefore, the electron density deviation, $n_{1,s}$, is zero everywhere within the sth sublayer.

Next, we will dertermine the n_1 in the other sublayers. Consider the boundary at $r = r_{s-1}$ (refer to Fig. 3.1(b)) and using the same boundary conditions as used in Chapter 3, such as

Tangential components of $\vec{E}$ and $\vec{H}$ fields are continuous (4.67)

$$n_{o,s-1} V_{(s-1)r} - n_{o,s} V_{sr} = 0 \qquad \text{at } r = r_{s-1} \tag{4.68}$$

$$\frac{n_{1,s-1}}{n_{o,s-1}} - \frac{n_{1,s}}{n_{o,s}} = 0 \qquad \text{at } r = r_{s-1} \ . \tag{4.69}$$

Since $n_{1,s}$ and V_{sr} are zero as indicated in Eqs. (4.60) and (4.57), Eqs. (4.68) and (4.69) yield

$$H_n^{(1)'}(k_{p,s-1}r_{s-1})\, G_{s-1,n} + H_n^{(2)'}(k_{p,s-1}r_{s-1})\, I_{s-1,n} = 0 \tag{4.70}$$

and

$$H_n^{(1)}(k_{p,s-1}r_{s-1})\, G_{s-1,n} + H_n^{(2)}(k_{p,s-1}r_{s-1})\, I_{s-1,n} = 0 \tag{4.71}$$

respectively. Eqs. (4.70) and (4.71) are similar to Eqs. (4.59) and (4.54), thus, we have

$$G_{s-1,n} = I_{s-1,n} = 0 \ . \tag{4.72}$$

By successive matching of the boundary conditions at all other boundaries, we can show the total vanishing of electroacoustic mode in the plasma medium. Therefore, Maxwell's equations given in Eq. (4.28) to Eq. (4.31) can be simplified for this particular case to the following equations:

$$\nabla \times \vec{E}_m = -j\omega\mu_o \vec{H}_m \tag{4.73}$$

$$\nabla \times \vec{H}_m = j\omega\xi_m \vec{E}_m \tag{4.74}$$

$$\nabla \cdot \vec{E}_m = 0 \tag{4.75}$$

$$\nabla \cdot \vec{H}_m = 0 \ . \tag{4.76}$$

These equations are the same set of equations used in the cold plasma case in Chapter 2. Physically, it implies that when a metallic cylinder coated by a layer of hot, non-uniform plasma is illuminated by a plane wave of TM polarization, the hot plasma behaves as a cold plasma and no electroacoustic wave is excited in the plasma layer. Only an electromagnetic wave exists in the plasma region. The electric field, $\vec{E}_m$, in the mth sublayer yields only a z component and is expressed as Eq. (4.47). The corresponding $\vec{H}$ field has components given by

$$H_{mr} = -\frac{j}{\omega\mu_o r} \sum_{n=o}^{\infty} n\sin(n\theta)\left[H_n^{(1)}(k_{e,m}r)\, D_{m,n} + H_n^{(2)}(k_{e,m}r)\, F_{m,n}\right] \tag{4.77}$$

$$H_{m\theta} = -j\sqrt{\frac{\xi_m}{\mu_o}} \sum_{n=o}^{\infty} \cos(n\theta)\left[H_n^{(1)'}(k_{e,m}r)\, D_{m,n} + H_n^{(2)'}(k_{e,m}r)\, F_{m,n}\right] \tag{4.78}$$

$$H_{mz} = 0. \tag{4.79}$$

4.6 Matching of Boundary Conditions at Interfaces

Since only electromagnetic waves exist in the plasma layer and other regions, the boundary conditions at interfaces are the same as that described for the cold plasma case in Chapter 2. Similar matching process as used in Sec. 2.6 of Chapter 2 can be employed here. However, in this case, the polarization of the incident wave is different from the case in Chapter 2, a different set of five simultaneous equations

can be obtained from matching the boundary conditions. These equations can be represented in matrix form as

$$\begin{bmatrix} Q_n(1,1) & Q_n(1,2) & Q_n(1,3) & 0 & 0 \\ Q_n(2,1) & Q_n(2,2) & Q_n(2,3) & 0 & 0 \\ 0 & Q_n(3,2) & Q_n(3,3) & Q_n(3,4) & Q_n(3,5) \\ 0 & Q_n(4,2) & Q_n(4,3) & Q_n(4,4) & Q_n(4,5) \\ 0 & 0 & 0 & Q_n(5,4) & Q_n(5,5) \end{bmatrix} \begin{bmatrix} A_n \\ B_n \\ C_n \\ D_{s,n} \\ F_{s,n} \end{bmatrix} = \begin{bmatrix} Q_n(1,6) \\ Q_n(2,6) \\ 0 \\ 0 \\ 0 \end{bmatrix} \tag{4.80}$$

where

$$Q_n(1,1) = -H_n^{(2)}(k_o c) \tag{4.81}$$

$$Q_n(1,2) = H_n^{(1)}(k_g c) \tag{4.82}$$

$$Q_n(1,3) = H_n^{(2)}(k_g c) \tag{4.83}$$

$$Q_n(1,6) = \epsilon_{on}(-j)^n J_n(k_o c) \tag{4.84}$$

$$Q_n(2,1) = -H_n^{(2)'}(k_o c) \tag{4.85}$$

$$Q_n(2,2) = \sqrt{\epsilon_g}\, H_n^{(1)'}(k_g c) \tag{4.86}$$

$$Q_n(2,3) = \sqrt{\epsilon_g}\, H_n^{(2)'}(k_g c) \tag{4.87}$$

$$Q_n(2,6) = \epsilon_{on}(-j)^n J_n'(k_o c) \tag{4.88}$$

$$Q_n(3,2) = -H_n^{(1)}(k_g b) \tag{4.89}$$

$$Q_n(3,3) = -H_n^{(2)}(k_g b) \tag{4.90}$$

$$Q_n(3,4) = H_n^{(1)}(k_{e,1} b)\, M_n(1,1) + H_n^{(2)}(k_{e,1} b)\, M_n(2,1) \tag{4.91}$$

$$Q_n(3,5) = H_n^{(1)}(k_{e,1}b)\, M_n(1,2) + H_n^{(2)}(k_{e,1}b)\, M_n(2,2) \tag{4.92}$$

$$Q_n(4,2) = -\sqrt{\epsilon_g}\, H_n^{(1)'}(k_g b) \tag{4.93}$$

$$Q_n(4,3) = -\sqrt{\epsilon_g}\, H_n^{(2)'}(k_g b) \tag{4.94}$$

$$Q_n(4,4) = \sqrt{\frac{\epsilon_1}{\epsilon_o}}\, H_n^{(1)'}(k_{e,1}b)\, M_n(1,1) + \sqrt{\frac{\epsilon_1}{\epsilon_o}}\, H_n^{(2)'}(k_{e,1}b)\, M_n(2,1) \tag{4.95}$$

$$Q_n(4,5) = \sqrt{\frac{\epsilon_1}{\epsilon_o}}\, H_n^{(1)'}(k_{e,1}b)\, M_n(1,2) + \sqrt{\frac{\epsilon_1}{\epsilon_o}}\, H_n^{(2)'}(k_{e,1}b)\, M_n(2,2) \tag{4.96}$$

$$Q_n(5,4) = H_n^{(1)}(k_{e,s}a) \tag{4.97}$$

$$Q_n(5,5) = H_n^{(2)}(k_{e,s}a) \quad . \tag{4.98}$$

The elements M(i,j)'s in Eqs. (4.91), (4.92), (4.95) and (4.96) are the entries of the matrix obtained from the product of the following matrices:

$$\begin{bmatrix} M_n(1,1) & M_n(1,2) \\ M_n(2,1) & M_n(2,2) \end{bmatrix}$$

$$= \left[L_n(k_{e,1}r_1)\right]^{-1}\left[L_n(k_{e,2}r_1)\right]\left[L_n(k_{e,2}r_2)\right]^{-1}\left[L_n(k_{e,3}r_2)\right] \cdots$$

$$\cdots \left[L_n(k_{e,s-1}r_{s-1})\right]^{-1}\left[L_n(k_{e,s}r_{s-1})\right] \tag{4.99}$$

with

$$\left[L_n(k_{e,m}r_m)\right] = \begin{bmatrix} H_n^{(1)}(k_{e,m}r_m) & H_n^{(2)}(k_{e,m}r_m) \\ \sqrt{\epsilon_m}\, H_n^{(1)'}(k_{e,m}r_m) & \sqrt{\epsilon_m}\, H_n^{(2)'}(k_{e,m}r_m) \end{bmatrix} . \tag{4.100}$$

4.7 Scattered Field in Free Space Region

The constant A_n which is the coefficient of the scattered fields in the free space region is of main interest and can be obtained from Eq. (4.80) by Cramer's Rule as

$$A_n = \frac{\Delta_{n1}}{\Delta_{n1}} \quad . \tag{2.101}$$

The two determinants, Δ_n and Δ_{n1}, are given as

$$\Delta_n = \begin{vmatrix} Q_n(1,1) & Q_n(1,2) & Q_n(1,3) & 0 & 0 \\ Q_n(2,1) & Q_n(2,2) & Q_n(2,3) & 0 & 0 \\ 0 & Q_n(3,2) & Q_n(3,3) & Q_n(3,4) & Q_n(3,5) \\ 0 & Q_n(4,2) & Q_n(4,3) & Q_n(4,4) & Q_n(4,5) \\ 0 & 0 & 0 & Q_n(5,4) & Q_n(5,5) \end{vmatrix} \tag{2.102}$$

and

$$\Delta_{n1} = \begin{vmatrix} Q_n(1,6) & Q_n(1,2) & Q_n(1,3) & 0 & 0 \\ Q_n(2,6) & Q_n(2,2) & Q_n(2,3) & 0 & 0 \\ 0 & Q_n(3,2) & Q_n(3,3) & Q_n(3,4) & Q_n(3,5) \\ 0 & Q_n(4,2) & Q_n(4,3) & Q_n(4,4) & Q_n(4,5) \\ 0 & 0 & 0 & Q_n(5,4) & Q_n(5,5) \end{vmatrix} \quad . \tag{2.103}$$

The expressions for $Q_n(i,j)$'s are given in Sec. 4.6.

Finally, the scattered fields in free space region are obtained as

$$E^s_{oz} = \sum_{n=o}^{\infty} \cos(n\theta)\, H^{(2)}_n(k_o r)\, A_n \tag{2.104}$$

$$E^s_{or} = E^s_{o\theta} = 0 \tag{2.105}$$

$$H_{or}^{s} = -\frac{j}{\omega\mu_o r}\sum_{n=o}^{\infty} n\sin(n\theta)\, H_n^{(2)}(k_o r)\, A_n \qquad (2.106)$$

$$H_{o\theta}^{s} = -\frac{j}{\zeta_o}\sum_{n=o}^{\infty} \cos(n\theta)\, H_n^{(2)'}(k_o r)\, A_n \qquad (2.107)$$

$$H_{oz}^{s} = 0 \qquad (2.108)$$

with A_n expressed as Eq. (2.101).

4.8 Some Special Cases

The electromagnetic scatterings from a plain plasma cylinder and a plasma-coated dielectric cylinder will be considered as two special cases of the problem studied in this chapter. These two cases can be solved by modifying the procedure and solutions obtained in the previous section. Since these modifications are similar to that derived in Sec. 2.8, only numerical results will be presented in the next section.

4.9 Numerical Results

The back scattered E fields from a plasma-coated metallic cylinder and from a plain plasma cylinder have been calculated as a function of $(\omega_p/\omega)^2_{ave.}$. In the numerical calculation, the collision frequency ν is assumed to be constant for all sublayers for simplicity (Reason for this assumption has been given in Sec. 2.9, Chapter 2). The series solutions are produced by summing up the first four terms only, because of the rapid convergence of series. The scattered fields are calculated at a distance from the z axis with $k_o r = 10$ for convenience. The dimensions for the glass tube, the plasma layer and the central cylindrical conductor are based on the actual dimensions of the experimental model.

These dimensions and the dielectric constant of glass and the operating frequency are given in Table 4.1.

Operating frequency	a (mm)	b (mm)	c (mm)	ϵ_g
f = 2.3 GHz	2.158	7	8	5

Table 4.1 Physical dimensions of plasma tube, dielectric constant of glass and operating frequency.

Numerical calculation shows that the inhomogeneity along radial direction has little effect on the back scattered E fields. A 13-sublayer model has been used to approximate the plasma density distribution which is given by Eq. (3.192) in Chapter 3. The result obtained for this 13-sublayer model is quite similar to that for a homogeneous plasma layer. Also, the numerical result shows that collision frequency has only a little effect on the back scattered E field. The results are plotted with the normalized back scattered E field, (E_o^s/E_o^i where E_o^s is the scattered E field and E_o^i is the incident field) as a function of $(\omega_p/\omega)^2_{ave.}$.

Figure 4.2 shows the back scattered E fields from plasma-coated metallic cylinders of various radii illuminated by a TM plane wave, as a function of $(\omega_p/\omega)^2_{ave.}$. A 13-sublayer model is used for the stratified plasma medium with a density distribution given by the Eq. (3.192) in Chapter 3. The collision frequency is assumed to be $\nu/\omega = 0.01$. It is observed that the scattered field increases only slightly as the value of $(\omega_p/\omega)^2_{ave.}$ is increased. It is also observed that a metallic cylinder of smaller radius gives a smaller scattered field, but the scattered field from a smaller metallic cylinder increases more rapidly

as the plasma density is increased. For a uniform plasma layer, the result is nearly the same as that of the non-uniform case and that is not shown in the figure.

Figure 4.3 is a plot of the back scattered E field from a plain plasma cylinder as a function of $(\omega_p/\omega)^2_{ave.}$ for two different collision frequencies, $\nu/\omega = 0.1$ and $\nu/\omega = 0.01$. The assumed density distribution of the plasma layer is expressed by Eq. (3.193) in Chapter 3. In the figure, it is observed that the back scattered E field reaches a minimum when the plasma density reaches at a value of $(\omega_p/\omega)^2_{ave.} = 1.96$. This phenomenon disappears when the effect of glass wall is neglected. For a smaller collision frequency the minimum in the back scattered E field tends to become more outstanding. The effect of the collision frequency on the other part of the curve is insignificant. In general, the amplitude of the back scattered E field from a plain plasma cylinder is smaller than that from a plasma coated metallic cylinder. Also, the back scattered E field from a plain plasma cylinder with uniform density distribution is nearly the same as that of a non-uniform density distribution case.

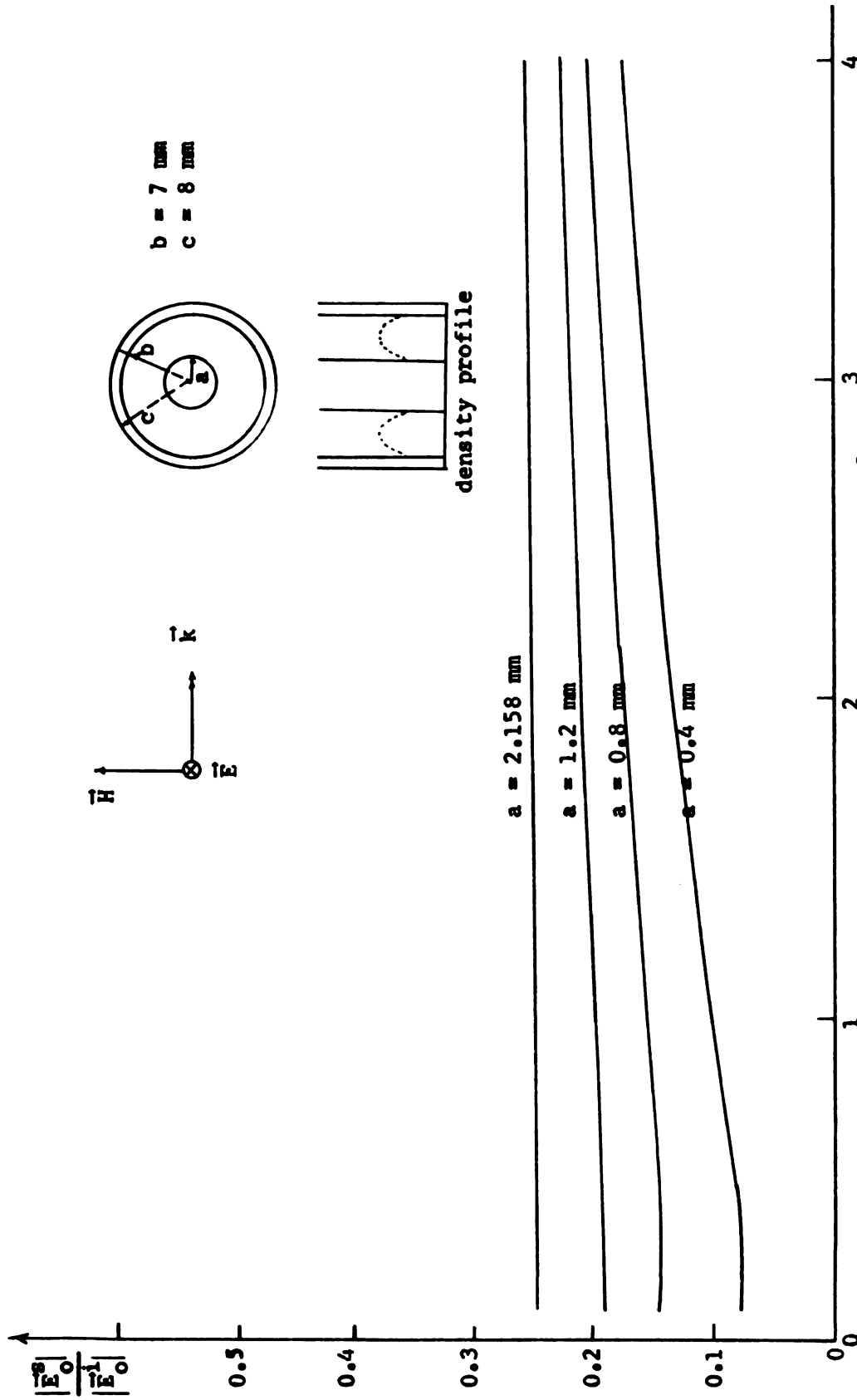

Fig. 4.2 Theoretical back scattered E field from a plasma-coated metallic cylinder for various radii as a function of $(\omega_p/\omega)^2_{ave.}$ for a parabolic plasma density distribution with a 13-sublayer model. ($f = 2.3$ GHz, $\theta = 180^o$, $k_o r = 10$, $\nu/\omega = 0.01$)

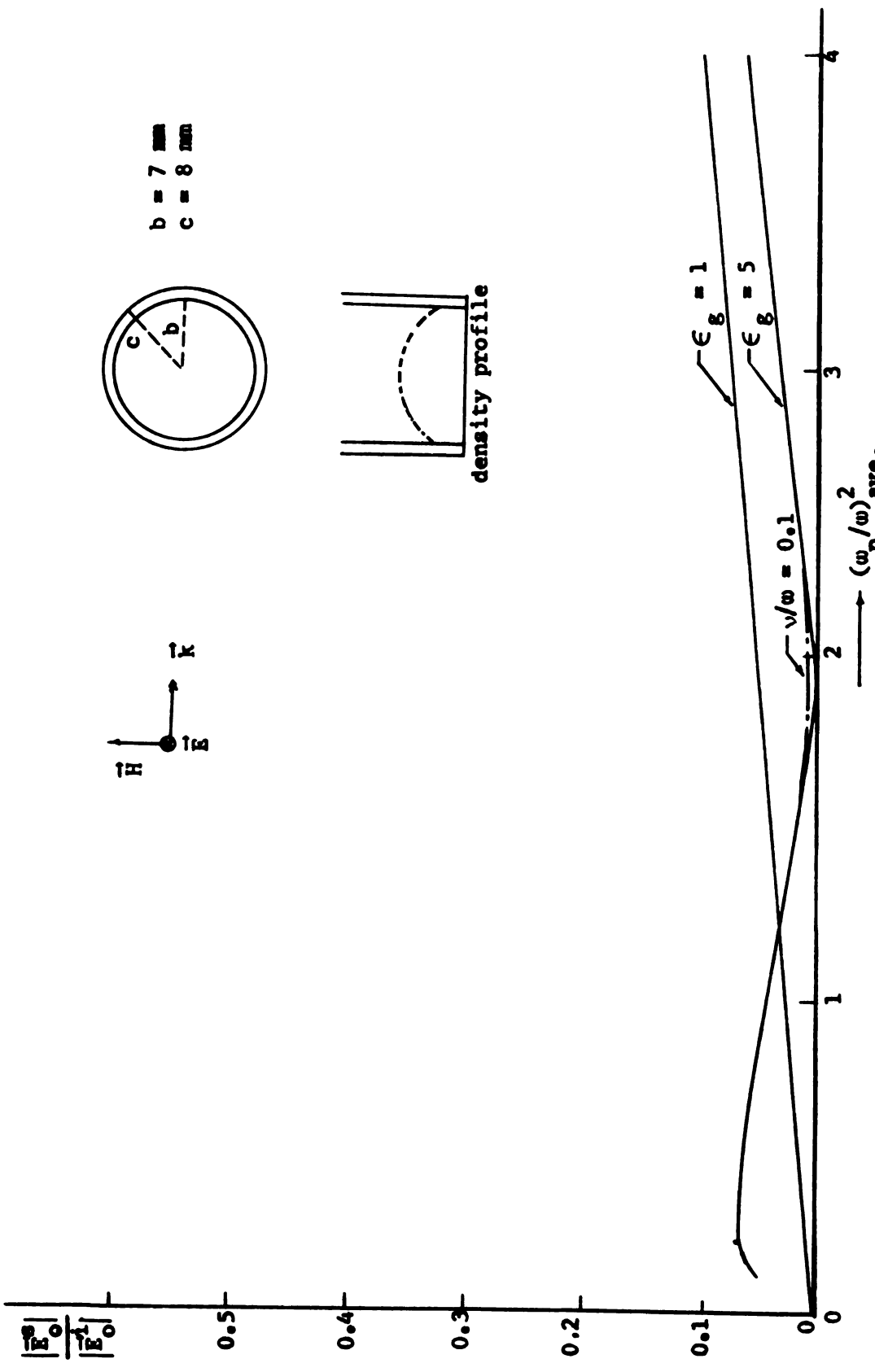

Fig. 4.3 Theoretical back scattered E field from a plain plasma cylinder as a function of $(\omega_p/\omega)^2_{ave.}$ for a parabolic plasma density distribution with a 13-sublayer model. (f = 2.3 GHz, θ = 180°, kor = 10, ν/ω = 0.01)

CHAPTER 5

EXPERIMENTAL INVESTIGATION OF THE SCATTERING FROM A PLASMA-COATED METALLIC CYLINDER AND A PLAIN PLASMA CYLINDER

5.1 Introduction

The electromagnetic scatterings from a plasma-coated metallic cylinder when illuminated by incident TE and TM waves have been studied theoretically in the preceding chapters. Although there have been a number of theoretical studies on the subject conducted by researchers in this area, very few experimental studies have been reported in the literature. Vandenplas[7] has conducted experiments on the scatterings from a plain plasma cylinder and a plasma-coated glass cylinder. However, to our best knowledge, Ho and Chen[26] are the only researchers who have investigated experimentally the scattering from a plasma-coated metallic cylinder.

Our experiment on the scattering from a plasma-coated metallic cylinder has been conducted inside of a waveguide While Ho and Chen conducted their experiment in free space. Kerźar and Weissglass[27] performed the experiment using a similar technique we used but they studied a plain plasma cylinder only.

The main task of this experimental investigation is to measure the back scattered fields from a plasma-coated metallic cylinder as a function of plasma density under a fixed operating frequency. This experiment has been performed for the purpose of checking theoretical

results developed in Chapters 2, 3 and 4. The resonance phenomenon and general behavior of the scattered field predicted by the theory have been qualitatively confirmed by the experiment.

5.2 Experimental Setup

The plasma-coated metallic cylinder was constructed by installing a metallic cylinder in the center of a cylindrical mercury-vapor discharge tube.

Two long mercury-vapor plasma tubes with outside and inside diameters of 16 and 14 mm were constructed. Installed in the center of one of the plasma tubes was a metallic cylinder of 4.316 mm diameter and 120 mm length. The plasma density was varied by sweeping the discharge current from zero to 600 mA which corresponded to a plasma density of $3.4 \times 10^{11}/cm^3$. The pressure of plasma was about 1 μ Hg.

In the experiment, the positive column parts of the plasma tubes were inserted into a S band rectangular waveguide (1 11/32"x 2 27/32") through holes on the waveguide wall. Two different arrangements for the plasma tube and the waveguide as shown in Figs. 5.1.1 and 5.1.2 have been considered in the experiment. In Fig. 5.1.1, the plasma tube is inserted through the narrow walls of the waveguide. This arrangement provides a situation of a plasma-coated metallic cylinder illuminated by a TE wave when the waveguide is excited by a TE_{10} mode. In Fig. 5.1.2, the plasma tube goes through the wide walls of the waveguide. For this case, the E field of the waveguide is in parallel with the plasma tube, thus, provide the situation of a plasma-coated metallic cylinder illuminated by a TM wave.

The schematic diagram of the experimental setup to measure the back scattered fields from a plasma-coated metallic cylinder and a plain plasma cylinder is shown in Fig. 5.2.

The back scattered field is fed into Channel 1 of the dual-vertical-input of an oscilloscope and the transmitted wave (incident and forward scattered waves) is fed into Channel 2 of the vertical input. The horizontal input of the oscilloscope is swept with a 60-cycle voltage which is linearly proportional to the discharge current of the plasma tube. Since the discharge current of the plasma tube is approximately proportional to the plasma density, the intensities of back scattered and transmitted waves can be plotted as functions of the plasma density directly on the oscilloscope.

Figures 5.3.1, 5.3.2, 5.4.1, and 5.4.2 are photographs of the experimental arrangements and setups.

5.3 Experimental Procedure

To minimize the error caused by unmatched loads, the following preparations were made before the measurement.

(1) Remove the plasma tube from the waveguide and plug the holes on the waveguide wall to maintain an unperturbed situation for the waveguide.

(2) Turn the microwave oscillator to a desired operating frequency (2.3 GHz in our experiment) with a 1 KHz square wave modulation applied. Turn the horizontal sweep of the oscilloscope to "internal sweep." Two sets of square waves with different amplitudes will appear on the oscilloscope. The reflected wave appears on Channel 1 and the transmitted wave on Channel 2.

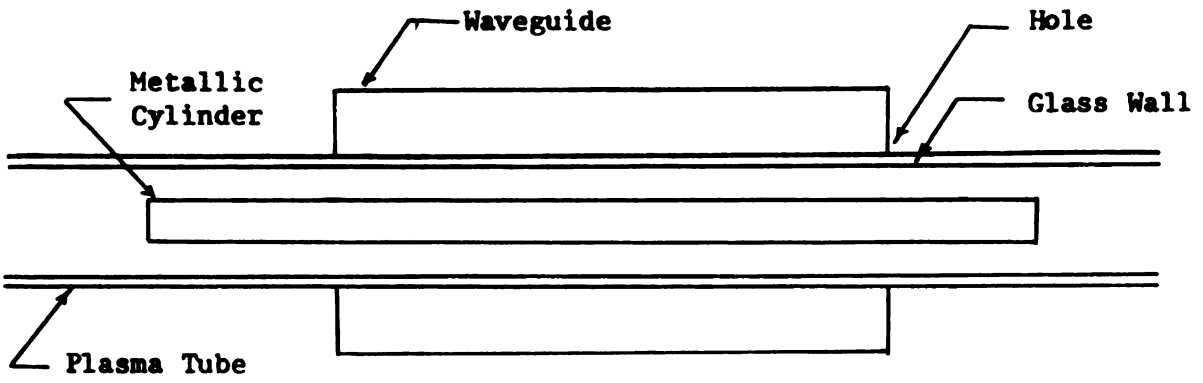

Fig. 5.1.1 Cross sectional view of a rectangular waveguide with an inserted plasma tube. (TE polarization)

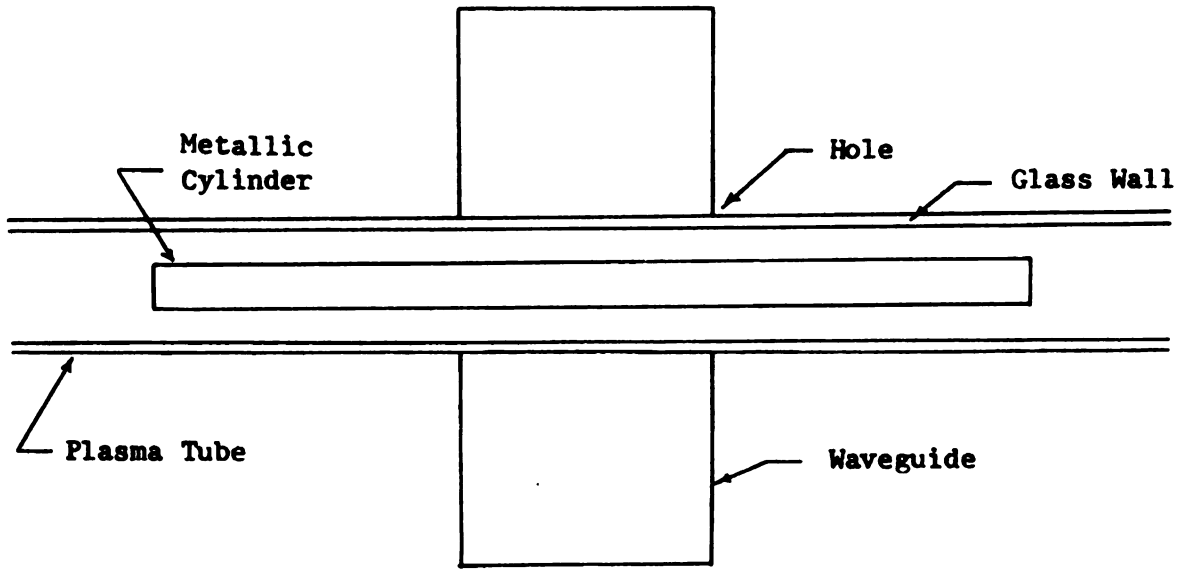

Fig. 5.1.2 Cross sectional view of a rectangular waveguide with an inserted plasma tube. (TM polarization)

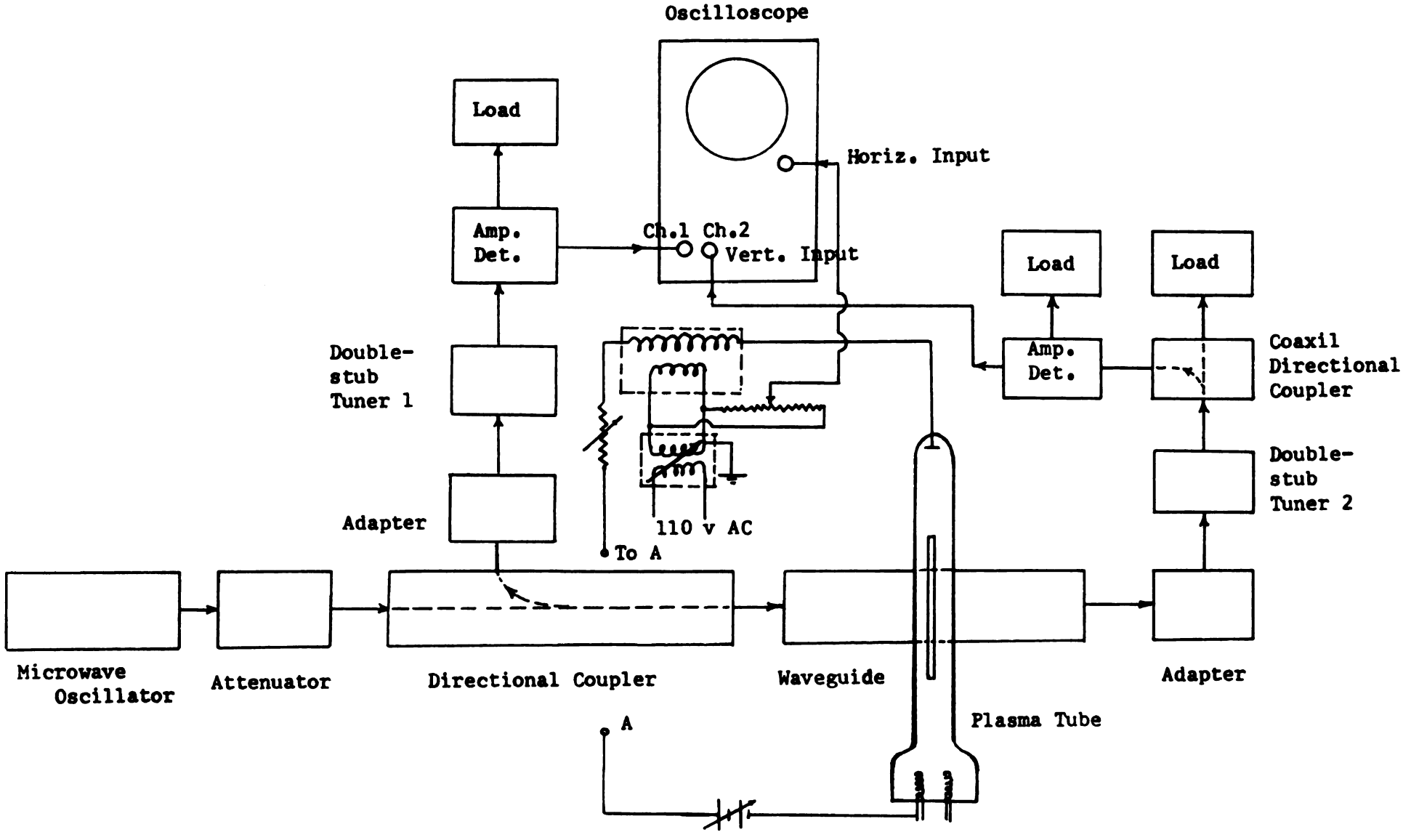

Fig. 5.2 Experimental setup for the measurement of scattered field .

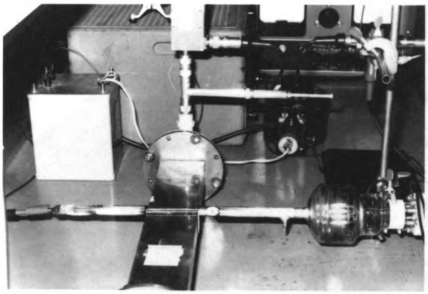

Fig. 5.3.1 The plasma discharge tube inserted in the waveguide.

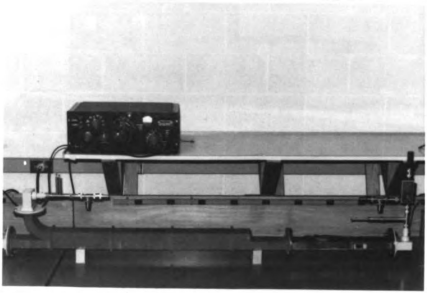

Fig. 5.3.2 The waveguide and directional coupler with double-stub tuners at both ends.

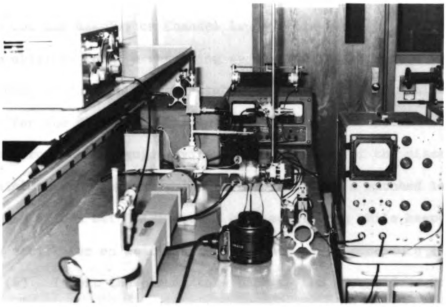

Fig. 5.4.1 Experimental set up for the measurement of scattered field with a TE incident wave.

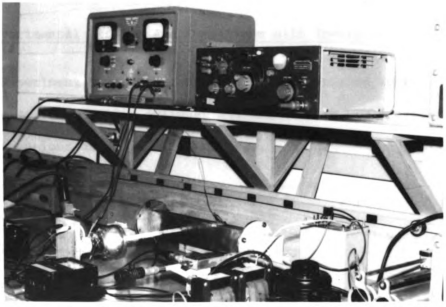

Fig. 5.4.2 Experiment set up for the measurement of scattered field with a TM incident wave.

(3) Adjust the double-stub tuner 1 to obtain a maximum amplitude for the display on Channel 1. By this way a highest sensitivity is obtained for the receiving system for the reflected wave.

(4) Adjust the double-stub tuner 2 to obtain a minimum amplitude for the display on Channel 1. This implies that the reflection from the waveguide system in the absence of the plasma tube is minimized or the waveguide is terminated by a matched load.

(5) Turn off 1 KHz square wave modulation while keep the microwave oscillator on at the same frequency as in procedure (2).

(6) Insert the plasma tube back to the waveguide. Start the plasma tube and connect the sweeping anode voltage to the horizontal input of the oscilloscope.

Two curves appearing on the oscilloscope are the reflected waves and the transmitted wave displayed as functions of discharge current which is proportional to the plasma density.

5.4 Experimental Results and Comparison with Theory

Experiment have been conducted with two plasma tubes. One is a plasma-coated metallic cylinder and the other a plain plasma cylinder. Their dimensions are given in Table 5.1.

Plasma-coated metallic cylinder			Plain plasma cylinder	
a (mm)	b (mm)	c (mm)	b (mm)	c (mm)
2.158	7	8	7	8

Table 5.1 Physical dimensions of plasma tubes.

The dielectric constant of glass wall is assumed to be 5 in the theoretical calculation. The operating frequency is fixed at 2.3 GHz and the discharge current is varied in the experiment. Since the plasma density is proportional to the discharge current and $(\omega_p/\omega)^2$ is proportional to plasma density, the displays on the oscilloscope are the plots of the intensities of the reflected and transmitted waves as functions of $(\omega_p/\omega)^2$. Thus, these displays can be compared directly with the theoretical results calculated in the preceding chapters.

5.4.1 Experimental and Theoretical Results

Figures 5.5 and 5.6 are experimental results of the reflected waves (back scattered fields) from a plasma-coated metallic cylinder when illuminated by a TE wave as functions of the discharge current or the plasma density. The transmitted wave (incident and forward scattered waves) is also shown in the lower part of Fig. 5.5.(a). It is noted that the sensitivities of the oscilloscope for the transmitted and reflected waves were adjusted separately to obtain symmetrical displays. Double tracing of the displayed curves is due to hysteresis phenomenon of the plasma. Figure 5.5.(b) shows the reflected wave only.

To show the detailed behavior of the curve of the reflected wave, the reflected wave was measured carefully at lower and higher discharge currents separately. Figure 5.6.(a) shows the detailed behavior of the reflected wave in the lower discharge current range. Figure 5.6.(b) shows the same quantity for the higher discharge current range. In these two figures, the dipolar resonance occurs at 210 mA

of the discharge current and the quadrupolar resonance occurs at 275 mA. The temperature resonances are shown in the left hand side of the dipolar resonance in Fig. 5.6.(a) appearing as small ripples.

Figure 5.7 shows the theoretical result of back scattered E field from a corresponding plasma-coated metallic cylinder when illuminated by a TE wave. Two values of collision frequency are assumed to be $\nu/\omega = 0.001$ and $\nu/\omega = 0.01$. Figure 5.7.(a) is obtained based on a cold plasma theory and a 13-sublayer model. Figure 5.7.(b) is obtained based on a hot plasma theory with a 3-sublayer model and the v_o/c ratio of 0.01 Both in Figs. 5.7.(a) and 5.7.(b), the non-uniform plasma density distribution is assumed to be expressed by Eq. (3.192) of Chapter 3.

Figure 5.8 shows the experimental results of the back scattered E field from a plain plasma cylinder when illuminated by a TE wave. The dipolar resonance is identified as the highest peak at the right of Fig. 5.8.(a) while a number of temperature resonances appearing at the left. The quadrupolar resonance is shown at the right of the dipolar resonance in Fig. 5.8.(b).

Figure 5.9.(a) and 5.9.(b) are the theoretical results of the back scattered E field from a plain plasma cylinder plotted as a function of $(\omega_p/\omega)^2_{ave.}$ based on a cold plasma theory and a hot plasma theory, respectively. The ratio v_o/c is assumed to be 0.0133 in the hot plasma theory. In both theories a non-uniform plasma density expressed by Eq. (3.193) of Chapter 3 is assumed.

Figure 5.10 shows the results of the back scattered E field from a plasma-coated metallic cylinder when illuminated by a TM wave.

Experimental result on the reflected wave is shown in Fig. 5.10.(a) as a function of the discharge current. As we have discussed in Chapter 4, for an incident TM wave, the cold and hot plasma theories both predict the same solution for the scattered field. Therefore, the theoretical back scattered E field shown in Fig. 5.10.(b) applies both for the cold and hot plasma cases. The collision frequency is assumed to be $\nu/\omega = 0.01$ in the theoretical calculation. The non-uniform plasma density distribution is assumed to be expressed by Eq. (3.192) of chapter and a 13-sublayer model is used.

Figure 5.11 shows the results of the back scattered E field from a plain plasma cylinder when illuminated by a TM wave. Experimental results on the reflected and transmitted waves as functions of the discharge current are shown in Fig. 5.11.(a). The theoretical result on the reflected wave is shown in Fig. 5.11.(b). The non-uniform plasma density is assumed to be expressed by Eq. (3.193) of Chapter 3 and a 13-sublayer model is used in theoretical calculation.

5.4.2 Comparison Between Experiment and Theory

For the case of the back scattered E field from a plasma-coated metallic cylinder illuminated by a TE wave, the dipolar and quadrupolar resonances are predicted both by the cold and hot plasma theories. The temperature resonances are predicted only by the hot plasma theory. All those dipolar, quadrupolar and temperature resonances are observed in the experiment as shown in Figs. 5.5 and 5.6. In the hot plasma theory, the theoretical value of $(\omega_{p,q}/\omega_{p,d})^2$, where $\omega_{p,q}$ and $\omega_{p,d}$ are the plasma frequencies corresponding to the quadrupolar and dipolar resonances, is 1.27. With the cold plasma theory

the value of $(\omega_{p,q}/\omega_{p,d})^2$ is found to be 1.24. Experimentally as in Fig. 5.5.(b), the value of I_q/I_d, where I_q and I_d are the discharge currents corresponding to the quadrupolar and dipolar resonances, is observed to be 1.28. Thus, for the location of the dipolar and quadrupolar resonances, experiment and theory come to a very good agreement. As for the shape of the curve, the quadrupolar resonance observed in the experiment is a rather smooth peak while the theory predicts a sharp peak. The temperature resonances are seen to occur to the left of the dipolar resonance. Those resonances occured at plasma densities where the value of $(\omega_p/\omega)^2$ are less than 0.7 are not detected in the experiment.

For the back scattered E field from a plain plasma cylinder illuminated by a TE wave, the temperature resonances are observed experimentally as shown in Fig. 5.8. The dipolar resonance occurs at the extreme right of Fig. 5.8.(a). The quadrupolar resonance occurs at a discharge current of I = 440 mA in Fig. 5.8.(b). The magnitude of quadrupolar resonance in this case appears to be larger than the case of a plasma-coated metallic cylinder. The theoretical prediction of the temperature resonances gives weaker amplitude than that observed in the experiment. This discrepancy is probably due to the inaccuracy in the theoretical analysis since a computer subroutine for calculating Hankel functions with a large complex argument is not available.

For the case of the back scatterings from a plasma-coated metallic cylinder and a plain plasma cylinder when they are illuminated by a TM wave, theory and experiment agrees very satisfactorily as evidenced in Figs. 5.10 and 5.11. For both cases of a plasma-coated

metallic cylinder and a plain plasma cylinder, no resonance is observed experimentally or theoretically.

5.5 Discussion

The experimental investigation of the scattering from a plasma-coated metallic cylinder when illuminated by a TE or a TM wave gives satisfactory results which compare fairly closely with the theoretical results based on the hot plasma theory. The cold plasma theory also gives a fair agreement with experiment but it fails to predict the temperature resonances.

The main difficulty encounted in the theoretical study is the mathematical resonances associated with the stratification method. This has been discussed in Sec. 2.9 of Chapter 2. To avoid the mathematical resonances, it may be worthwhile to apply the differential equation method[2,5,7] to our problem if this study is to be extended in the future.

Finally, the experiment in this research was conducted in a waveguide while our theory assumed the free space situation. In spite of these differences, theory and experiment agree quite satisfactory. For a future extention, it may be suggested to conduct the experiment in free space.

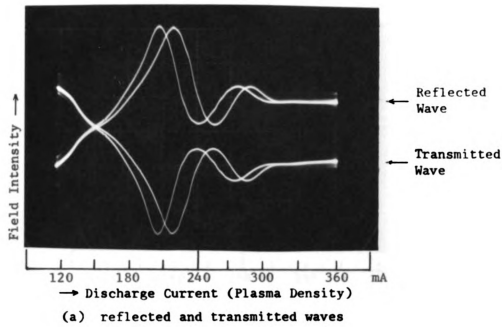

Fig. 5.5 Experimental results of the back scattered E field from a plasma-coated metallic cylinder as a function of the discharge current with a TE incident wave.

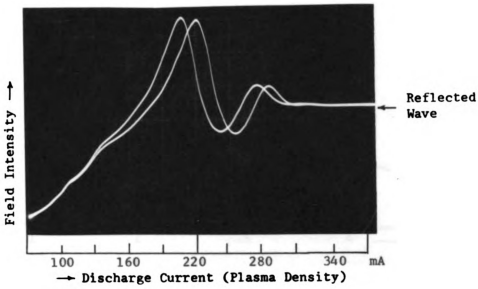

(a) lower discharge current range

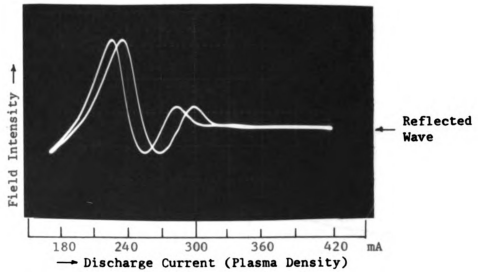

(b) higher discharge current range

Fig. 5.6 Experimental results of the back scattered E field from a plasma-coated metallic cylinder as a function of the discharge current with a TE incident wave.

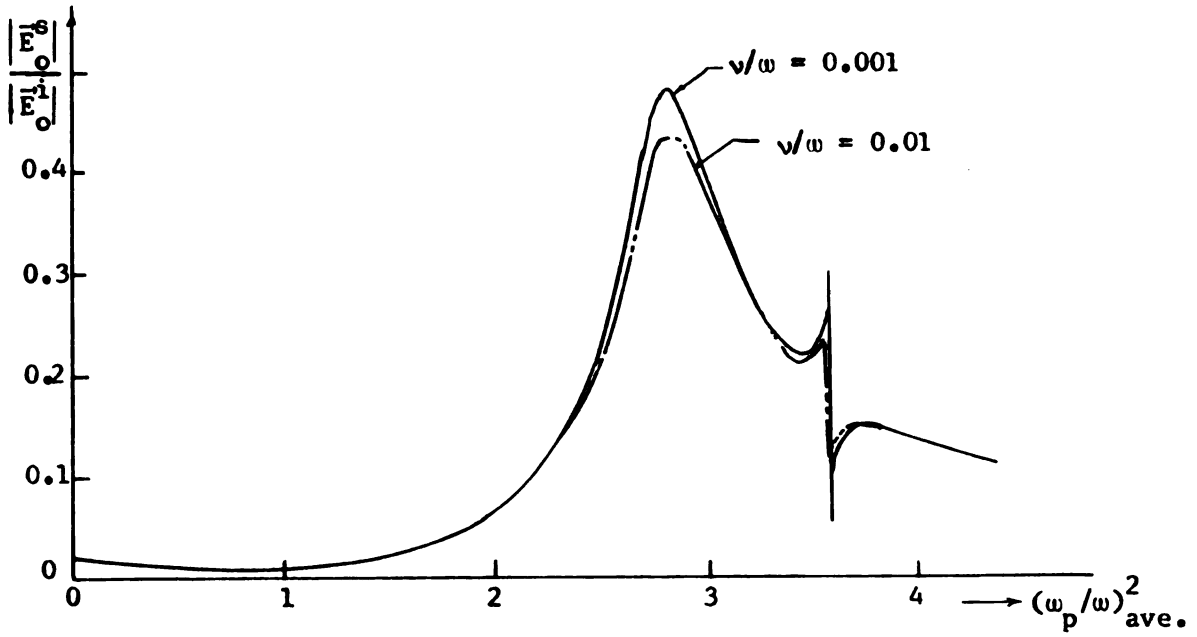

(a) cold plasma theory with 13-sublayer model

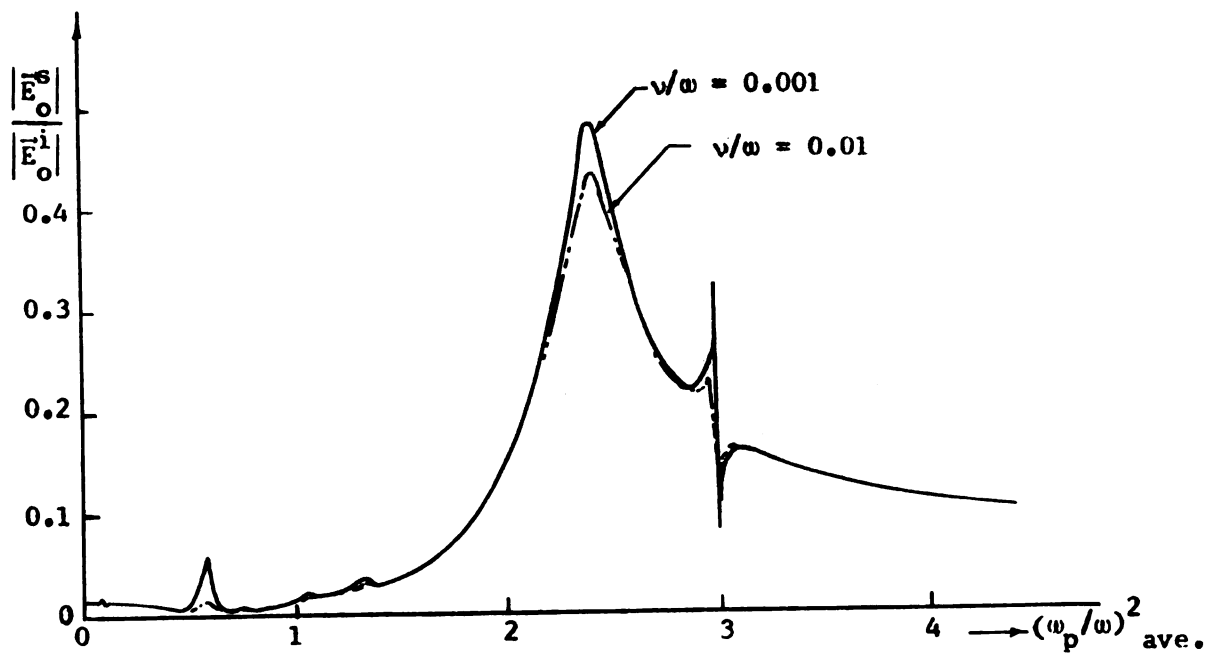

(b) hot plasma theory with 3-sublayer model and $v_o/c = 0.01$

Fig. 5.7 Theoretical back scattered E field from a plasma—coated metallic cylinder as a function of $(\omega_p/\omega)^2_{ave.}$ with a TE incident wave and a parabolic density dist. ($k_o r = 10$, $\theta = 180^o$)

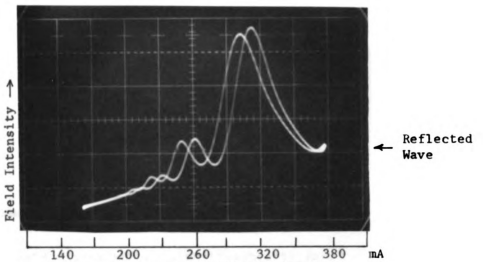

(a) dipolar and temperature resonances

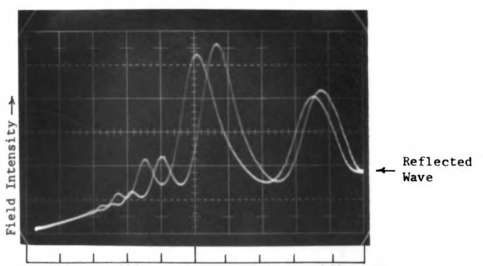

(b) dipolar, quadrupolar and temperature resonances

Fig. 5.8 Experimental results of the back scattered E field from a plain plasma cylinder as a function of the discharge current with a TE incident wave.

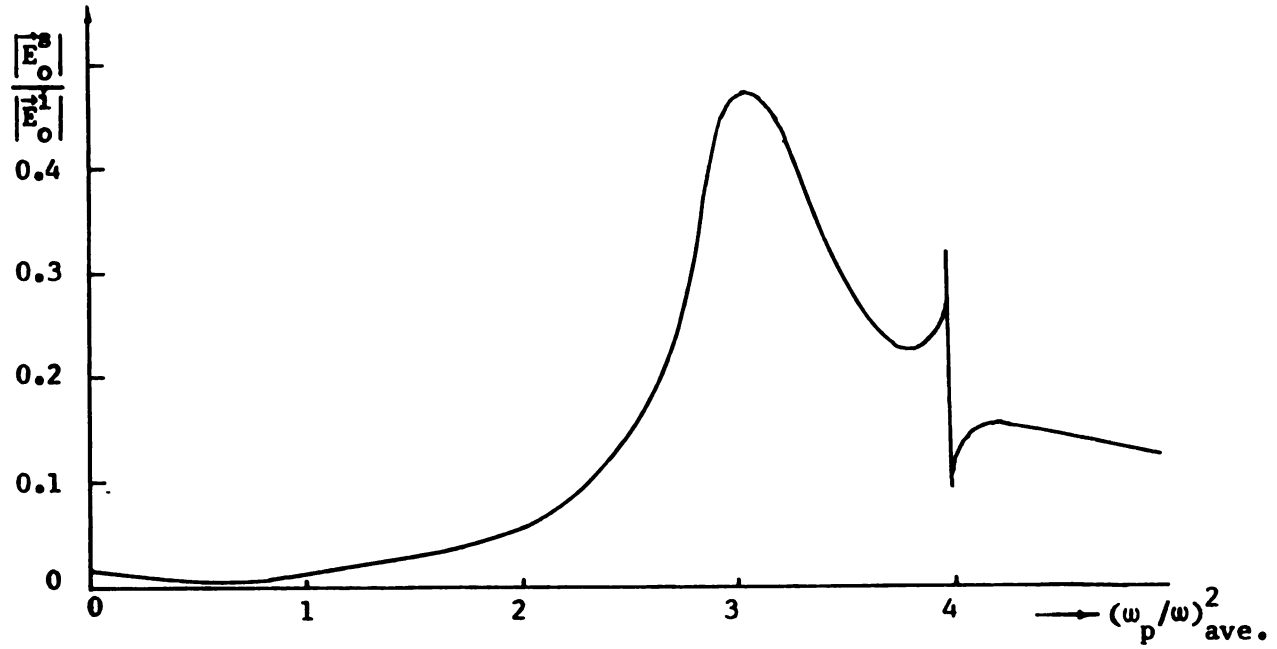

(a) cold plasma theory with 13-sublayer model

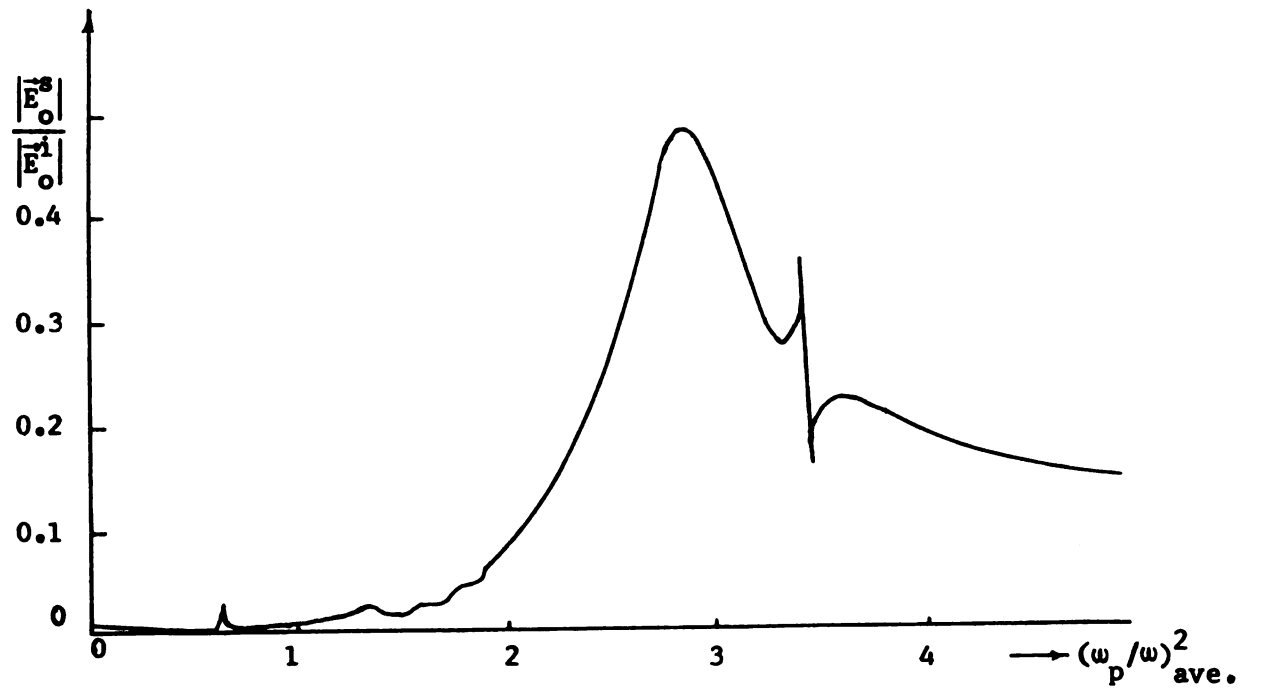

(b) hot plasma theory with 3-sublayer model and $v_o/c = 0.01333$

Fig. 5.9 Theoretical back scattered E field from a plain plasma cylinder as a function of $(\omega_p/\omega)^2_{ave.}$ with a TE incident wave and a parabolic density dist. ($k_o r = 10$, $\nu/\omega = .001$, $\theta = 180^o$)

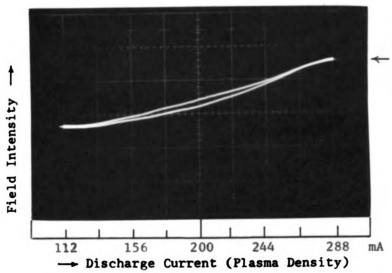

(a) experiment result

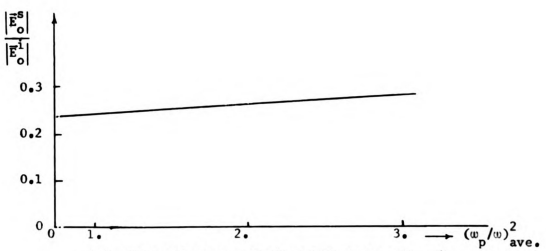

(b) theoretical result ($\theta = 180$, $k_o r = 10$, $\nu/\omega = 0.01$)

Fig. 5.10 Experimental & theoretical results of the back scattered E field from a plasma-coated metallic cylinder with a TM incident wave.

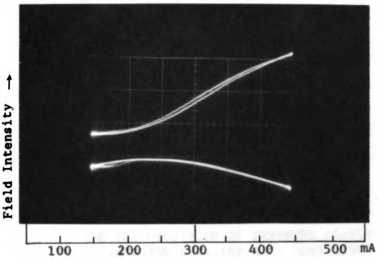

(a) experiment result

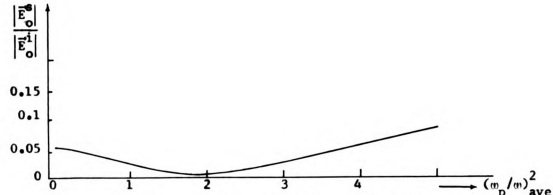

(b) theoretical result ($\theta = 180^o$, $k_o r = 10$, $\nu/\omega = 0.01$)

Fig. 5.11 Experimental and theoretical results of the back scattered E field from a plain plasma cylinder with a TM incident wave.

APPENDIX A

THE DECOMPOSITION OF PRESSURE GRADIENT INTO THE D.C. AND A.C. COMPONENTS

APPENDIX A

THE DECOMPOSITION OF PRESSURE GRADIENT INTO THE D.C. AND A.C. COMPONENTS

The pressure gradient, ∇P, of Eq. (3.75) is considered and decomposed into the d.c. and a.c. components as follows:

If a static pressure (d.c. case) is concerned, the pressure is established by an isothermol process. That is, the temperature of the gas is fixed to a constant value, and we have

$$P = n_e kT \tag{A.1}$$

where T is the fixed temperature of gas, n_e is electron density of the plasma and k is Boltzmann's constant.

If an external force disturbes n_e in such a way that

$$n_e(\vec{r},t) = n_o(\vec{r}) + n_1(\vec{r},t) \tag{A.2}$$

and n_e is a fast function of time, such as a high frequency disturbance, then the temperature of gas is not fixed simply due to the fact that not enough time is allowed to exchange energy in the gas to keep the temperature constant. In such case, the adiabatic law is used. that is

$$P n^{-\gamma} = \text{constant} \tag{A.3}$$

where γ is the ratio of specific heat such that

$$\gamma = \frac{c_p}{c_v} = \frac{m+2}{m} \tag{A.4}$$

with m = degree of freedom of gas.

In a high frequency plasma oscillation, the motion of electron is usually in one direction only. So that we can assume $m = 1$. This leads to $\gamma = 3$.

For the case of a small r.f. perturbation, as in Eq. (A.2), the relationship between the pressure and the electron density is

$$P n_e^{-\gamma} = P_o n_o^{-\gamma} = \text{constant} \tag{A.5}$$

since initially $P = P_o$ and $n_e = n_o$. Then

$$P = P_o \left(\frac{n_e}{n_o} \right)^{\gamma}. \tag{A.6}$$

P_o is the static pressure established by an isothemal process, so that

$$P_o = n_o k T. \tag{A.7}$$

From Eq. (A.6), we have

$$\begin{aligned} \nabla P &= \nabla \left[P_o \left(\frac{n_e}{n_o} \right)^{\gamma} \right] \\ &= \left(\frac{n_e}{n_o} \right)^{\gamma} \nabla P_o + P_o \nabla \left(\frac{n_e}{n_o} \right)^{\gamma}. \end{aligned} \tag{A.8}$$

The substitution of Eq. (A.2) in Eq. (A.8) leads to

$$\begin{aligned} \nabla P &= \left(1 + \frac{n_1}{n_o} \right)^{\gamma} \nabla P_o + P_o \nabla \left(1 + \frac{n_1}{n_o} \right)^{\gamma} \\ &= \left(1 + \frac{n_1}{n_o} \right)^{\gamma} kT \nabla n_o + kT n_o \left[\gamma \left(1 + \frac{n_1}{n_o} \right)^{\gamma - 1} \right. \\ &\qquad \left. \cdot \frac{n_o \nabla n_1 - n_1 \nabla n_o}{n_o^2} \right] \end{aligned} \tag{A.9}$$

or

$$\nabla P = kT\left[\left(1+\frac{n_1}{n_o}\right)^{\gamma} - \gamma\left(1+\frac{n_1}{n_o}\right)^{\gamma-1}\frac{n_1}{n_o}\right]\nabla n_o + \gamma kT\left(1+\frac{n_1}{n_o}\right)^{\gamma-1}\nabla n_1 \quad . \tag{A.10}$$

If $n_1 \ll n_o$, Eq. (A.10) yields

$$\nabla P = kT\nabla n_o + \gamma kT\nabla n_1 \quad . \tag{A.11}$$

In the above expression, the terms, $kT\,\nabla n_o$ and $\gamma kT\,\nabla n_1$, are the d.c. and a.c. components of the pressure gradient respectively.

REFERENCES

REFERENCES

(1) T. R. Kaiser and R. L. Closs, "Theory of Radio Reflections from Meteor Trails : I," The Phil. Magazine, Ser. 7, Vol. 43, No. 336, pp. 1 - 32, Jan. 1952.

(2) G. H. Keitel, "Certain Mode Solutions of Forward Scattering by Meteor Trails," Proc. of IRE, pp. 1481 - 1487, Oct. 1955.

(3) Y. Ohba, "Diffraction by a Conducting Circular Cylinder Clad by an Anisotropic Plasma Sheath," Canadian J. of Phys., Vol. 41, pp. 881 - 889, 1963.

(4) H. C. Chen and D. K. Cheng, "Scattering of Electromagnetic Waves by an Anisotropic Plasma-Coated Conducting Cylinder," IEEE Trans. Antennas and Propagation, Vol. AP - 12, pp. 348 - 353, May 1964.

(5) C. Yeh and W. V. T. Rusch, "Interaction of Microwaves with an Inhomogeneous and Anisotropic Plasma Column," J. of Appl. Phys., Vol. 36, No. 7, pp. 2302 - 2306, July 1965.

(6) C. C. H. Tang, "Backscattering from Dielectric-Coated Infinite Cylindrical Obstacles," J. of Appl. Phys., Vol. 28, No. 5, pp. 628 - 633, May 1957.

(7) P. E. Vandenplas, "Electron Waves and Resonances in Bounded Plasma," Interscience Publishers, N. Y., 1968.

(8) K. Fong, "Computation of Backscattering Cross Section of Plasma-Clad Metal Cylinders by the 'Layer Method'," IEEE Trans. Antennas and Propagation, pp. 138 - 140, Jan. 1968.

(9) J. A. Stratton, "Electromagnetic Theory," McGraw-Hill Book Co.,N. Y., p. 374, 1941.

(10) N. Herlofson, "Plasma Resonance in Ionospheric Irregularities," Arkiv För Fysik, Vol. 3, pp. 247 - 297, Feb. 1951.

(11) P. E. Vandenplas and A. M. Messian, "Equations of a Hot Inhomogeneous Plasma Model-II, Perturbed Scalar Pressure Approximation," Plasma Physics (J. of Nuclear Engery, Part c), Vol. 6, pp. 459 - 468, 1964.

(12) T. J. Killian, "The Uniform Positive Column of an Electric Discharge in Mercury Vapor," Phys. Review, Vol. 35, pp. 1238 - 1252, May 1930.

(13) J. L. Shohet and A. J. Hatch, "Eigenvalues of a Microwave Cavity Filled with a Plasma of Variable Radial Density," J. of Appl. Phys., Vol. 41, No. 6, pp. 2610 - 2618, May 1970.

(14) A. Dattner, "Plasma Resonance," Ericsson Tech., Vol. 3, No. 2, pp. 309 - 350, 1957.

(15) J. V. Parker, J. C. Nickel and R. W. Gould, "Resonance Oscillations in a Hot Nonuniform Plasma," The physics of Fluids, Vol. 7, No. 9, pp. 1489 - 1500, Sep. 1964.

(16) F. W. Crawford, "Internal Resonances of a Discharge Column," J. of Appl. Phys., Vol. 35, No. 5, pp. 1365 - 1369, May 1964.

(17) F. W. Crawford and G. S. Kino, "The Mechanism of Tonks-Dattner Resonances of a Discharge Column," Proc. of the Sixth International Conference on Ionization Phenomena in Gases, Paris, July 1963.

(18) J. R. Wait, "Scattering of Electromagnetic and Electroacoustic Waves by a Cylindrical Object in a Compressible Plasma," Radio Science J. of Research NBS/USNC-URSI, Vol. 69D, No. 2, pp. 247 - 256, Feb. 1965.

(19) J. A. Fejer, "Scattering of Electromagnetic Waves by a Plasma Cylinder," The Physics of Fluids, Vol. 7, No. 3, pp. 439 - 445, Mar. 1964.

(20) L. Spitzer, "Physics of Fully-Ionized Gases," Interscience, 1956.

(21) M. H. Cohen, "Radiation in a Plasma. II. Equivalent Sources," Phys. Review, Vol. 126, No. 2, pp. 389 - 397, April 1962.

(22) A. H. Kritz and D. Mintzer, "Propagation of Plasma Waves across a Density Discontinuity," Phys. Review, Vol. 117, No. 2, pp. 382 - 386, Jan. 1960.

(23) K. A. Haynes and D. Kahn, "Wave Propagation across a Two-Fluid Plasma Density Discontinuity," The Physics of Fluids, Vol. 8, No. 9, pp. 1681 - 1688, Sept. 1965.

(24) S.R. Seshadri, I. L. Morris and R. J. Mailloux, "Scattering by a Perfectly Conducting Cylinder in a Compressible Plasma," Canadian J. of Phys., Vol. 42, pp. 465 - 476, March 1964.

(25) "Hand Book of Mathematical Functions," Dover Publications, Inc., N. Y.

(26) B. Ho and K. M. Chen, "Electroacoustic Resonance in Plasma Layer Surrounding a Metallic Cylinder," Proc. of IEEE, Vol. 56, No. 9 pp. 1600 - 1602, Sept. 1968.

(27) B. Keržar and P. Weissglas, "Plasma Microwave Interaction," J. of Appl. Phys., Vol. 36, No. 8, pp. 2479 - 2484, Aug. 1965.